UNIVERSITY OF CALIFORNIA SAN DIEGO

Elucidating Novel Regulatory Mechanisms of the Tumor Suppressor Phosphatase PHLPP1

A dissertation submitted in partial satisfaction of the
requirements for the degree Doctor of Philosophy

in

Biomedical Sciences

by

Agnieszka Teresa Grzechnik Kawashima

Committee in charge:

Professor Alexandra C. Newton, Chair
Professor Arshad Desai
Professor Jack E. Dixon
Professor Christopher K. Glass
Professor J. Silvio Gutkind
Professor Lorraine Pillus

2020

The dissertation of Agnieszka Teresa Grzechnik Kawashima is approved, and it is acceptable in quality and form for publication on microfilm and electronically:

_____

_____

_____

_____

_____

_____

Chair

University of California San Diego

2020

DEDICATION

For my son Luke,

By far my most exciting and successful science experiment

TABLE OF CONTENTS

LIST OF FIGURES

LIST OF TABLES

LIST OF SUPPLEMENTAL DATASETS

ACKNOWLEDGEMENTS

I would like to first and foremost express my gratitude to my mentor, Dr. Alexandra Newton. Thank you for the guidance and support during this journey, and for giving me the space to explore interesting new stories off the beaten path. I also would like to acknowledge my committee members – Drs. Arshad Desai, Jack Dixon, Chris Glass, Silvio Gutkind, and Lorraine Pillus – for their time and insightful comments. Thank you to all of my collaborators who provided valuable insight and technical assistance during my graduate career.

I would like to thank all members of the Newton lab, both past and present, for their support and enthusiasm. Even though science itself has its ups and downs, this group of scientists always made my time in the lab enjoyable. I would like to particularly thank the other PHLPP-er in the lab during my tenure, Dr. Ksenya Cohen-Katsenelson. I always felt grateful to have a bay mate who was equally as interested and enthusiastic about my project as I was. Thanks for always looking out for me and for all the fun times in Bay E. To Alexander Jones, who replaced Ksenya in Bay E – it was nice to have someone else keen on learning about phosphatases in a kinase-loving lab. Also, big thank you to Maya Kunkel, Gema Lordén, and An-Angela Van, who made even the hardest days in the lab enjoyable – thank you for all the laughs, coffee breaks, and Korean barbecue expeditions.

Thank you to the entire Grzechnik and Kawashima families, and to all of my extended Polish family here in San Diego and in Poland. Your support has always meant so much to me. To my parents – Sławek and Izabela – who have always supported me as I forged my own path in this world. Thank you for always being there when I needed help, but also giving me the space to figure out my own direction in life.

Finally, and most importantly, I wish to thank my husband Tad. Thank you for always listening as I rambled on and on about my project. Thank you for joining me in lab during nights and weekends when I did not want to be there alone. A lot of life happened for us in these past seven years – from getting married to buying our first house to bringing Luke into this world – I can't imagine going through it with anyone else.

Chapter 1, in part, is an adaptation of material that appears in "PHLPPing through history: a decade in the life of PHLPP phosphatases", as published in *Biochemical Society Transactions* 2016 by Agnieszka T. Grzechnik and Alexandra C. Newton. The dissertation author was the primary author of these literature reviews.

Chapter 2, in full, has been submitted for publication under the title "The PHLPP1 N-Terminal Extension is a Mitotic Cdk1 Substrate and Controls an Interactome Switch", as published by Agnieszka T. Kawashima, Cassandra Wong, Charles C. King, Pablo Lara-Gonzalez, Arshad Desai, Anne-Claude Gingras, and Alexandra C. Newton. The dissertation author was the primary investigator and author of the material.

Chapter 3, in full, is a reprint of material that appears in "PHLPP1 Counter-Regulates STAT1-mediated Inflammatory Signaling", as published by Ksenya Cohen-Katsenelson, Joshua D. Stender, Agnieszka T. Kawashima, Gema Lordén, Satoshi Uchiyama, Victor Nizet, Christopher K. Glass, and Alexandra C. Newton. The dissertation author was a co-first author, along with Ksenya Cohen-Katsenelson and Joshua D. Stender, on this publication.

VITA

2011 Bachelor of Science (Biochemistry), University of California Los Angeles

2020 Doctor of Philosophy (Biomedical Sciences), University of California San Diego

PUBLICATIONS

Kawashima AT, Wong C, King CC, Lara-Gonzalez P, Desai A, Gingras AC, Newton AC. 2020. The PHLPP1 N-terminal extension is a mitotic Cdk1 substrate and controls and interactome switch. *Manuscript submitted for publication.*

Kawashima AT, Newton AC. 2020. Pharmacology on Target. *Trends in Pharmacological Sciences*, **41**: 227-230.

Cohen Katsenelson K*, Stender JD*, **Kawashima AT***, Lordén G, Uchiyama S, Nizet V, Glass CK, Newton AC. 2019. PHLPP1 counter-regulates STAT1-mediated inflammatory signaling. *Elife*. **8,** e48609. **authors contributed equally*

Grzechnik AT, Newton AC. 2017. PH Domain Leucine-Rich Repeat Protein Phosphatase (PHLPP). *Encyclopedia of Signaling Molecules*. Choi S, ed. (New York: Springer), pp.1-7.

Grzechnik AT, Newton AC. 2016. PHLPPing through history: a decade in the life of PHLPP phosphatases. *Biochem Soc Trans*. **44**, 1675-1682.

Lee YJ, Lee CY, **Grzechnik AT,** Gonzales-Zubiate F, Vashisht AA, Lee A, Wolschlegel J, Chanfreau DF. 2013. RNA Polymerase I stability couples cellular growth to metal availability. *Mol Cell.* **51**, 105-115.

ABSTRACT OF THE DISSERTATION

Elucidating Novel Regulatory Mechanisms of the Tumor Suppressor Phosphatase PHLPP1

by

Agnieszka Teresa Grzechnik Kawashima

Doctor of Philosophy in Biomedical Sciences

University of California San Diego, 2020

Professor Alexandra C. Newton, Chair

In the fifteen years since the tumor suppressor phosphatase PH domain Leucine-rich repeat Protein Phosphatase 1 (PHLPP1) was initially discovered in the search for the enzyme that dephosphorylates Akt at the hydrophobic motif (Ser473), a number of new substrates of PHLPP1 have been identified, suggesting a broad and varied role for this newly classified serine/threonine phosphatase. Not surprisingly, deregulation of PHLPP1 signaling has been implicated in a diverse set of disease states, ranging from cancer to diabetes to inflammation. However, there was still progress to be made to better understand how PHLPP1 itself is regulated. This thesis expands on

the knowledge of how PHLPP1 localization, expression, protein interactions, and function are all dynamically regulated in the cell. First, mechanistic studies reveal that the previously unstudied PHLPP1 N-terminal extension, which accounts for the first roughly 30% of the protein sequence, is dynamically regulated by phosphorylation during mitosis and is required for a mitotic "switch" in the PHLPP1 interactome. Second, biochemical analysis of this N-terminal extension revealed that it houses a nuclear localization signal, allowing it to control PHLPP1 localization and function in the context of inflammatory signaling pathways. Finally, these studies exposed that PHLPP1 expression levels are dramatically reduced in the absence of extracellular glutamine, suggesting that PHLPP1 expression is sensitive to environmental nutrient levels. Taken together, these studies not only provide novel insight into how PHLPP1 functions in a normal physiological context but also how its regulation can go awry in various disease states.

Chapter 1 – Introduction to PH domain Leucine-rich repeat Protein Phosphatase 1 (PHLPP1)

Protein Phosphatases

Protein phosphorylation is one of the major mechanisms by which cells transduce signals. Over 300,000 phosphorylation sites have been identified, with about 60% occurring on Serine (Ser) residues, and 25% on Threonine (Thr) residues (1). For every phosphorylation event, there is a corresponding dephosphorylation event, yet our understanding of the structure, function, and regulation of the 40 or so Ser/Thr protein phosphatases lags behind that of the 400 or so Ser/Thr protein kinases (2). In part, the greater understanding of protein kinases stems from their common architecture and catalytic mechanisms. In contrast, there is considerable variation in the enzymes that remove phosphate (3). Unlike protein kinases, which phosphorylate substrates at conserved motifs, a single phosphatase can regulate a wide variety of substrates, not targeting a specific consensus sequence. Rather, regulatory regions on the phosphatase provide the specificity required for targeting substrates. The three serine/threonine phosphatase families -the phosphoprotein phosphatases (PPP), metal-dependent protein phosphatases (PPM), aspartate-based phosphatases (FCP/SCP)- encode these regulatory regions in different ways. While the PPP family has regulatory domains encoded for on separate subunits, PPM and FCP/SCP family members have regulatory regions and catalytic domain encoded for on a single peptide. This review focuses on a newly discovered member of the PPM family, the PH domain Leucine Rich Repeat Protein Phosphatases (PHLPP).

The PHLPP Family: Domain Composition and Function

The PHLPP phosphatases, which comprise of PHLPP1 and PHLPP2, are part of the PP2C family of Ser/Thr phosphatases which, along with pyruvate dehydrogenase phosphatase, make up the metal-dependent protein phosphatase (PPM) family. PPM members are similar to other Ser/Thr

phosphatases in that they require a divalent cation, preferably Mn^{2+} or Mg^{2+}, for catalytic activity. Biochemical analysis has revealed that the activity of the purified PHLPP2 PP2C domain is dependent on the presence of Mn^{2+} (4). Divalent cations are coordinated by four conserved aspartate residues into the active site of the phosphatase. The active site of human PHLPP has a unique architecture, with only three of these four conserved acidic residues; this may account for the lower catalytic activity of the PHLPP PP2C domain compared to PP2Cα, the most well studied PP2C phosphatase (4).

PP2C phosphatases are unique from other Ser/Thr phosphatases due to their insensitivity to a number of common phosphatase inhibitors, such as okadaic acid and microcystin (5). PHLPP inhibitors were recently discovered by a chemical and virtual screen of the National Cancer Institute (NCI) repository (6). Two compounds were identified to selectively inhibit activity of PHLPP1 and PHLPP2 with *in vitro* IC_{50} values in the 5 μM range, compared to *in vitro* IC_{50} values in the 100 μM range for PP2Cα and PP1. Treatment of cells with these inhibitors increases Akt phosphorylation and suppress cellular apoptosis (6), promotes chondrocyte proliferation (7), decreases chaperone-mediated autophagy (8), and raises levels of Akt activity in rat cortical neurons resulting in a neuroprotective phenotype (9). The identification of such inhibitors not only provides a pharmacological breakthrough to studying PHLPP activity *in vitro* and in cells, but also offers the first steps to creating a potential therapeutic drug to inhibit PHLPP activity.

The first identified substrate of both PHLPP1 and PHLPP2 was the pro-oncogenic AGC kinase, Akt (Figure 1.1.A) (10). Specifically, PHLPP inactivates Akt by dephosphorylating a key regulatory serine residue (Ser473) in the C-terminal tail of Akt. Further work demonstrated that PHLPP1 is able to directly dephosphorylate other AGC kinases at their hydrophobic motifs, most notably protein kinase C (PKC, Figure 1.1.B) (11), thus reducing the steady state levels of this

enzyme, and ribosomal protein S6 kinase (S6K, Figure 1.1.A) (12). Thus, PHLPP1 was dubbed the 'hydrophobic motif phosphatase'. In the decade since this initial discovery that PHLPP1 dephosphorylates Akt, several other non-AGC kinase PHLPP1 substrates have been revealed. For example, the pro-apoptotic kinase Mammalian Sterile 20-like kinase 1 (Mst1), a member of the STE kinase family, is also a substrate of PHLPP1 (Figure 1.1.A) (13). By removing an inhibitory phosphorylation on Thr387, PHLPP1 activates Mst1 and induces apoptosis. Thus, dephosphorylation by PHLPP1 inactivates pro-survival kinases such as Akt and activates pro-apoptotic kinases such as Mst1.

Most PHLPP signaling pathways discovered to date have involved the activity of cytoplasmic PHLPP. Recent evidence suggests a novel nuclear signaling role for PHLPP1 (Figure 1.1.D). PHLPP1 suppresses histone phosphorylation and acetylation to negatively affect transcription of receptor tyrosine kinases, such as the Epidermal Growth Factor Receptor (EGFR) (14). Chemical modifications to the histone N-terminal tail can dramatically alter chromatin structure, playing a key role in regulating gene expression, DNA replication, and DNA repair (15). Loss of PHLPP1 not only resulted in an increase in global histone phosphorylation and acetylation, two marks associated with actively transcribed genes, but it also resulted in increased histone lysine acetylation in the EGFR promoter. Amplified signaling by RTKs is associated with diverse human cancers, as a result of somatic gain-of-function mutations of the RTKs, gene amplification, or epigenetic changes that result in increased receptor expression (16). Interestingly, another study identified that PHLPP1 is able to directly dephosphorylate RAF1 (c-RAF) (17), a kinase downstream of EGFR and Ras (Figure 1.1.C) (18). RAF1 was identified as a PHLPP1 interacting protein via co-immunoprecipitation coupled to mass spectrometry. Further analysis showed that PHLPP1 is able to dephosphorylate RAF1 at Ser338, resulting in the inactivation of RAF1. These

lines of data suggest a complex role for PHLPP1 in regulating, both directly and indirectly, the MEK/ERK signaling cascade. Thus, this epigenetic role of PHLPP1 is likely a major contributor to the tumor suppressive properties of the enzyme.

PHLPP is evolutionarily conserved from yeast to humans (19). Intriguingly, the yeast homologue of PHLPP, Cyr1, is part of the same gene as the only adenylate cyclase encoded in the *Saccharomyces cerevisiae* genome (20). In yeast, the cyclic AMP (cAMP)/Protein Kinase A (PKA) signaling pathway is vital for nutritional sensing and growth (21), with deletion of the gene encoding Cyr1 resulting in G1 phase cell cycle arrest (20). Increases in extracellular glucose concentration result in RAS-associated activation of adenylate cyclase and the production of cAMP, a critical cofactor for the enzyme PKA. Elevation of cAMP leads to robust changes in the transcriptome that support growth and fermentation (22). Whether mammalian PHLPP has retained any function in regulating cAMP/PKA signaling from its distant yeast homologue remains to be investigated.

How do the PHLPP phosphatases find their targets at the right place and the right time? The presence of distinct regulatory domains on the PHLPP polypeptide provide this specificity. These PHLPP1 and PHLPP2 are relatively large proteins (180 kDa and 150 kDa, respectively) and encode similar regulatory regions, including a Pleckstrin Homology (PH) domain, multiple Leucine Rich Repeats (LRRs), a catalytic Mn^{2+}-dependent PP2C phosphatase domain, and an unstructured C-terminal tail that ends in a PDZ (post synaptic density protein PSD95, Drosophila disc large tumor suppressor DLG1, and zonula occludens-1 protein zo-1) binding ligand (Figure 1.2) (10). These various regulatory domains are critical for proper targeting of PHLPP to its substrates. For example, the PH domain is required for PHLPP1 to target PKC, the LRR is required for the suppressive effect on RTK transcription, and the PDZ domain is required for

dephosphorylation of Akt. Additionally, the C-terminal extension (CTE) of PHLPP1 interacts with various protein scaffolds, including the plasma membrane scaffold Scrib (23) and the deubiquitinating complex of USP1/UAF1 (sometimes referred to as WDR48) (24-27). The main structural difference between these two phosphatases is that PHLPP1 has a long unstructured N-terminal tail that is approximately 60 kDa in size and makes up roughly 30% of the amino acid sequence. The function of this N-terminal extension (NTE) has been unclear as no studies to date have focused on the characterization of the NTE. What is known is that the NTE is not required for PHLPP1 to target specific substrates, namely Akt, PKC, and S6K. Identification of how this unstructured NTE regulates the function of PHLPP1 has been a primary focus of this dissertation.

Regulation of PHLPP Expression

While much work has gone into uncovering physiological targets of PHLPP1, there remains a gap in our understanding of how PHLPP1 itself is regulated. Multiple recent studies have focused on how PHLPP1 transcription is controlled in the context of bone development (Figure 1.3.A). Akt signaling plays a profound role in promoting chondrocyte proliferation, but must be suppressed upon terminal differentiation (28). Novel evidence suggests that Histone Deacetylase 3 (HDAC3) promotes Akt activity by suppressing transcription of the PHLPP1 gene (29). Upon stimulation with transforming growth factor beta (TGFβ), a potent activator of chondrogenesis, HDAC3 association with the PHLPP1 promoter was observed, resulting in decreased transcription of PHLPP1. Further work demonstrated that PHLPP1 expression was elevated in human patients with osteoarthritis due to a decrease in methylation of the PHLPP1 promoter, an event associated with transcriptional activation (30). Furthermore, mice lacking PHLPP1 are not as susceptible to cartilage deterioration in a surgically-induced osteoarthritis

model (31). A follow-up study utilized the PHLPP inhibitor NSC117079 in a mouse model of osteoarthritis, showing that it has a therapeutic benefit; following surgical destabilization of the meniscus, mice treated with this inhibitor were more active and had increased production of cartilage extracellular matrix components required for bone healing (32). These studies not only reveal how PHLPP1 expression is regulated during bone morphogenesis, but also suggest therapeutic potential for PHLPP inhibitors.

A number of recent studies have focused on how PHLPP expression is regulated by micro RNAs (miRNA) (Figure 1.3.B). miRNA regulates protein expression by promoting mRNA degradation or inhibiting translation of mRNA. The first reported miRNA to target PHLPP was miR-190, which targets the 3' untranslated region (UTR) of PHLPP1 (33). In this study, exposure to arsenic resulted in activation of Akt signaling and an increase in phosphorylation of Ser473. This was accounted for by an increase in miR-190 levels, resulting in down-regulation of PHLPP1 protein expression. A number of miRNAs that are deregulated in cancer have been shown to regulate both PHLPP1 and PHLPP2 expression levels. In hepatocellular carcinoma (HCC), miR-331-3p, which targets both PHLPP1 and PHLPP2, is significantly over-expressed (34). miR-3127 is also over-expressed in HCC, and can function to suppress expression of not only PHLPP1 and PHLPP2, but also Inositol Polyphosphate Phosphatase 4A (INPP4A) and Inositol Polyphosphate-5-Phosphatase J (INPP5J) (35), two enzymes involved in inositol metabolism. miR-205 has been shown to target the 3’UTR of PHLPP2 and Phosphatase and Tensin Homologue (PTEN), and is in a region of the genome that is frequently amplified in non-small cell lung cancer (NSCLC) (36). In glioma, up-regulation of miR-93 results in a marked inhibition of PHLPP2, PTEN and Forkhead Box O3 (FOXO3) expression (37). An interesting commonality between a number of these miRNAs is that they not only target PHLPP, but also PTEN, another tumor suppressor phosphatase

that suppresses PI3K/Akt signaling, further cementing the importance of Akt signaling in tumorigenesis.

Translational control of PHLPP1 expression appears to be regulated in part by the mammalian Target of Rapamycin Complex 1 (mTORC1) (Figure 1.3.C). mTORC1 is a multi-subunit complex with kinase activity that is sensitive to the natural compound, rapamycin, unlike its sister complex, mTORC2 (38). mTORC1 plays a key role in regulating translation mostly through its ability to inactivate the translational inhibitor Eukaryotic Translation Initiation Factor 4E Binding Protein 1 (4E-BP1) and activate ribosomal protein S6K. By sensing changes in nutrient and energy levels, mTORC1 is able to ensure protein synthesis is shut off during times of stress. Treatment of cells with rapamycin results in down-regulation of both PHLPP1 and PHLPP2 (39). Knock-down of key components of the mTORC1 complex, such as mTOR or Raptor, resulted in a similar outcome. As PHLPP mRNA levels and rate of degradation of PHLPP protein was unaffected by rapamycin treatment, the data suggests that PHLPP translational rates are sensitive to mTORC1 activity. Intriguingly, a recent study suggests a role in which free Raptor, which is normally associated with the mTORC1 complex, interacts and binds PHLPP2, resulting in PHLPP2 protein stabilization and reduced signaling through Akt (40). In aged obese mice, levels of free Raptor decline, resulting in a reduction of PHLPP2 protein stability and prolonged signaling through Akt (40). The authors suggest that this leads to increased *de novo* lipogenesis and formation of fatty liver. These studies propose that the mTORC1 complex has a multi-faceted role in regulating PHLPP expression.

Multiple lines of evidence suggest a role for ubiquitination in the regulation of PHLPP1 protein stability (Figure 1.3.C). After phosphorylation at a phospho-degron motif by Glycogen Synthase Kinase 3β (GSK3β), PHLPP1 is recognized by beta-Transducin Repeats-containing

Trotein (β-TrCP), a subunit of the Skp-Cullin 1-F-box protein (SCF) ubiquitin E3 ligase complex, and ubiquitinated, resulting in protein degradation (41). The interaction between PHLPP1 and β-TrCP is further enhanced by the binding of the co-chaperone protein, Suppressor of G2 Allele SKP1 (SGT1) (42). As GSK3β is phosphorylated by Akt leading to its catalytic inactivation, Akt activity acts to promote PHLPP1 protein stability by inhibiting ubiquitination, a possible mechanism to shut down Akt activity after initial stimulation. GSK3β activity is regulated by the kinase Greatwall (GWL) (43), although the mechanism of this regulation is unclear. Over-expression of GWL results in a decrease in the levels of inhibitory phosphorylation on GSK3β at Ser9 and Ser21, resulting in increased ubiquitin-mediated degradation of PHLPP1.

A number of other studies have implicated deubiquitinating enzymes in PHLPP1 regulation as well. Namely, a number of deubiquitinases, including Ubiquitin Specific Peptidase 1 (USP1) (44), USP12 (25), and USP46 (45), have been shown to interact with and deubiquitinate PHLPP1, resulting in increased protein stability. Considering that these enzymes play a role in stabilizing PHLPP1, a bona fide tumor suppressor, it is not surprising that the expression and activity of these deubiquitinases are down-regulated during tumorigenesis. A somatic mutation in the protein WD Repeat Domain 48 (WDR48), which is required to recruit USP12 to PHLPP1, occurs in colon adenocarcinoma (25). Cellular studies have shown that this mutation results in a down-regulation of PHLPP1 protein levels, and thus an increase in Akt signaling output (25). Additionally, reduced levels of USP46 are correlated with a down-regulation of PHLPP1 expression in colorectal cancer (45).

PHLPP and Disease

Maintaining balanced levels of PHLPP1 expression is key for preventing pathologies, as changes in the steady-state levels of PHLPP1 are correlated with a number of diseases. The most well characterized example of this is in cancer, as both PHLPP1 and PHLPP2 have been identified as tumor suppressors, largely attributed to PHLPP-dependent suppression of pro-survival signaling through the PI3K/Akt signaling pathway. Both PHLPP1 and PHLPP2 expression is lost in diverse cancers (46-49). Mouse models have also been used to show that the loss of PHLPP1 expression results in tumor progression. PHLPP1 knock-out mice develop prostate neoplasias, which progress to carcinomas when combined with partial loss of PTEN (50). These same knock-out mice, when crossed with an Apc (Min) colon cancer mouse model, had more aggressive and invasive tumors compared to either the PHLPP1 knock-out or Apc (Min) mice alone (51). Outside of cancer progression, loss of PHLPP1 expression may play a role in circadian rhythm disorders. The transcription of the PHLPP1 gene, originally identified as the SCN Circadian Oscillatory Protein (SCOP), oscillates in a circadian manner in the rat suprachiasmatic nucleus, a bundle of neurons that is responsible for maintaining the circadian clock (52). Although the mechanism is unclear, mice lacking PHLPP1 have deficiencies in light-induced resetting of the circadian rhythm (53). While no connections have been made yet, it would be of interest to determine if loss of PHLPP1 expression in humans is linked with any circadian rhythm disorders.

On the other end of the spectrum, a number of other diseases are characterized by up-regulation of PHLPP1 levels. First, multiple reports have shown that PHLPP1, but not PHLPP2, levels are higher in both the skeletal muscle and adipose tissue of diabetic patients compared to their healthy counterparts (54, 55). PHLPP1 selectively dephosphorylates Akt2 (56), the Akt isozyme that plays an important role in insulin-stimulated glucose uptake, in cells. Thus, one

possible mechanism for why cells become insensitive to insulin in diabetic patients is because PHLPP1 levels become elevated. Akt also plays an important role in regulating cardiac cell survival. PHLPP1 knockout mice have been reported to display a cardio-protective phenotype following cardiac stress (57). Therefore, suppressing PHLPP expression in the context of the heart would provide therapeutic benefits.

A growing body of evidence now implicates PHLPP1 in the regulation of the immune response. Several studies have reported that PHLPP1, through suppressing Akt activity, promotes maturation of regulatory T cells (Tregs) which play a role in suppressing the immune response (58-60). These studies identify that PHLPP1 is expressed at higher levels in Tregs compared to conventional T cells, and that Tregs reduce Akt phosphorylation and activity during the maturation process. Tregs from PHLPP1 knock-out mice had a reduced immunosuppressive potential, signifying a key role for PHLPP1 in the immune response. In glioma tumor samples, an increase in inflammatory cytokines (TNF-alpha, IL-17, and IL-1β) were correlated with a loss of PHLPP1 protein expression (61). This same phenotype could be replicated in cell culture using siRNA to reduce PHLPP1 levels in U-251 glioma cells. PHLPP1 expression and activity is dynamically regulated in other immune cells, such as macrophages. Leptin signaling in macrophages results in a reduction in PHLPP1 levels and an increase in Akt pSer473 after infection with *Salmonella* Typhimurium, resulting in a decreased ability for these macrophages to clear infection (62). A separate study showed that LPS stimulation of macrophages resulted in the down-regulation of PHLPP1 transcription via the loss of SP1 transcription factor activity (63). Two studies have implicated PHLPP1 in the negative regulation of the inflammatory transcription factor STAT1 (64, 65). Specifically, these studies identified that PHLPP1 directly dephosphorylates STAT1 in

macrophages followed cytokine stimulation. One of these studies is highlighted in this dissertation (Chapter 3).

Negative regulation of Akt by both PHLPP1 and PHLPP2 plays an important role in both suppressing and promoting various disease phenotypes. Furthermore, PHLPP1 signaling has now been implicated in a diverse set of diseases, indicating that maintaining PHLPP1 homeostasis in the cell is critical. This indicates the potential importance of tissue-specific expression of PHLPP1, especially in the context of drug development. For example, if a systemic PHLPP1 inhibitor was designed to treat diabetes or to promote cardiac cell survival during a myocardial infarction, would it potentially promote cellular transformation in other tissues where loss of PHLPP expression or activity is associated with cancer? This provides a challenge that needs to be addressed by understanding the different players involved in tissue-specific PHLPP signaling.

Concluding Remarks

PHLPP is a relatively recent entrant into the arena of cell signaling, yet research in the past fifteen years has secured a firm place for PHLPP as a key regulator, through diverse mechanisms, of cellular homeostasis. Its dysregulation tips the balance from survival/proliferation to apoptosis/cell arrest. No longer considered just the 'hydrophobic motif' phosphatase, the roles of PHLPP are expanding to include much broader functions such as regulating the epigenome. The coming years will likely unveil more substrates, pathways, and diseases in which PHLPP is involved. Additionally, a better understanding of how PHLPP itself is regulated will provide great insight into how its loss or over-abundance can destabilize cellular signaling. This dissertation has zoned in specifically on this central question and presents three novel areas of study to define this question. Chapter 2 reveals how a previously uncharacterized region of PHLPP1, the N-terminal

extension (NTE), regulates a PHLPP1 interactome "switch" during mitosis. The work described in this chapter also revealed that the NTE is reversibly regulated by post-translational modifications. Chapter 3 presents the identification of a previously undescribed nuclear localization signal in the PHLPP1 NTE, providing a mechanism to explain how PHLPP1 functions in the nucleus. The work described in Chapter 4 sheds light onto how PHLPP1 expression is regulated in cell culture, showing that PHLPP1 expression is down-regulated as cells reach confluency in two-dimensional cell culture due to the depletion of extracellular glutamine. Taken together, the work presented here sheds new light on PHLPP1 biology in both healthy and diseased cells.

Acknowledgements

We thank members of the Newton laboratory for helpful suggestions. The present work was supported by National Institutes of Health (GM067946) to A. C. N. A.T.G was supported in part by the UCSD Graduate Training Program in Cellular and Molecular Pharmacology through an institutional training grant from the National Institutes of General Medical Sciences (T32 GM007752).

Chapter 1, in full, is an adaptation of the material that appears in "PHLPPing through history: a decade in the life of PHLPP phosphatases", as published in *Biochemical Society Transactions* (2016) by Agnieszka T. Grzechnik and Alexandra C. Newton. The dissertation author was the primary author of these literature reviews.

FIGURES:

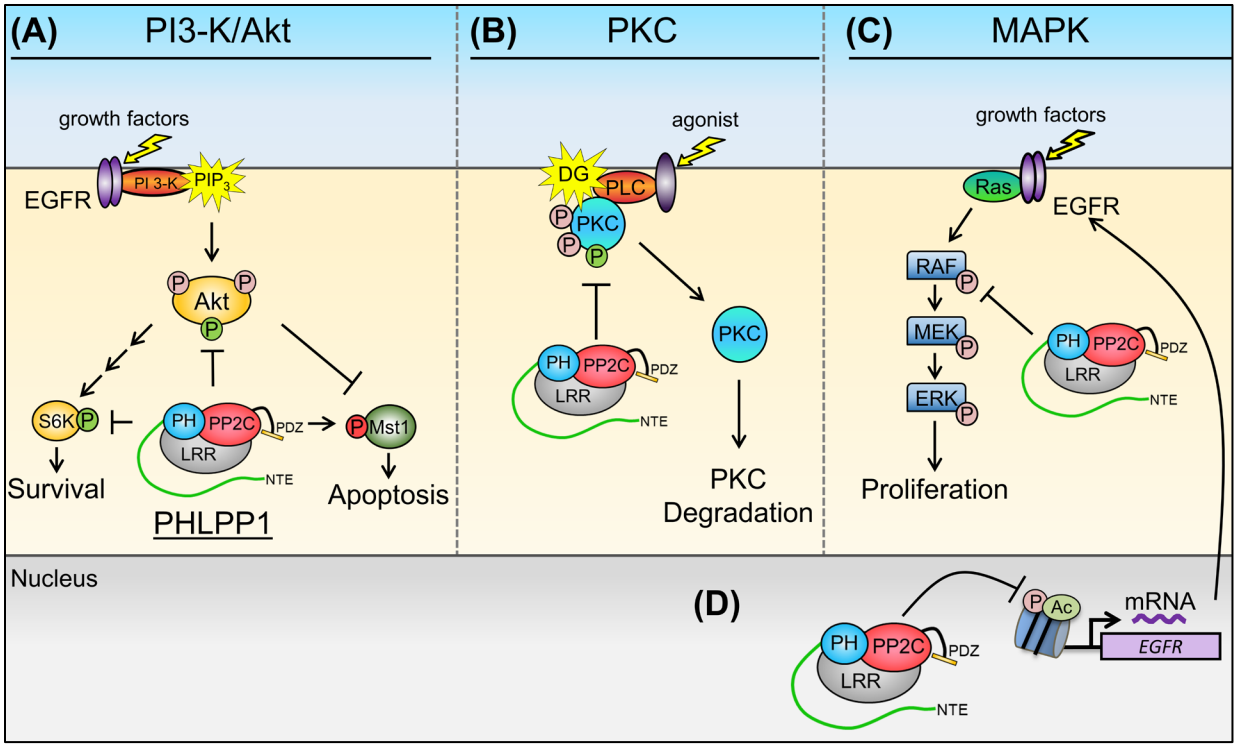

Figure 1.1: PHLPP1 signaling in the cell. PHLPP1 regulates a number of cellular pathways. **(A)** PHLPP1 regulates PI3-K/Akt signaling at various nodes. PHLPP1 dephosphorylates both Akt and S6K at their hydrophobic motifs (green circle), leading to their inactivation. PHLPP1 dephosphorylates non-AGC kinases as well, such as an inhibitory site (red circle) on the pro-apoptotic kinase, Mst1, leading to its activation. **(B)** PHLPP1 dephosphorylates PKC at its hydrophobic motif, resulting in decreased PKC stability and an indirect decrease in kinase activity. **(C)** PHLPP1 regulates Mitogen Activated Protein Kinase (MAPK) signaling. PHLPP1 dephosphorylates the kinase RAF1, providing a route for dampening MAPK proliferative signaling. **(D)** A novel nuclear role for PHLPP1 has been identified in regulating the epigenome; PHLPP1 is able to suppress histone acetylation and phosphorylation to reduce gene expression of receptor tyrosine kinases, such as EGFR. The mechanism of this regulation has yet to be determined.

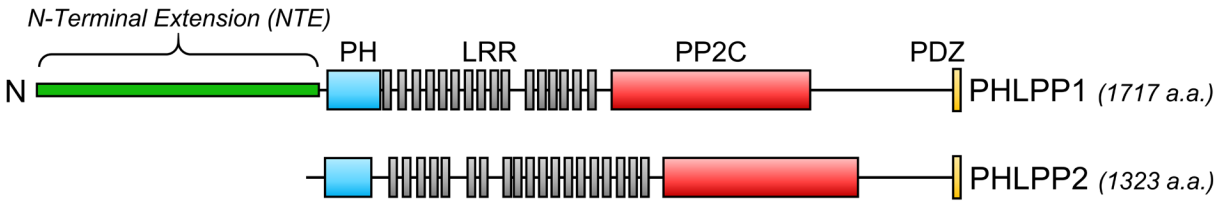

Figure 1.2: Domain structure of human PHLPP. The PHLPP family of phosphatases is composed of two isozymes, PHLPP1 and PHLPP2. Both isozymes have similar structural domains, including a Pleckstrin Homology (PH) domain required for targeting to PKC, a Leucine Rich Repeat (LRR) required for nuclear PHLPP function, a PP2C phosphatase domain, and a C-terminal extension (CTE) required for binding scaffolds such as Scribble, and a PDZ binding ligand at the extreme C-terminus that is required for targeting to Akt. PHLPP1 has a large N-terminal extension (NTE, residues 1-512) that is approximately 60 kDa in size that is not present in PHLPP2. The PP2C domain between these two isozymes is 58% homologous and both require Mg^{2+} or Mn^{2+} for catalytic activity.

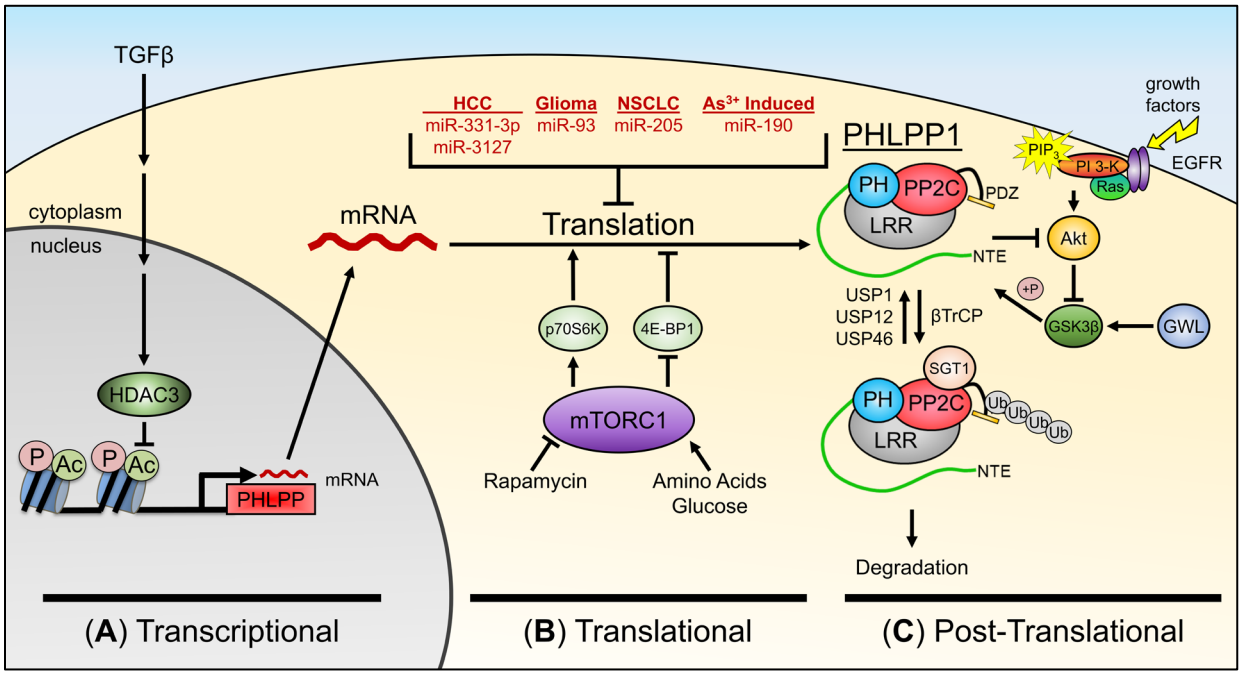

Figure 1.3: PHLPP1 regulation at the transcriptional, translational, and post-translational level. (A) PHLPP1 transcription is regulated by HDAC3 during chondrogenesis. Stimulation of chondrocytes with TGFβ results in activation of HDAC3. HDAC3 will then deacetylate the PHLPP1 promoter, resulting in decreased transcription of PHLPP1. **(B)** PHLPP1 mRNA translation is regulated by miRNA and mTORC1. A number of different miRNAs target the 3' UTR of both PHLPP1 and PHLPP2. These various miRNAs are frequently up-regulated in a number of different cancers, including hepatocellular carcinoma (HCC), glioma, and non-small cell lung cancer (NSCLC). Arsenic exposure induces miR-190, which can target the 3' UTR of PHLPP1 mRNA. The mTORC1 complex enhances PHLPP1 translation. Treatment of cells with rapamycin, which inhibits mTORC1 activity, results in decreased translation of PHLPP1 mRNA. **(C)** PHLPP1 is regulated by ubiquitination. Upon phosphorylation of a phosphor-degron motif in the PP2C domain of PHLPP by GSK3β, βTrCP-dependent ubiquitination of PHLPP1 occurs, resulting in degradation of PHLPP1 protein. Activity of the kinase Greatwall (GWL), results in increased GSKβ activity. Association of the co-chaperone, SGT1, enhances the interaction between PHLPP1 and βTrCP, resulting in greater degradation of PHLPP1. PHLPP1 can be deubiquitinated by a number of enzymes, including USP1, USP12, and USP46.

Chapter 2 – The PHLPP1 N-Terminal Extension is a Mitotic Cdk1 Substrate and Controls an Interactome Switch

ABSTRACT

PH domain Leucine-Rich Repeat Protein Phosphatase 1 (PHLPP1) is a tumor suppressor that directly dephosphorylates a wide array of substrates, most notably the pro-survival kinase Akt. However, little is known about the molecular mechanisms governing PHLPP1 itself. Here we report that PHLPP1 is dynamically regulated in a cell cycle-dependent manner, and deletion of PHLPP1 results in mitotic delays and increased rates of chromosomal segregation errors. We show that PHLPP1 is hyperphosphorylated during mitosis by Cdk1 in a functionally uncharacterized region known as the PHLPP1 N-terminal extension (NTE). A proximity-dependent biotin identification (BioID) interaction screen revealed that during mitosis, the NTE is required for the dissociation of PHLPP1 from plasma membrane scaffolds, such as Scribble. Additionally, PHLPP1 gains close proximity to the kinetochore and mitotic spindles as evidenced by increased binding of proteins such as KNL1 and TPX2. Our data are consistent with a model in which phosphorylation of PHLPP1 during mitosis regulates binding to its mitotic partners and allows accurate progression through mitosis. The finding that PHLPP1 binds mitotic proteins in a cell cycle- and phosphorylation-dependent manner may have relevance to its tumor suppressive function.

INTRODUCTION

Dynamic changes in protein phosphorylation critically regulate accurate and timely progression through the cell cycle. Phosphorylation is particularly important during mitosis to ensure that the replicated genome is evenly divided between two daughter cells. Errors in this process can result in aneuploidy, a hallmark of cancer (66). Phospho-proteomic analyses have identified over one thousand proteins whose phosphorylation increases during mitosis, with the

majority of sites displaying [S/T]-[P] motifs that are recognized by cyclin-dependent kinases (Cdk) (67, 68). In addition to activation of kinases, most notably Cdk1 bound to cyclin B, inactivation of protein phosphatases such as protein phosphatase 2A (PP2A) drives the massive increase in protein phosphorylation. However, this cellular state of heightened protein phosphorylation is short lived. Reactivation of protein phosphatases (69) and activation of the E3 ubiquitin ligase Anaphase Promoting Complex (APC/C), which degrades key mitotic proteins such as cyclin B (70-72), occur during the final stages of mitosis. Phosphorylation of mitotic substrates by the Cdk1-cyclin B complex has diverse effects, including regulating the localization (73, 74), activity (75-77), stability (78), and interactome of substrate proteins (79). Given the massive phosphorylation changes that accompany mitosis (67, 68), it is increasingly apparent that many other mitotic kinases and phosphatases orchestrate mitotic responses, and many may do so downstream of Cdk1.

The PH domain Leucine-Rich Repeat Protein Phosphatases 1 and 2 (PHLPP1 and PHLPP2) are emerging as key players opposing context-dependent signaling events (80). These two family members of the PPM 'shrub' of the phosphatome (81) were originally discovered for their role in dephosphorylating a key regulatory site on Akt, the hydrophobic motif (Ser473 on Akt1), to suppress the activity of this oncogenic kinase (10, 82). Supporting a tumor suppressive role, the *PHLPP1* gene locus is frequently deleted in cancer (47, 48, 83, 84), and genetic deletion in a mouse model promotes tumor progression in both prostate (85) and colorectal cancer (51). While the importance of PHLPP1 signaling in the context of disease has mostly been attributed to its regulation of Akt and other AGC kinases (11, 12, 86), an increasing number of substrates involved in other biological pathways are being identified. Notably, PHLPP1 suppresses inflammatory signaling by dephosphorylating the transcription factor STAT1 (64), controls receptor tyrosine kinase transcription by suppressing histone phosphorylation (14), maintains

regulatory T-cell development (58), and promotes bone morphogenesis (29, 32, 87). A role in mitosis was recently suggested in a study showing that PHLPP1 dephosphorylates and stabilizes the outer-kinetochore protein SGT1, resulting in proper kinetochore assembly (88).

PHLPP family members have low catalytic activity and their scaffolding to protein substrates is essential for effective downstream signaling. This is achieved through specific regulatory modules that are part of the same polypeptide, contrasting with most other Ser/Thr phosphatases whose regulatory modules are distinct polypeptides. In addition to a catalytic PP2C phosphatase domain, both PHLPP1 and PHLPP2 have a Pleckstrin Homology (PH) domain, multiple Leucine-Rich Repeats (LRRs), and an unstructured C-terminal extension (CTE) capped by a PDZ binding ligand (80). The main structural difference between the two family members is a unique, approximately 50 kDa N-terminal extension (NTE) on PHLPP1 which contains a bipartite arginine-rich nuclear localization signal (NLS) (64). This region has no known domain homology and is not required for targeting of shared PHLPP targets, such as Akt (10, 82), protein kinase C (PKC) (11), and ribosomal protein S6 kinase 1 (S6K1) (12). Each of these domains confers specificity required for substrate targeting. For example, Akt dephosphorylation in cells depends on an intact PDZ ligand (82), PKC dephosphorylation depends on the PH domain (11), and STAT1 binding and dephosphorylation requires the NTE (64). Additionally, the binding of PHLPP1 to the plasma membrane scaffold Scribble (Scrib) depends on determinants in the CTE distinct from the PDZ ligand, and this interaction was shown to be necessary for the dephosphorylation of Akt Ser473 in epithelial cells (23). Identification of key binding partners to the NTE and CTE have opened up the possibility that these unstructured and understudied regions of the enzyme play critical roles in regulating PHLPP1 interactions and localization.

Here we determined that the PHLPP1 NTE is a substrate of Cdk1, and that the NTE functions to switch the PHLPP1 protein-interaction network during mitosis. Specifically, we report that endogenous PHLPP1 protein undergoes a distinct and reversible electrophoretic mobility shift in mitotic cells as a result of hyperphosphorylation on the NTE. Biochemical analysis and phospho-mass spectrometry uncovered 13 previously undescribed mitotic phospho-sites within the NTE, all exhibiting a minimal Cdkl recognition motif, [S/T]-[P]. *In vitro* and cellular assays utilizing the Cdk1 inhibitor RO-3306 confirmed that the NTE is a Cdk1 substrate. A proximity-dependent biotin identification (BioID) screen revealed that the NTE regulates the interactome of PHLPP1 during mitosis, dampening PHLPP1 interactions with plasma membrane scaffolds such as Scrib and promoting interactions with the kinetochore and mitotic spindle assembly proteins. Importantly, mouse embryonic fibroblasts (MEFs) lacking PHLPP1 had increased errors in chromatin segregation and a mitotic delay phenotype, as assessed by fluorescence microscopy. Taken together, these results identify PHLPP1 as a Cdk1 substrate and a new player in the field of mitotic signaling.

RESULTS

PHLPP1 expression and phosphorylation is dynamically regulated during the cell cycle.

To determine how PHLPP1 is regulated during the cell cycle, we utilized two different cell cycle synchronization techniques. RPE1 cells were synchronized using either a double-thymidine block to enrich for G1/S cells or a thymidine/nocodazole block followed by a mitotic shake-off to isolate mitotic cells, and PHLPP1 levels were assessed (Figure 2.1.A). We observed a 3-fold increase in PHLPP1 expression after nocodazole treatment (lane 3). Additionally, a substantial electrophoretic mobility shift on PHLPP1 occurred in nocodazole-treated cells. To determine the

kinetics of this mobility shift, HEK-293A cells were treated with nocodazole for various amounts of time (Figure 2.1.B). While the upper band was detected as early as 4 hours after treatment with nocodazole (lane 3), it took > 12 hours to become predominant (lane 7-10), a result that is consistent with long-term treatment synchronizing the cell population in mitosis. Additionally, the presence of the upper band correlated with a depletion of Cdk1 pTyr15 and increase in H3 pSer10, two markers of mitosis.

To determine if the mitosis-dependent electrophoretic mobility shift of PHLPP1 resulted from phosphorylation, lysates from nocodazole-treated cells were incubated with either purified lambda phosphatase (Figure 2.1.C, lane 5) or buffer only (Figure 2.1.C, lane 4) for 30 min at 25°C. The shift observed in mitotic cells (lane 3) collapsed after 30 min of lambda phosphatase treatment (lane 5), indicating that the mobility shift resulted from phosphorylation. When asynchronous cells (lanes 1 and 2) were treated with lambda phosphatase (lane 2), a faster mobility species was also observed, demonstrating that PHLPP1 is phosphorylated under basal conditions.

We next addressed whether the phosphorylation was reversed during mitotic exit. RPE1 cells were synchronized in mitosis using a thymidine/nocodazole block, followed by a mitotic shake-off (Figure 2.1.D). Mitotic cells were collected, washed, and released into nocodazole-free media, allowing cells to resume and exit mitosis. Cyclin B1, which is degraded during mitotic exit, and Cdk1 Tyr15 phosphorylation, which occurs during mitotic exit, were analyzed to track mitotic progression. Exit from mitosis was accompanied by dephosphorylation of PHLPP1, assessed by the increase in electrophoretic mobility, with the appearance of the dephosphorylated species correlating with the increase in mitotic exit markers. Additionally, the steady-state levels of PHLPP1 decreased, with a 5-fold reduction in protein levels observed 90 min post mitotic release

(lane 4). Thus, PHLPP1 expression and phosphorylation state are dynamically regulated during the cell cycle.

Mitotic PHLPP1 phosphorylation occurs on the PHLPP1 N-Terminal Extension (NTE).

To elucidate which region of PHLPP1 is phosphorylated during mitosis, truncated PHLPP1 mutants were expressed in asynchronous and mitotic HeLa cells (Figure 2.2.A). While full-length (FL) PHLPP1 exhibited a mobility shift following nocodazole treatment, a construct lacking the N-terminal extension (ΔNTE) did not (Figure 2.2.B). Additionally, the NTE alone had a mobility shift when expressed in nocodazole-treated cells. Endogenous PHLPP2, the other PHLPP family member which lacks the NTE that is present on PHLPP1, does not shift during mitosis (Figure 2.2.B), further suggesting that the NTE mediates the mitosis-induced electrophoretic mobility shift of PHLPP1.

We utilized phospho-mass spectrometry to determine which residues in the NTE are phosphorylated during mitosis. HeLa cells expressing FLAG-tagged NTE were treated with DMSO or nocodazole, then purified and resolved on an SDS-PAGE gel (Figure 2.2.C). The faster mobility species (dash), corresponding to the unphosphorylated NTE, was excised from the DMSO-treated condition (Figure 2.2.D, lane 1), and the slower mobility species (asterisk) was excised from the nocodazole-treated condition (Figure 2.2.D, lane 2). Gel slices were digested with trypsin and analyzed by ultra-high-pressure liquid chromatography (UPLC) coupled with tandem mass spectrometry (MS/MS) to identify phosphorylated peptides (Supplemental Dataset 1). A mitotic enrichment score was calculated by dividing the total spectral counts of the nocodazole-treated sample by the DMSO-treated samples for each phosphorylated residue. This analysis revealed that 13 residues had a ≥3-fold increase in spectral counts of phosphorylated peptides in

the nocodazole-treated cells compared to the DMSO control, while two residues, Ser50 and Thr56, were phosphorylated to similar levels in both samples (Figure 2.2.E). Additionally, the residues modified were grouped in clusters rather than evenly spread out along the NTE (Figure 2.2.F). These clusters also appeared in regions of the NTE that are predicted to be intrinsically disordered (Figure 2.2.G). Intrinsic disorder prediction was completed by analysis of the PHLPP1 amino acid sequence using the IUPRED2 long disorder prediction tool using the default parameters (89). These data reveal that PHLPP1 is hyperphosphorylated at the NTE following nocodazole treatment.

The PHLPP1 NTE is a substrate of Cdk1.

Almost all of the identified phosphorylation sites in the NTE occur on serine or threonine residues followed by a proline, the motif for a proline-directed kinase such as Cdk1, the master regulator of mitosis (90). Additionally, two of the residues, Ser450 and Thr451, are part of a canonical consensus motif for Cdk1, [S/T]-[P]-[X]-[R/K], and previous studies have illustrated that Cdk1 can target a minimal sequence of [S/T]-[P] (91, 92). To determine if the PHLPP1 NTE is a Cdk1 substrate, we incubated FLAG-tagged PHLPP1 NTE, purified from asynchronous 293T cells, with recombinant Cdk1-cyclin B1 and ATP. This resulted in an electrophoretic mobility shift of the NTE as assessed by western blot (Figure 2.3.A). Rather than accumulating all upper or all lower band, we observed a number of intermediate bands, supporting the multiple sites identified by mass spectrometry. Additionally, samples resolved on a PhosTag gel displayed several bands, further suggesting multiple phosphorylated residues (Figure 2.3.B). Treatment of the FLAG-NTE with lambda phosphatase resulted in a collapse of the slower migrating species to a species

migrating faster than that of untreated PHLPP1, likely reflecting basal phosphorylation on the Ser50 and Thr56 residues identified by mass spectrometry (Figure 2.3.A, lane 1).

We next employed a pharmacological approach to determine whether Cdk1 catalyzes the phosphorylation of PHLPP1 in cells. Treatment of mitotic HeLa cells with the Cdk1 active site inhibitor RO-3306 for 30 min prior to lysis resulted in collapse of the endogenous PHLPP1 mobility shift (Figure 2.3.C, lane 4). This collapse was not observed when cells were treated with either an Aurora Kinase A/B inhibitor (ZM-447439, lane 5) or a Polo-like Kinase 1/3 inhibitor (GW843682X, lane 6). To determine whether this mobility shift could be induced in non-mitotic cells (when Cdk1 is not fully active), asynchronous cells were treated with the phosphatase inhibitor Calyculin A (lane 2) for 30 min prior to lysis in order to preserve any transient phosphorylation events. Although phosphatase inhibition resulted in a small electrophoretic mobility shift, this species of PHLPP1 migrated below that of the hyperphosphorylated PHLPP1 observed in nocodazole-treated cells. These data reveal that Cdk1 activation is necessary for the hyperphosphorylation of PHLPP1 that results in a robust mobility shift.

Nocodazole treatment induces changes to the PHLPP1 interactome.

As mitotic phosphorylation events induce changes in protein-protein interactions (93), we hypothesized that the phosphorylation of the PHLPP1 NTE could alter the PHLPP1 interactome. To determine the differences in PHLPP1 protein-protein interactions between DMSO- and nocodazole-treated cells, we performed a proximity-dependent biotin identification (BioID) screen (94). A mutated form of the *E. coli* biotin ligase BirA R118G (BirA*) (95) and a 3XFLAG tag were fused to the N-terminus of full-length (FL) or truncated (ΔNTE) PHLPP1 and stably integrated into the tetracycline-inducible Flp-In T-REx HeLa cell system (Figure 2.4.A). As a

negative control to determine background biotinylation, a cell line expressing just the BirA*-3XFLAG tag was generated. Cells were treated with tetracycline to induce expression of BirA*-3XFLAG fusion proteins and then either DMSO to obtain asynchronous cells or thymidine/nocodazole to block cells in mitosis (Figure 2.4.B). When lysates from cells expressing BirA*-3XFLAG-PHLPP1 (FL) were resolved on an SDS-PAGE gel and probed with an anti-FLAG antibody, a mobility shift of the construct was observed. Thus, fusion of BirA*-3XFLAG to PHLPP1 did not appear to prevent hyperphosphorylation of the NTE (Figure 2.4.C). After synchronization, biotin was added to cells 12 hours prior to harvest to allow for biotinylation of proteins proximal to the BirA*-3XFLAG-PHLPP1 fusion proteins. Following cell lysis, biotinylated proteins were purified using streptavidin-conjugated beads and analyzed by nano-HPLC (high-pressure liquid chromatography) coupled to mass spectrometry. The data set was analyzed using the computational tool SAINTexpress (96) to define high-confidence proximity interactions and visualized by a dot plot (Figure 2.4.D-H, Supplemental Dataset 2).

A number of previously identified PHLPP1 interacting proteins, such as Scrib (23, 97), USP1 (26, 27, 98), WDR48 (24, 25, 98), WDR20 (99), and SGT1 (42, 88), were identified in the BioID screen, indicative of the ability of this screen to identify known PHLPP1 interactors. To assess the PHLPP1 mitotic interactome, we determined which prey had ≥ 2-fold increase in nocodazole-treated cells compared to DMSO-treated cells (Figure 2.4.E). Gene ontology (GO) analysis using g:Profiler (100) revealed an enrichment of proteins found at mitotic spindles, such as TPX2, tubulin (TUBA1A, TUBA4A, TUBB4B), and kinesins (KIF23, KIF5B, KIF15). Additionally, several kinetochore proteins, namely Bub1B, Knl1, Spindly (SPDL1), and CENP-F, were identified, suggesting that PHLPP1 is in close proximity to a number of key mitotic signaling scaffolds. We also assessed which interactions were decreased by ≥ 2-fold in nocodazole-treated

compared to DMSO-treated cells (Figure 2.4.F). GO analysis identified an enrichment for prey involved in regulation of cell-cell anchoring junctions, such as Scrib, Dlg5, and cortactin (CTTN), and proteins involved in amino acid transport across the plasma membrane, such as 4F2hc (SL3A2), LAT1 (SLC7A5), and ASCT2 (SLC1A5). These data indicate that during interphase, PHLPP1 interacts with scaffolds at the plasma membrane, but mitosis disrupts these interactions, allowing PHLPP1 to switch binding partners and re-localize to key mitotic signaling complexes.

We next asked whether the NTE plays a role in this localization change, considering it is heavily modified during mitosis. To answer this question, we determined which prey displayed either a ≥ 2-fold enrichment or ≥ 2-fold depletion in nocodazole-treated cells expressing the ΔNTE construct compared to cells expressing full-length PHLPP1 (Figure 2.4.G). We observed that NTE deletion enhanced the interaction with proteins localized to the plasma membrane, such as Scrib, Dlg5, and 4F2hc (SLC3A2), and decreased the interaction with mitotic spindle proteins, such as tubulin (TUBA1A, TUBA4A, TUBB4B) and dynein (DYNC1H1). These data suggest that the NTE is critical in releasing PHLPP1 from its plasma membrane-associated interactions. Furthermore, deletion of the NTE under basal conditions resulted in enhanced pulldown of plasma membrane-associated proteins (Figure 4H), revealing that the NTE plays a general role in regulating PHLPP1 protein-protein interactions and localization outside of mitosis.

Immortalized *Phlpp1*$^{-/-}$ mouse embryonic fibroblasts exhibit increased rates of mitotic defects compared to wild-type cells.

Since the BioID data suggested that PHLPP1 could be in proximity to mitotic signaling hubs, we hypothesized that PHLPP1 may function to regulate mitosis. To initially determine if PHLPP1 activity is required to maintain mitotic fidelity, we asked if the deletion of PHLPP1

resulted in any obvious mitotic defects. We performed live-cell imaging of *Phlpp1*$^{-/-}$ (KO) and *Phlpp1*$^{+/+}$ (WT) MEFs stably expressing a monomeric red fluorescent protein (mRFP)-tagged histone H2B to visualize chromatin dynamics during mitosis. Mitotic cells were scored on four individual parameters: 1) mitotic duration from nuclear envelope breakdown (NEBD) to anaphase (Figure 2.5.A, B), 2) evidence of lagging chromosomes during anaphase (Figure 2.5.C), 3) multipolar spindle formation (Figure 2.5.D), and 4) anaphase bridge formation (Figure 2.5.E). While no significant difference was observed between WT and KO MEFs in the percentage of cells forming multipolar spindles (Figure 2.5.H; 5% ± 2% vs. 2% ± 1%, respectively) or anaphase bridges (Figure 2.5.I; 5% ± 2% vs. 2% ± 1%, respectively), lagging chromosomes were more prevalent in the KO MEFs compared to WT MEFs (Figure 2.5.G; 54% ± 2% vs. 32% ± 4%, respectively). Additionally, these lagging chromosomes can often form micronuclei, small extra-nuclear bodies containing chromatin that are a marker of genomic instability (101). DAPI staining revealed that micronuclei were observed more frequently in KO compared to WT MEFs (Figure 2.5.J; 19% ± 1% vs. 8.6% ± 0.7%, respectively). The KO MEFs exhibited more frequent defects in chromosomal alignment, as evidenced by the increased amount of time spent between NEBD and anaphase (Figure 2.4.A, B, F; 43 min ± 1 min vs. 34 min ± 1 min, respectively). Thus, cells lacking PHLPP1 exhibit subtle but measurable mitotic defects, suggesting a role for PHLPP1 in mitotic regulation. Further experimentation and analysis are required to determine whether these defects are due to the mitotic function of the PHLPP1 NTE.

DISCUSSION

Here we identify the tumor suppressor phosphatase PHLPP1 as a component of the intricate machinery that maintains accuracy during the cell cycle, with its loss causing errors in cell division

(Figure 2.6). We show that PHLPP1 is a substrate for Cdk1, the master regulator of mitosis. Studies *in vitro* and in cells reveal that Cdk1 phosphorylates PHLPP1 at multiple [S/T]-[P] sites on the NTE as cells enter mitosis and that this region of the protein determines the cellular interactome of the phosphatase. The finding that PHLPP1 is involved in cell cycle regulation unveils a new player to oppose the plethora of phosphorylation events associated with cell division.

The phosphorylation of PHLPP1 by Cdk1 as cells enter mitosis suggests that the phosphatase may be one of the mitotic targets of Cdk1, whose activity is necessary for faithful cell division. Proper and timely activation of Cdk1 is essential for the accurate completion of cell division; deletion of the gene encoding Cdk1 results in early embryonic lethality in mice (102, 103) and expression of a Cdk1 lacking inhibitory phosphorylation sites (Thr14Ala/Tyr15Ala) in adult mice results in DNA damage and eventual death (103). Furthermore, increased Cdk1 expression and activity are associated with cancer progression and poor prognosis (104-108). Complete inhibition of Cdk1 by the active site inhibitor RO-3306 arrests cells at the G2/M transition (109) while partial inhibition results in mitotic delays and errors in chromatin segregation resulting in micronuclei formation (110, 111). The finding that cells lacking PHLPP1, which we establish as a Cdk1 substrate, display mitotic delays and increased chromatin segregation errors identify the phosphatase as one of the downstream targets of Cdk1 whose phosphorylation ensures mitotic fidelity.

Cdk1 phosphorylates the relatively understudied PHLPP1 NTE. This region of the protein accounts for almost 20% of the entire peptide (residues 1-512 out of 1717) and is predicted to be intrinsically disordered and unstructured, a desirable attribute for a potential kinase suitor. Interestingly, PHLPP2 lacks this NTE and does not undergo the dramatic electrophoretic mobility shift observed for PHLPP1. Both biochemical and mass spectrometry results indicate that the NTE

is phosphorylated at multiple sites by Cdk1 during mitotic entry and that the phosphorylated species is removed during mitotic exit, either by dephosphorylation or degradation of the phospho-protein. Our data do not inform whether Cdk1 is actively discriminating which sites it phosphorylates or the stoichiometry of the phosphorylation, but given the large electrophoretic mobility shift and detection of intermediate species, many sites are modified per single molecule. Of the 13 sites identified, only one (Thr451) adheres to the optimal Cdk1 consensus sequence of [S/T]-[P]-[X]-[K/R] (91, 92). Interestingly, the phosphorylated residues are roughly clustered in two regions (residues 317-345 and 409-451), consistent with reports that many Cdk1 substrates are phosphorylated multiple times in clusters within regions predicted to be intrinsically disordered (112). Furthermore, these clusters are reported to occur in large numbers at rapidly evolving regions rather than on conserved residues (112), suggesting that the degree of phosphorylation of a substrate could be more significant than the specific sites being phosphorylated. These data identify the unique NTE of PHLPP1 as a phosphorylation switch that coordinates with the cell cycle.

BioID analysis identified large changes in the interactome of PHLPP1 through its NTE and, through changes observed upon nocodazole treatment, the phosphorylation state of the NTE. For this analysis, we created stable cell lines encoding only one copy of BirA*-FLAG-tagged PHLPP1 (or a construct lacking the NTE). Full-length PHLPP1 associated primarily with proteins that are enriched in plasma membrane-associated functions, such as amino acid transport and regulation of cell-cell anchoring junctions. Interestingly, several of the identified partners are known Cdk1 substrates, including Filamin A (FLNA) (113), Plectin (PLEC) (114), and Cortactin (CTTN) (115). It is of note that several known PHLPP1 binding partners, including Scrib, USP1, WDR48, WDR20 and SGT1, were identified as hits in this screen. Deletion of the NTE enhanced

the interaction with a large number of proteins, suggesting that the NTE functions to preclude binding of interaction partners. This includes Scrib as well as WDR48 (25), another established target that interacts with the CTE of PHLPP1. These data suggest that the NTE functions to reversibly shield the CTE and other binding determinants from potential binding partners. Conversely, deletion of the NTE abolished the interaction with another set of proteins, notably mitotic spindle proteins such as TUBA1A. Thus, the NTE controls the PHLPP1 interactome.

The Cdk1-mediated phosphorylation of PHLPP1 during mitosis may provide a mechanism to control the reversible shielding of binding determinants on PHLPP1. Consistent with this, BioID revealed that association with Scrib and WDR48 was reduced in cells expressing full-length BirA*-FLAG-PHLPP1 during mitosis (where a phosphorylated NTE is present) compared to non-mitotic cells (unphosphorylated NTE). Furthermore, pull down of Scrib and WDR48 during mitosis was restored if the truncated form of PHLPP1 (ΔNTE) was expressed. Thus, the reversible regulation of binding partners mediated by phosphorylation of the NTE may be an important regulatory mechanism that defines PHLPP1 signaling.

Our finding that PHLPP1 KO MEFs exhibit mitotic delays and have increased mitotic errors, resulting in micronuclei formation compared to WT MEFs suggests that PHLPP1 plays a role in maintaining mitotic fidelity. Whether these defects are attributed to the inability for PHLPP1 to localize and function properly via the NTE is an open question. A recent study reported that knock-down of PHLPP1 in HeLa cells results in an increased rate of abnormal spindle formation and centrosomal defects (88), supporting the possibility that loss of PHLPP1 directly affects centrosomal maturation and spindle formation. Our BioID screen identified several targets that are in a complex with the mitotic kinase Aurora A, a known regulator of mitotic spindle maturation. These proteins included TPX2, Ch-TOG/XMAP215 (CKAP5), KIF11, and HURP

(DLGAP5) (116). Importantly, their interaction with PHLPP1 are apparently enhanced in nocodazole-treated cells compared to untreated cells. Whether PHLPP1 regulates Aurora A kinase activity to maintain mitotic fidelity is a mechanism that has yet to be explored.

Another mechanism that could explain the mitotic defect phenotype observed in the PHLPP1 KO MEFs is through PHLPP1-dependent regulation of Akt activity. Several studies have shown that Akt is active during mitosis and that activation of Akt can override the G2/M checkpoint, even in the presence of DNA damage (117-119). Furthermore, Akt inhibition can result in abnormal spindle formation (120). The release of PHLPP1 from the Scrib scaffold during mitosis could provide a potential mechanism for how Akt activity is increased during mitosis. Tethering of PHLPP1 to Scrib allows better access to Akt (23), so its release from the scaffold would be expected to enhance Akt activity during mitosis. Taken together, our data are consistent with a model in which Cdk1 phosphorylates the NTE of PHLPP1, inducing a conformational change that releases PHLPP1 from plasma membrane-bound substrates and unmasks determinants that promote binding to centrosomal proteins.

The identification of PHLPP1 as a novel mitotic phosphatase unveils novel insight into how PHLPP1 functions as a tumor suppressor as errors in mitosis can result in aneuploidy, a hallmark of cancer. Thus, in addition to its previously characterized functions of suppressing signaling pathways, it plays a role in the fundamental process of cell division. Furthermore, the identification of the unstructured NTE as a key regulator of the PHLPP1 interactome suggests that allosteric modulators have potential to control deregulated PHLPP1 signaling in disease. Our findings provide a new lens to view PHLPP1 function during cancer.

MATERIALS AND METHODS

Materials and Antibodies.

The pharmacological reagents used in this study are as listed: Biotin (BB0078, BioBasic), Calyculin A (9902, Cell Signaling), GW843682X (sc-203202, Santa Cruz Biotechnology), RO-3306 (270-463, Enzo Life Sciences), Tetracycline (TET701, BioBasic), ZM-447439 (sc-200696, Santa Cruz Biotechnology). The pCDNA3-HA-tagged PHLPP1 construct was described previously (121). The pCDNA3-HA-tagged PHLPP1 N-terminal Extension (NTE) construct was described previously (64). The pCDNA3-HA-tagged PHLPP1 ΔNTE construct was described previously (10). The PHLPP1 NTE was subcloned into the pCMV-3XFLAG vector (E4401, Sigma Aldrich). Full-length PHLPP1 and the PHLPP1 NTE were subcloned via Gateway cloning (Thermo Fisher Scientific) into pDEST 5' BirA*-FLAG pcDNA5 FRT TO (122). All DNA plasmid transfections were done using Effectene (301425, Qiagen), following the manufacturer's instructions. Antibodies used in this study are as listed: Cdk1 (cdc2) total (77055, Cell Signaling), Cdk1 (cdc2) pY15 (9111, Cell Signaling), Cyclin B1 (4138, Cell Signaling), FLAG M2 (F3165, Sigma Aldrich), H3 total (39163, Active Motif), H3 pS10 (39253, Active Motif), HA clone 3F10 (11867423001, Roche), Hsp90 (610418, BD Transductions), PHLPP1 (22789-1-AP, Proteintech), PHLPP2 (A300-661A, Bethyl Laboratories), Tubulin (T6074, Sigma-Aldrich), Vinculin (13901, Cell Signaling).

Cell Culture.

MEFs from WT or *Phlpp1*$^{-/-}$ mice stably expressing shp53 and GFP were a kind gift from the group of Dr. Lloyd Trotman (CSHL) and have been previously described (85). MEFs, HeLa (ATCC), HEK-293T, and HEK-293A (a kind gift from the lab of Dr. Kun-Liang Guan, UCSD)

cells were grown in Dulbecco's modified Eagle medium (DMEM, 10-013-CV, Corning), and RPE1 cells (a kind gift from the lab of Dr. Karen Oegema, UCSD) were grown in DMEM/Hams F-12 50/50 mix (10-092-CV, Corning). All cell lines were supplemented with 10% fetal bovine serum (S11150, Atlanta Biologicals) and 1% penicillin/streptomycin (15140-122, Gibco), and cultured at 37°C in 5% (vol/vol) CO_2. Cells showed no evidence of *Mycoplasma* contamination using a PCR-based protocol (123) and showed no evidence of contamination.

Cell Cycle Synchronization.

To block cells in G1/S, a double-thymidine block was used. Thymidine (T9250, Sigma Aldrich) was added to cells to a final concentration of 2 mM for 24 h. Thymidine-containing media was then removed, and cells were washed four times with PBS and incubated with fresh media for 8 h, after which thymidine was added to cells to a final concentration of 2 mM for 16 h, after which cells were lysed. To block cells in mitosis, a thymidine/nocodazole block was used. Following a single thymidine block, cells were washed and incubated in fresh media for 3 h, followed by the addition of nocodazole (2190, Cell Signaling) to a final concentration of 50 ng/mL (RPE1 cells) or 100 ng/mL (HEK-293A, HeLa cells). After 16 h, mitotic cells were harvested by a mitotic shake-off. For mitotic release experiments, mitotic cells were pooled by mitotic shake-off, centrifuged at 150 x *g* for 3 min, and then resuspended in 10 mL PBS. This step was repeated three times to ensure removal of nocodazole-containing media. Cells were then resuspended in fresh growth media, re-plated, and lysed at various time points.

Cell Lysis and Western Blot.

Cells were lysed in buffer containing 20 mM Tris (pH 7.5), 150 mM NaCl, 1 mM EDTA, 1 mM EGTA, 1% Triton X-100, 2.5 mM sodium pyrophosphate, 1 mM Na_3VO_4, 1 mM DTT, 1 mM PMSF, 1 µM microcystin, 20 µM benzamidine, and 40 µg/mL leupeptin and sonicated briefly. Following a 10 min incubation at 4°C, lysates were centrifuged, and soluble fractions were separated by SDS-PAGE gel or PhosTag gels containing 100 µM PhosTag reagent (a kind gift from the lab of Dr. Dario Alessi, University of Dundee) and 100 µM $MnCl_2$, followed by transfer to PVDF membranes (BioRad). Membranes were blocked with 5% milk for 1 h at room temperature and analyzed by immunoblotting with specific antibodies. Detection and quantification of western blots was conducted by chemiluminescence on a FluorChem Q imaging system (ProteinSimple).

Lambda Phosphatase Assay.

Cells were lysed in buffer containing 20 mM Tris (pH 7.5), 150 mM NaCl, 1% Triton X-100, 1 mM DTT, 1 mM PMSF, 20 µM benzamidine, and 40 µg/mL leupeptin. Following a 10 min incubation at 4°C, lysates were centrifuged, and soluble fractions were incubated with 1X NEBuffer for Protein MetalloPhosphatases (PMP), 1 mM $MnCl_2$, and either 1 µL (400 units) lambda phosphatase (P0753, NEB) or 1 µL NEBuffer for PMP. Samples were incubated at room temperature for 30 min, after which reactions were terminated by the addition of protein sample buffer containing 250 mM Tris HCl, 8% (w/v) SDS, 40% (v/v) glycerol, 80 µg/mL bromophenol blue, and 2.86 M β-mercaptoethanol.

FLAG-PHLPP1 NTE Purification for Phospho-Mass Spectrometry.

pCMV-3XFLAG-PHLPP1-NTE was transfected into HeLa cells using Effectene. Media was replaced 24 h later with fresh media containing either 100 ng/mL nocodazole or DMSO for 16 h, after which cells were lysed in a buffer containing 20 mM Tris (pH 7.5), 150 mM NaCl, 1 mM EDTA, 1 mM EGTA, 1% Triton X 100, 2.5 mM sodium pyrophosphate, 1 mM Na_3VO_4, 1 mM DTT, 1 mM PMSF, 1 mM microcystin, 20 mM benzamidine, and 40 mg/ml leupeptin. The detergent-solubilized cell lysates were incubated with anti-FLAG M2 affinity gel (30 ml per plate, Sigma-Aldrich, A2220) for 1 h at 4˚C, washed four times in lysis buffer, and then eluted using protein sample buffer. Eluted samples were analyzed by western blot to determine the presence of the FLAG epitope. The remainder of the samples was separated on an 8% SDS-PAGE gel. Following staining with Coomassie Blue, relevant bands were excised from the gel and processed further for phospho-mass spectrometry.

Phospho-mass Spectrometry of PHLPP1 NTE.

For in gel digest, colloidal Coomassie gel slices were washed three times with 100 mM ammonium bicarbonate in 5-15% acetonitrile (ACN) for 15 min. The gel pieces were dried in a SpeedVac, and subsequently reduced by mixing with 10 mM DTT in 100 mM ammonium bicarbonate at 56°C for 30 min. Gel pieces were dehydrated by incubation with 55 mM iodoacetamide in 100 mM ammonium bicarbonate, followed by increasing concentrations of acetonitrile:100 mM ammonium bicarbonate (50%, 75%, 95%). For digestion, samples were incubated with trypsin (0.01 µg/µl) in 100 mM ammonium bicarbonate at 37°C overnight. Peptides were extracted twice by addition of 50 µL 0.2% formic acid and 65% ACN and vortexed at room temperature for 30 min. The supernatant was dried in a SpeedVac, after which a total of 50 µL

50% ACN-0.2% formic acid was added to the sample, followed by a 30 min vortex at room temperature.

Trypsin-digested peptides were subsequently analyzed by ultra-high-pressure liquid chromatography (UPLC) coupled with tandem mass spectroscopy (LC-MS/MS) using nano-spray ionization. The nanospray ionization experiments were performed using a TripleTOF 5600 hybrid mass spectrometer (ABSCIEX) interfaced with nano-scale reversed-phase UPLC (Waters corporation nano ACQUITY) using a 20 cm-75 micron ID glass capillary packed with 2.5 µm C18 (130) CSH™ beads (Waters corporation). Peptides were eluted from the C18 column into the mass spectrometer using a linear gradient (5%–80%) of ACN at a flow rate of 250 µl/min for 1 h. The buffers used to create the ACN gradient were: Buffer A (98% H_2O, 2% ACN, 0.1% formic acid, and 0.005% TFA) and Buffer B (100% ACN, 0.1% formic acid, and 0.005% TFA. MS/MS data were acquired in a data-dependent manner in which the MS1 data was acquired for 250 ms at m/z of 400 to 1250 Da and the MS/MS data was acquired from m/z of 50 to 2,000 Da. The Independent data acquisition (IDA) parameters were as follows; MS1-TOF acquisition time of 250 ms, followed by 50 MS2 events of 48 ms acquisition time for each event. The threshold to trigger MS2 event was set to 150 counts when the ion had the charge state +2, +3 and +4. The ion exclusion time was set to 4 s.

The collected data were analyzed using Protein Pilot 5.0 (ABSCIEX) for peptide identifications. MS/MS spectra were searched against only human PHLPP1 (UniProtKB Accession - O60346 (PHLP1_HUMAN)). Database parameters were set to allow 1 missed cleavage site per peptide with a mass tolerance of ± 10 ppm, a maximum charge of 4+, and a minimum allowed peptide length of 6 amino acids. The following variable modifications were selected for: acetylation, amidation, carbamidomethylation, carboxylation, deamidation,

dehydration, demethylation, formylation, formylation, oxidation, phosphorylation, and sodium adducts. Search parameters were set based on all possible PTM peptides generated for this specific protein. To determine mitotic enrichment, the number of peptides identified that include the phosphorylated residue were counted (total spectral counts). The following formula was used to calculate the mitotic enrichment: [Spectral Counts$_{+Nocodazole}$] / (1 + [Spectral Counts$_{+DMSO}$]). Any phosphorylated residue with an enrichment score of ≥3 was denoted as a mitotic phosphorylation. Data analysis and scoring parameters can be found in Supplemental Dataset 1.

Intrinsic Disorder Prediction.

To predict regions of intrinsic disorder in the PHLPP1 amino acid sequence, IUPred2A prediction software was used (https://iupred2a.elte.hu/) (89). The full length PHLPP1 amino acid sequence was queried using the IUPred2 long disorder setting.

***In vitro* Cdk1 Kinase Assay.**

pCMV-3XFLAG-PHLPP1-NTE was transfected into HEK-293T cells using Effectene. Cells were collected 72 h post-transfection and lysed in a buffer containing 20 mM Tris (pH 7.5), 150 mM NaCl, 1 mM EDTA, 1 mM EGTA, 1% Triton X 100, 2.5 mM sodium pyrophosphate, 1 mM Na_3VO_4, 1 mM DTT, 1 mM PMSF, 1 mM microcystin, 20 mM benzamidine, and 40 mg/ml leupeptin. The detergent-solubilized cell lysates were incubated with anti-FLAG M2 affinity gel (30 ml per plate, Sigma-Aldrich, A2220) for 1 h at 4˚C and washed four times in lysis buffer. FLAG-tagged NTE was eluted from the beads for 1 h at 4˚C in a buffer containing 0. 5mg/mL 3XFLAG Peptide (F4799, Sigma), 50 mM HEPES (pH 7.4), 100 mM NaCl, 1 mM DTT, 0.01% Igepal, and 10% glycerol. Samples were centrifuged, and the eluate was transferred to new tube.

Protein concentration and purity was measured by Bradford assay (#5000006, BioRad) and SDS/PAGE gel. Each reaction (50 µL total volume) contained 60 ng purified FLAG-NTE, 0.3 units recombinant human Cdk1-cyclin B1 (14-450, EMD Millipore), and 1 mM ATP in a buffer containing 50 mM Tris-HCl (pH 7.5), 10 mM $MgCl_2$, 0.1 mM EDTA, 2 mM DTT, and 0.01% Brij 35 (NEBuffer for Protein Kinases, B6022, NEB). Samples were incubated at 30˚C for various time points, and reactions were terminated by the addition of protein sample buffer, followed by western blot analysis.

BioID - Cell Line Generation and Cell Cycle Synchronization.

BirA*-FLAG constructs were generated via Gateway cloning (Thermo Fisher Scientific) into pDEST 5' BirA*-FLAG pcDNA5 FRT TO and used to generate stable cell lines in HeLa Flp-In T-REx cell pools as in (122). To obtain a mitotic population, cells were plated on a 150 mm plate and treated with thymidine (2 mM final concentration) and tetracycline (1 µg/mL final concentration) to induce expression of BirA*-tagged proteins. After 24 h, cells were washed twice with PBS and incubated in cell culture media containing tetracycline (1 µg/mL final concentration). After 3 h, nocodazole (100 ng/µL final concentration) was added to the cells. After 4 h, biotin was added to the cells at a final concentration of 50 µM. Cells were harvested 12 h later. For asynchronous cells, the same treatment protocol was used, but the addition of thymidine and nocodazole was omitted.

BioID - Streptavidin Affinity Purification and Data Acquisition.

Cell pellets were resuspended in a 1:4 ratio of pellet weight to radio-immunoprecipitation assay (RIPA) buffer [50 mM Tris-HCL (pH 7.5), 150 mM NaCl, 1% NP-40, 1 mM EGTA, 4.5

mM $MgCl_2$ and 0.4% SDS), supplemented with benzonase (250 U/ml, E1014, Sigma Aldrich) and 1X Protease Inhibitor Cocktail (P8340, Sigma Aldrich)]. Cells were lysed by one freeze-thaw cycle, then gently agitated on a nutator at 4°C for 30 min, followed by centrifugation at 16,000 x *g* for 20 min at 4°C. The supernatant was transferred to 1.5 ml microcentrifuge tubes, and 25 µl of 60% streptavidin-sepharose bead slurry (17-5113-01, GE Healthcare) was added. Following overnight incubation at 4°C with rocking, beads were washed with 2% SDS buffer (2% SDS, 50 mM Tris pH 7.5), twice with RIPA buffer, and three times with 50 mM ammonium bicarbonate pH 8.0 (ABC). After removal of the last wash, beads were resuspended in 50 mM ABC (100 µl) with 1 µg of trypsin (T6567, Sigma-Aldrich) and rocked at 37°C for 4 h. Then, an additional 1 µg of trypsin (in 2 µl of 50 mM ABC) was added to each sample, and samples were incubated at 37°C with rocking overnight. Beads were centrifuged at 500 x *g* for 1 min, and the supernatant (pooled peptides) was transferred to a new tube. Beads were rinsed with MS-grade H_2O (100 µl), and the rinse was combined with the pooled peptide sample. 10% formic acid was added to the supernatant to a final concentration of 2%. The pooled supernatant was centrifuged at 16,000 x *g* for 5 min to pellet remaining beads. 230 µl of the pooled supernatant was transferred to a new 1.5 ml microcentrifuge tube, and samples were dried using a vacuum concentrator. Tryptic peptides were resuspended in 10 µl of 5% formic acid, and 2.5 µl was used for each analysis.

Peptides were analyzed by nano-HPLC (high-pressure liquid chromatography) coupled to MS. Nano-spray emitters were generated from fused silica capillary tubing (100 µm internal diameter, 365 µm outer diameter) using a laser puller (Sutter Instrument Co., model P-2000, heat = 280, FIL = 0, VEL = 18, DEL = 2000). Nano-spray emitters were packed with C18 reversed-phase material (Reprosil-Pur 120 C18-AQ, 3µm) in methanol using a pressure injection cell. 5 µl of sample (2.5 µl of each sample with 3.5µl of 5% formic acid) was directly loaded at 800 nl/min

for 20 min onto a 100 µm x 15cm nano-spray emitter. Peptides were eluted from the column with an acetonitrile gradient generated by an Eksigent ekspert™ nanoLC 425, and analyzed on a TripleTOF™6600 instrument (AB SCIEX, Concord, Ontario, Canada). The gradient was delivered at 400 nl/min from 2% acetonitrile with 0.1% formic acid to 35% acetonitrile with 0.1% formic acid using a linear gradient of 90 min. This was followed by a 15 min wash with 80% acetonitrile with 0.1% formic acid and equilibration for another 15 min to 2% acetonitrile with 0.1% formic acid, resulting in a total of 120 min for the DDA (data-dependent acquisition) protocol. The first MS1 scan had an accumulation time of 250 ms within a mass range of 400-1800 Da. This was followed by 10 MS/MS scans of the top 10 peptides identified in the first DDA scan, with an accumulation time of 100 ms for each MS/MS scan. Each candidate ion was required to have a charge state from 2-5 and a minimum threshold of 300 counts per second, isolated using a window of 50 mDa. Previously analyzed candidate ions were dynamically excluded for 7 seconds.

BioID - MS Data Analysis.

Mass spectrometry data generated were stored, searched, and analyzed using ProHits laboratory information management system (LIMS) platform (124). Within ProHits, WIFF files were converted to an MGF format using the WIFF2MGF converter and to a mzML format using ProteoWizard (V3.0.10702) and the AB SCIEX MS Data Converter (V1.3 beta). The DDA data was then searched using Mascot (V2.3.02) (125) and Comet (V2016.01 rev.2) (126). The spectra were searched with the human and adenovirus sequences in the RefSeq database (version 57, January 30th, 2013) acquired from NCBI, supplemented with "common contaminants" from the Max Planck Institute (http://maxquant.org/contaminants.zip) and the Global Proteome Machine (GPM; ftp://ftp.thegpm.org/fasta/cRAP/crap.fasta), forward and reverse sequences (labeled

"gi|9999" or "DECOY"), sequence tags (BirA, GST26, mCherry and GFP), and streptavidin, for a total of 72,481 entries. Database parameters were set to search for tryptic cleavages, allowing up to 2 missed cleavages sites per peptide with a mass tolerance of 35ppm for precursors with charges of 2+ to 4+ and a tolerance of 0.15 amu for fragment ions. Variable modifications were selected for deamidated asparagine and glutamine, and oxidized methionine. Results from each search engine were analyzed through TPP (the Trans-Proteomic Pipeline, v.4.7 POLAR VORTEX rev 1) via the iProphet pipeline (127). Data analysis can be found in Supplemental Dataset 2.

BioID - SAINT Analysis.

SAINTexpress (version 3.6.1) was used as a statistical tool to calculate the probability of potential protein-protein interactions from background contaminants using default parameters (96). SAINT analysis was performed using two biological replicates per bait for DDA. Four negative control experiments were used for the SAINT analysis: 2 biological replicates each of empty-3xFLAG and empty-BirA*FLAG stable cell lines, treated with DMSO. Controls were not compressed, and two unique peptide ions and a minimum iProphet probability of 0.99 were required for protein identification. SAINT probabilities were calculated independently for each sample, averaged (AvgP) across biological replicates, and reported as the final SAINT score. Only SAINT scores with a FDR ≤ 1% were considered high-confidence protein interactions. Data was visualized using ProHitz-viz (128). Data analysis can be found in Supplemental Dataset 2. The BioID data has been deposited as a complete submission to the MassIVE repository (https://massive.ucsd.edu/ProteoSAFe/static/massive.jsp) and assigned the accession number MSV000085628. The ProteomeXchange accession is PXD020003. The dataset is currently available for reviewers at ftp://MSV000085628@massive.ucsd.edu. Please login with username

MSV000085628_reviewer; password: PHLPP1. The dataset will be made public upon acceptance of the manuscript.

Time-lapse Imaging of H2B-mRFP Expressing MEFs.

WT or *Phlpp1*$^{-/-}$ KO MEFs stably expressing H2B-mRFP were generated using lentivirus. Briefly, HEK-293T cells were transfected with H2B-mRFP cloned into the pCDH-EF1 vector (a kind gift from the lab of Dr. Karen Oegema, UCSD), as described in (129), and the packaging plasmids psPAX2 (12260, Addgene) and pMD2.G (12259, Addgene), using Fugene 6 (E2691, Promega). 48 h after transfection, virus-containing culture was added to WT and KO MEFs along with 8 μg/mL polybrene. FACS sorting of RFP-expressing cells was performed to isolate single clones to generate clonal lines. One day prior to imaging, cells were plated in 8 well μ-slides (80826, Ibidi). Time-lapse imaging was performed on a deconvolution microscope (DeltaVision Elite; Applied Precision) equipped with a charge-coupled device camera (pco.edge 5.5 sCMOS; PCO) and a 60x 1.42NA PlanApo N objective (Olympus). 5x5 μm z-stacks without binning were acquired at 2 min 30 s intervals over a 14 h period using an environmental control chamber set to 37°C in 5% (vol/vol) CO_2. For mRFP-tagged H2B, 5% illumination intensity and 50 ms exposure was used. Images were analyzed using ImageJ (NIH) and scored on four separate parameters: 1) time (min) from nuclear envelope breakdown (NEBD) to anaphase, 2) percent of mitotic cells exhibiting chromatin segregation errors, 3) percent of mitotic cells exhibiting multipolar spindle formation, and 4) percent of mitotic cells that formed an anaphase bridge. For both the WT and KO MEFs, three clonal lines were imaged and analyzed separately, and the results from each analysis were combined to calculate an average and standard error of the mean (SEM). Statistical significance was determined using a Student's t-test.

Micronuclei Quantification.

WT and *Phlpp1*$^{-/-}$ KO MEFs were plated on glass coverslips in a 6-well plate. Media was removed 24 h after plating, and cells were washed with PBS, then stained and fixed with DAPI (10236276001, Roche) diluted in 100% methanol (1 μg/mL final concentration) for 15 min at 37°C. Cover slips with methanol-fixed cells were washed with PBS and images acquired on a Zeiss Axiovert 200M microscope (Carl Zeiss Microimaging Inc) using an iXon Ultra 888 EMCCD camera (ANDOR) controlled by MetaFluor software (Molecular Devices). Imaging analysis was performed on ImageJ software (NIH). For each slide, multiple fields of view were quantified. The number of cells with micronuclei were divided by the total number of cells counted, generating the percent of cells with micronuclei. Data over three separate experiments were averaged and SEM calculated. Statistical significance was determined using a Student's t-test.

ACKNOWLEDGMENTS

We thank members of the Newton and Dixon laboratories for helpful discussion. We kindly thank Sourav Banerjee (UCSD) and Jack Dixon (UCSD) for performing FACS cell sorting. We kindly thank Dr. Lloyd Trotman's lab (CSHL) for the WT and *Phlpp1*$^{-/-}$ MEFs. We kindly thank Dr. Kun Liang Guan's lab (UCSD*)* for the HEK-293A cells. We kindly thank Dr. Karen Oegema's lab (UCSD) for the RPE1 cells and the pCDH-EF1 vector. We kindly thank Dr. Dario Alessi's lab (University of Dundee) for the PhosTag reagent.

This work was supported by NIH R35 GM122523 (A.C.N.), NIH GM067946 (A.C.N.), NIH P01DK054441 (A.C.N.), NIH R01 GM074215 (A.D.) and the Canadian Institutes of Health Research (CIHR FDN 144301 to A.C.G.). BioID experiments were performed at the Network Biology Collaborative Centre at the Lunenfeld-Tanenbaum Research Institute, a facility supported

by Canada Foundation for Innovation funding, by the Ontarian Government and by Genome Canada and Ontario Genomics (OGI-139). A.T.G. was supported in part by the University of California, San Diego Graduate Training Grant in Cellular and Molecular Pharmacology through the National Institutes of Health Institutional Training Grant T32 GM007752 from the NIGMS. A.C.G. is the Canada Research Chair (Tier 1) in Functional Proteomics.

Chapter 2, in full, has been submitted for publication under the title "The PHLPP1 N-Terminal Extension is a Mitotic Cdk1 Substrate and Controls an Interactome Switch", as published by Agnieszka T. Kawashima, Cassandra Wong, Charles C. King, Pablo Lara-Gonzalez, Arshad Desai, Anne-Claude Gingras, and Alexandra C. Newton. The dissertation author was the primary investigator and author of the material.

Author contributions are as stated: A.T.K., C.W., and C.C.K. performed the experiments. C.W. designed and performed the BioID screen under the supervision of A.C.G. C.C.K. performed the phospho-mass spectrometry. A.T.K. performed the remaining experiments and generated the figures. P.L. and A.D. provided assistance and equipment for time-lapse fluorescence microscopy. A.T.K and A.C.N. wrote the manuscript, and all authors edited the manuscript. A.T.K. and A.C.N. conceived the project.

FIGURES

Figure 2.1: PHLPP1 expression and phosphorylation are cell cycle dependent. (A) Western blot of RPE1 cells treated with either DMSO (asynchronous), double-thymidine block (G1/S), or thymidine/nocodazole block (M). Graph represents the quantification of four independent experiments. Values expressed as the mean relative (rel.) units ± SEM of the ratio of total PHLPP1 to loading control (Hsp90) normalized to +DMSO control. *p<0.05, **p<0.005 (Student's t-test). Lanes in blot irrelevant to this experiment were removed (indicated by dashed line) **(B)** Western blot of HEK-293A cells treated with nocodazole (100 ng/mL) for indicated amounts of time in hours (h). **(C)** Lysates from asynchronous (lane 1, 2) or nocodazole-treated (lane 3, 4, 5) HEK-293A cells were incubated at 25°C with or without ʎ phosphatase (ppase) for indicated amounts of time (min, minutes). All blots are probed against endogenous proteins. **(D)** Western blot of mitotic RPE1 cells that were collected, washed, and released from a thymidine/nocodazole block. Graphs represent the quantification of three independent experiments. Values expressed as the mean relative (rel.) units ± SEM of the ratio of total PHLPP1 to loading control (vinculin) normalized to the t=0 min. *p<0.05, **p<0.005 (One-way ANOVA). Numbers below each blot refer to the lane number. Asterisk refers to PHLPP1 electrophoretic mobility shift compared to faster mobility species (dash).

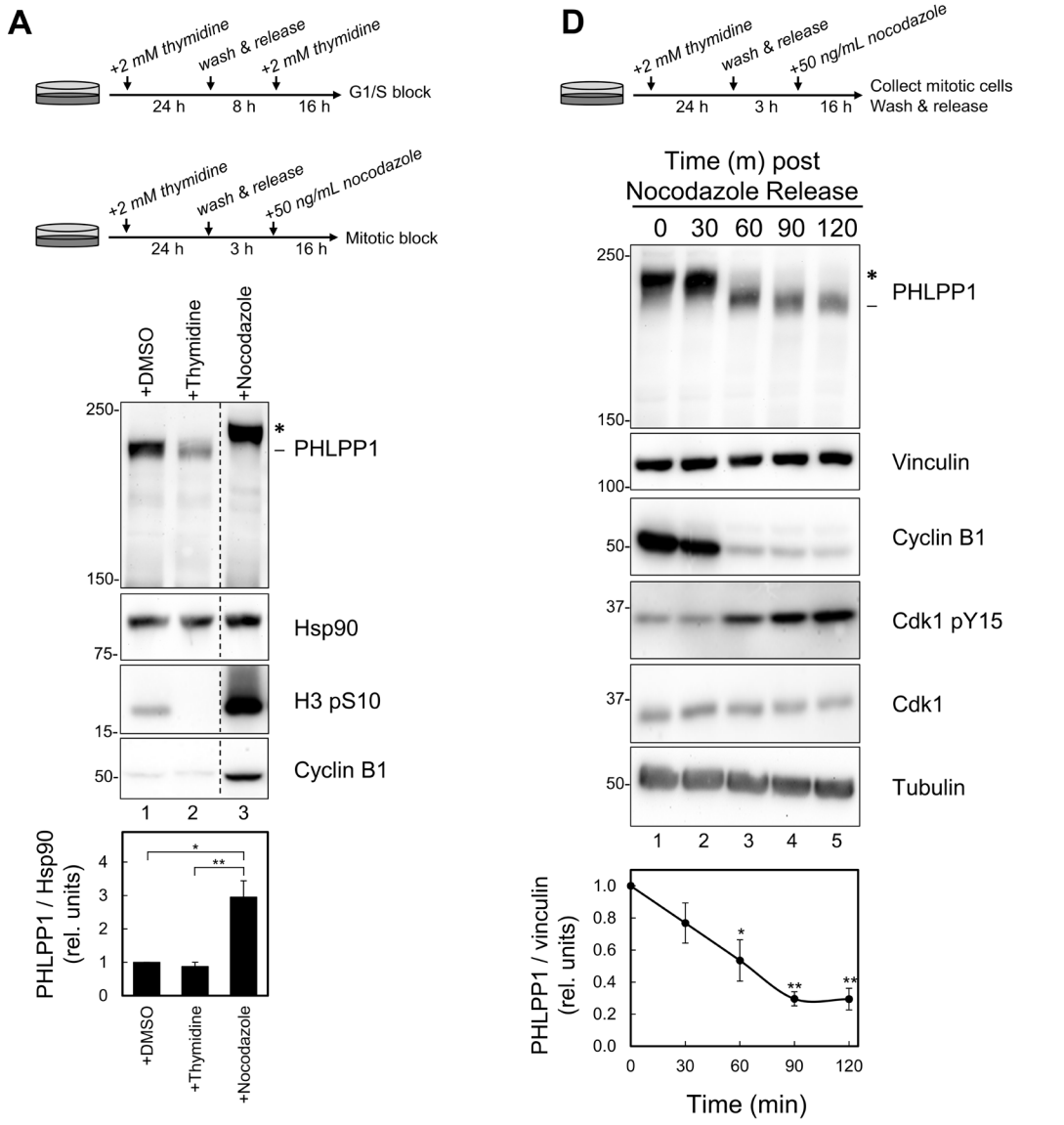
A
+2 mM thymidine
wash & release
+2 mM thymidine
24 h
8 h
16 h
G1/S block
+2 mM thymidine
wash & release
+50 ng/mL nocodazole
24 h
3 h
16 h
Mitotic block
+DMSO
+Thymidine
+Nocodazole
250-
150-
PHLPP1
Hsp90
75-
H3 pS10
15-
Cyclin B1
50-
1 2 3
PHLPP1 / Hsp90 (rel. units)
D
+2 mM thymidine
wash & release
+50 ng/mL nocodazole
24 h
3 h
16 h
Collect mitotic cells
Wash & release
Time (m) post Nocodazole Release
0 30 60 90 120
PHLPP1
Vinculin
100-
Cyclin B1
Cdk1 pY15
37-
Cdk1
Tubulin
1 2 3 4 5
PHLPP1 / vinculin (rel. units)
Time (min)
B
+Nocodazole (100 ng/mL)
0 2 4 6 8 10 12 14 16 18 :Time (h)
PHLPP1
Cdk1 pY15
Cdk1
H3 pS10
H3
1 2 3 4 5 6 7 8 9 10
C
:Nocodazole
:λ ppase
0 30 0 30 30 :Time (min)
PHLPP1
Hsp90
1 2 3 4 5

Figure 2.2: Mitotic PHLPP1 phosphorylation occurs within the unstructured N-terminal extension (NTE). (A) Schematic of HA-tagged PHLPP1 constructs used in this study: full-length PHLPP1 (amino acids 1-1717, FL), N-terminally truncated PHLPP1 (amino acids 513-1717, ΔNTE), and C-terminally truncated PHLPP1 (amino acids 1-512, NTE). **(B)** Western blot of DMSO or nocodazole-treated HeLa cells over-expressing HA-tagged constructs from (A) using an anti-HA antibody. Samples were also analyzed for endogenous PHLPP2 using an anti-PHLPP2 antibody. **(C)** Schematic of experimental design for phospho-mass spectrometry. **(D)** FLAG-PHLPP1 NTE purified from DMSO or nocodazole-treated HeLa cells separated on a SDS-PAGE gel (left: Coomassie blue staining, right: western blot using FLAG antibody). **(E)** Table summarizing phospho-mass spectrometry results. The Mitotic Enrichment score was calculated as follows: (Spectral $\text{Counts}_{+\text{Nocodazole}}$) / (1 + Spectral $\text{Counts}_{+\text{DMSO}}$). **(F)** Schematic of mitotic phosphorylation sites (bolded, underlined) detected in the PHLPP1 NTE (proximal proline residues in red). **(G)** Top: diagram of PHLPP1 protein structure with mitotic phosphorylation clusters denoted. Bottom: predictions of intrinsic disorder tendency of PHLPP1 by IUPred2A long disorder (89). Scores above 0.5 (black line) indicate disordered regions. Numbers below each blot refer to the lane number. Asterisk refers to PHLPP1 electrophoretic mobility shift compared to faster mobility species (dash).

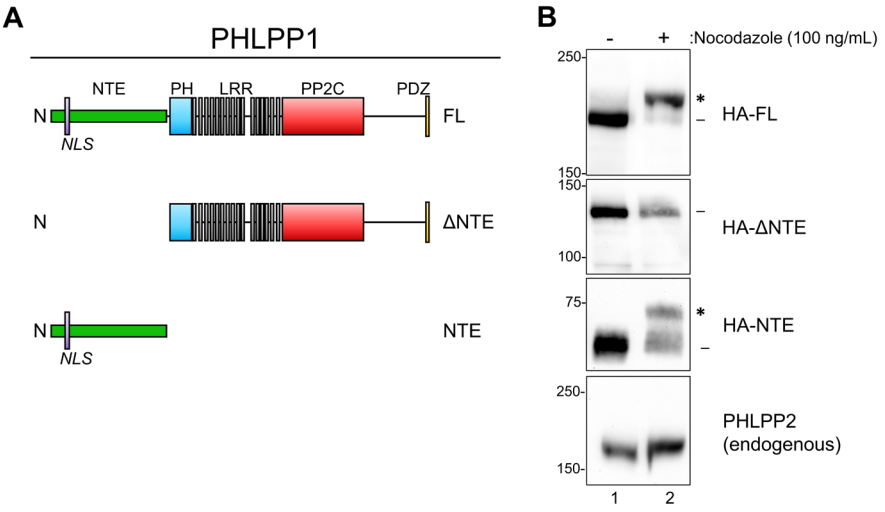

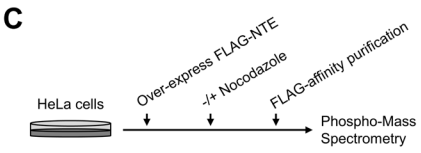

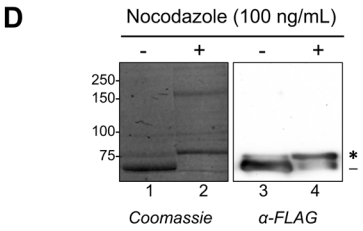

E

Residue	Spectral Counts (+DMSO)	Spectral Counts (+Nocodazole)	Mitotic Enrichment
Ser50	59	47	0.8
Thr56	8	15	1.7
Ser317	42	141	3.3
Ser321	16	98	5.8
Ser323	12	67	5.2
Ser324	13	122	8.7
Ser335	28	182	6.3
Ser336	24	272	10.9
Ser345	0	32	32.0
Thr409	1	22	11.0
Ser411	4	21	4.2
Ser412	6	52	7.4
Ser425	75	285	3.8
Ser450	11	57	4.8
Thr451	2	97	32.3

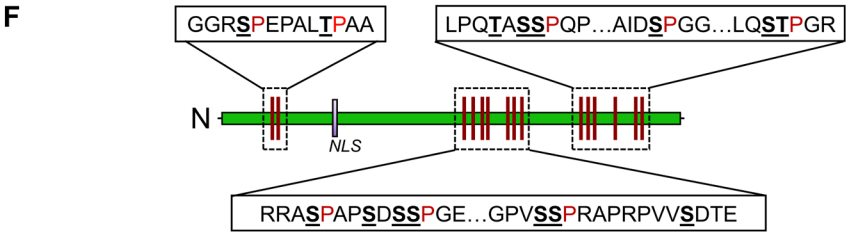

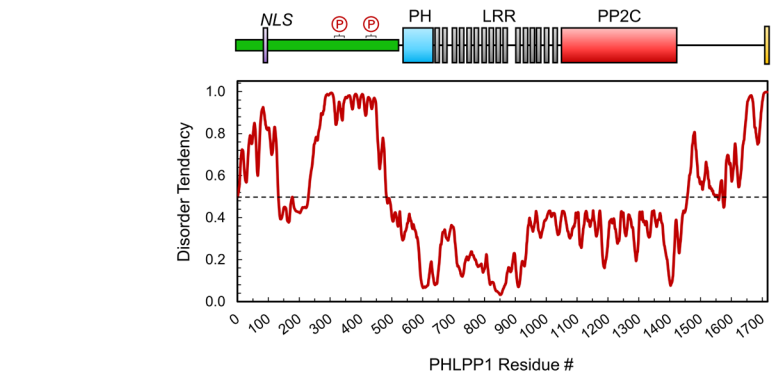

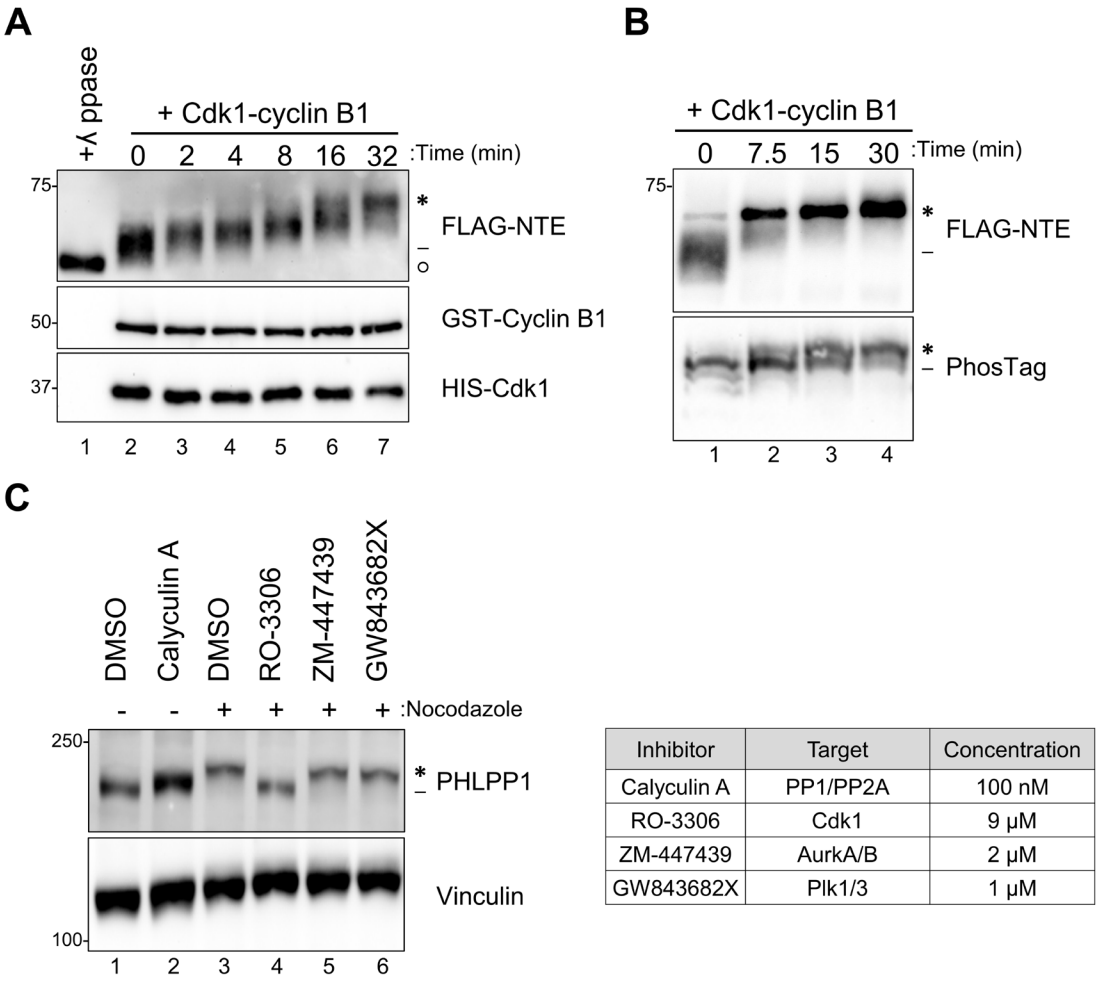

Inhibitor	Target	Concentration
Calyculin A	PP1/PP2A	100 nM
RO-3306	Cdk1	9 μM
ZM-447439	AurkA/B	2 μM
GW843682X	Plk1/3	1 μM

Figure 2.3: Cdk1 phosphorylates the PHLPP1 NTE during mitosis. (A) *In vitro* phosphorylation of FLAG-tagged PHLPP1 NTE with recombinant Cdk1-cyclin B1 (0.5 units/50 μL reaction). Purified NTE was incubated with either ʎ phosphatase (lane 1) or recombinant Cdk1-cyclin B1 (lanes 2-7) at 37°C for indicated time points. PHLPP1 NTE mobility shift was evaluated by western blot using an anti-FLAG antibody. GST-cyclin B1 and HIS-Cdk1 were probed by antibodies against cyclin B1 and Cdk1, respectively. **(B)** Purified NTE treated with recombinant Cdk1-cyclin B1 (1 unit/50 μL reaction) was probed by an anti-FLAG antibody on a SDS-PAGE (top) or PhosTag (bottom) gel. **(C)** HeLa cells were treated with nocodazole (100 ng/mL for 16 h), followed by various mitotic kinase inhibitors for 30 min prior to lysis as indicated: RO-3306 (Cdk1 inhibitor, 9 μM), ZM-447439 (Aurora A/B inhibitor, 2 μM), and GW843682X (Polo like kinase 1/3 inhibitor, 1 μM). Asynchronous cells were treated with the phosphatase inhibitor Calyculin A (100 nM) for 30 min prior to lysis. Triton-soluble lysates were subjected to western blot and probed for endogenous PHLPP1. Numbers below each blot refer to the lane number. Asterisk refers to PHLPP1 electrophoretic mobility shift compared to faster mobility species (dash).

Figure 2.4: A BioID screen to determine changes in the mitotic PHLPP1 interactome. **(A)** Tetracycline-inducible Flp-IN T-REx HeLa cells expressing the following constructs were generated: full-length PHLPP1 (amino acids 1-1717, FL) and N-terminally truncated PHLPP1 (amino acids 513-1717, ΔNTE), fused with BirA* biotin ligase (R118G mutation) and a 3X-FLAG tag. Additionally, cells expressing only the BirA*-3XFLAG tag were generated (BirA*). **(B)** BioID experimental workflow. **(C)** Western blot of BirA*-3XFLAG-PHLPP1 FL Flp-In T-REx HeLa cells treated with or without nocodazole. Blot was probed with an anti-FLAG antibody. **(D)** Legend for BioID dot plot analysis where AvgSpec refers to averaged spectral counts across the biological duplicates (BFDR, false discovery rate). Dot plot of prey identified that display either a **(E)** ≥ 2-fold enrichment in nocodazole-treated (mitotic) versus DMSO-treated (asynchronous) cells expressing full-length (FL) PHLPP1, or **(F)** ≥ 2-fold enrichment in DMSO-treated (asynchronous) versus nocodazole-treated (mitotic) cells expressing FL PHLPP1. **(G)** Dot plot of prey identified that display ≥ 2-fold enrichment or ≥ 2-fold depletion in nocodazole-treated ΔNTE cells compared to nocodazole-treated FL PHLPP1 expressing cells. **(H)** Dot plot of prey identified that display ≥ 2-fold enrichment or ≥ 2-fold depletion in DMSO treated ΔNTE cells compared to FL cells. Numbers below each blot refers to the lane number. Prey that are bolded and have an asterisk refer to previously identified PHLPP1 interacting proteins. Asterisk on western blot refers to PHLPP1 electrophoretic mobility shift compared to faster mobility species (dash).

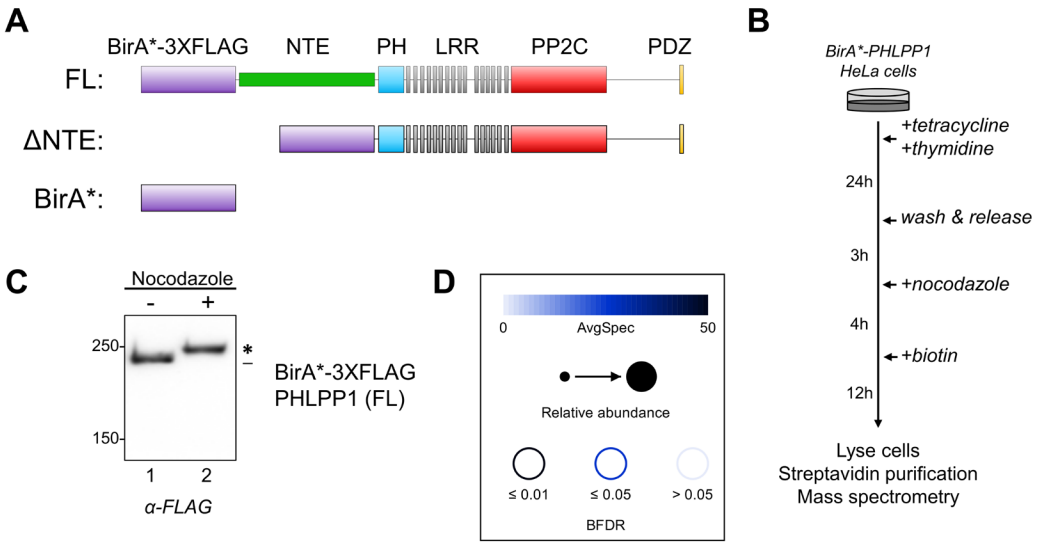

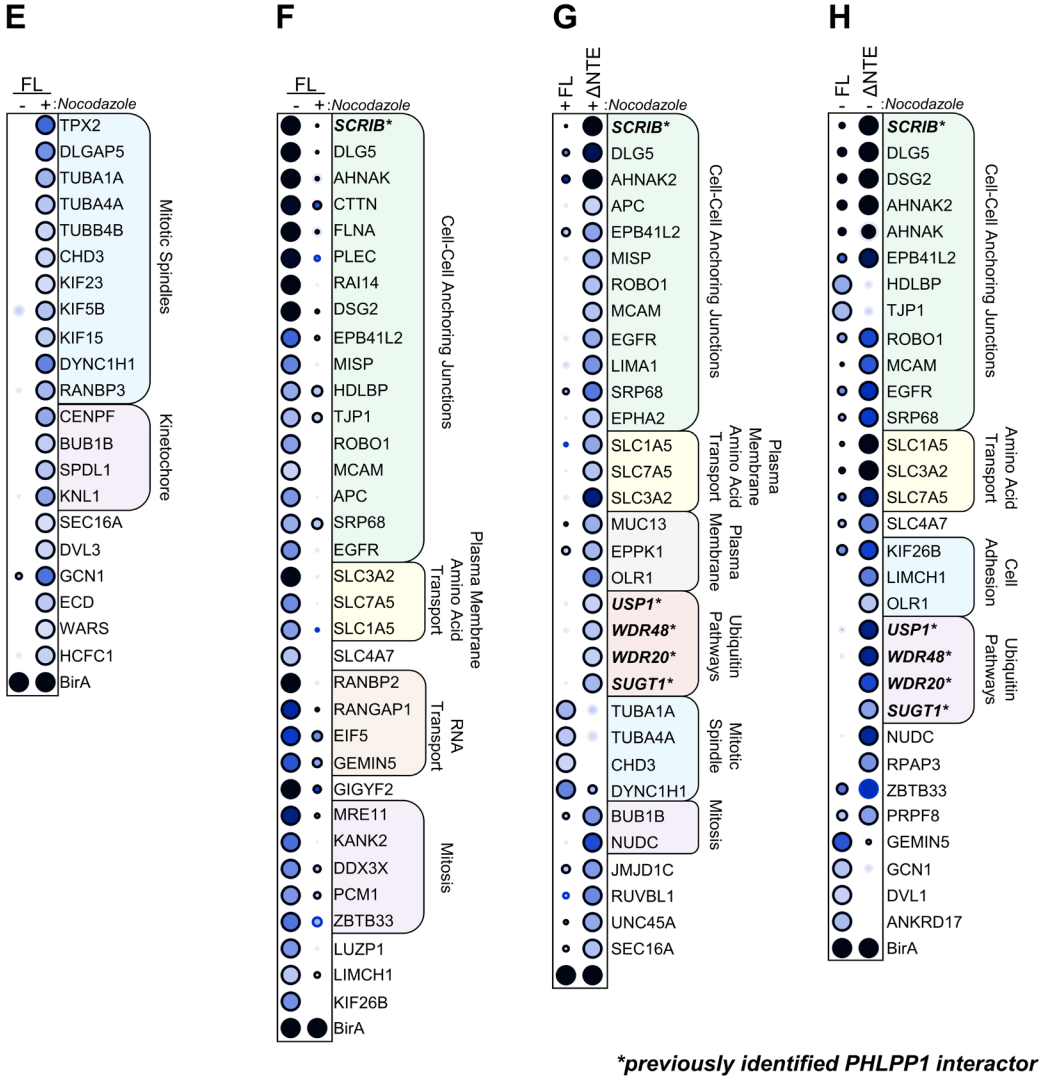

previously identified PHLPP1 interactor

Figure 2.5: *Phlpp1*$^{-/-}$ MEFs exhibit defects in mitosis. Time-lapse fluorescence microscopy to determine mitotic duration in **(A)** *Phlpp1*$^{+/+}$ (WT) and **(B)** *Phlpp1*$^{-/-}$ (KO) MEFs stably expressing mRFP-tagged H2B. Time when each frame was captured is denoted in minutes and seconds, where 0:00 was set as the first frame indicating nuclear envelope breakdown (NEBD). Single red asterisk refers to NEBD, and double red asterisk refers to beginning of anaphase. Representative images (from KO MEFs) of mitotic defects scored in WT and KO MEFs: **(C)** lagging chromosomes (highlighted by red arrow), **(D)** multipolar spindle formation, and **(E)** anaphase bridge formation (highlighted by red arrow). Scale bars for figures (A-E) indicate 10 μm. **(F-I)** Quantification of parameters listed in (A-E) of WT (n=185 cells) and KO (n=211 cells) MEFs. Three clonal lines were imaged and analyzed separately; results were then averaged and used to calculate the SEM. Values are expressed as the mean ± SEM. **p<0.005; ns, not significant (Student's t-test). **(J)** Representative image of DAPI stained WT and KO MEFs. Red arrows indicate cells containing micronuclei. Quantification of micronuclei-containing WT (n=4925) and KO (n=5302) cells from four independent experiments. Scale bars indicate 20 μm. Values are expressed as the mean ± SEM. **p<0.005 (Student's t-test).

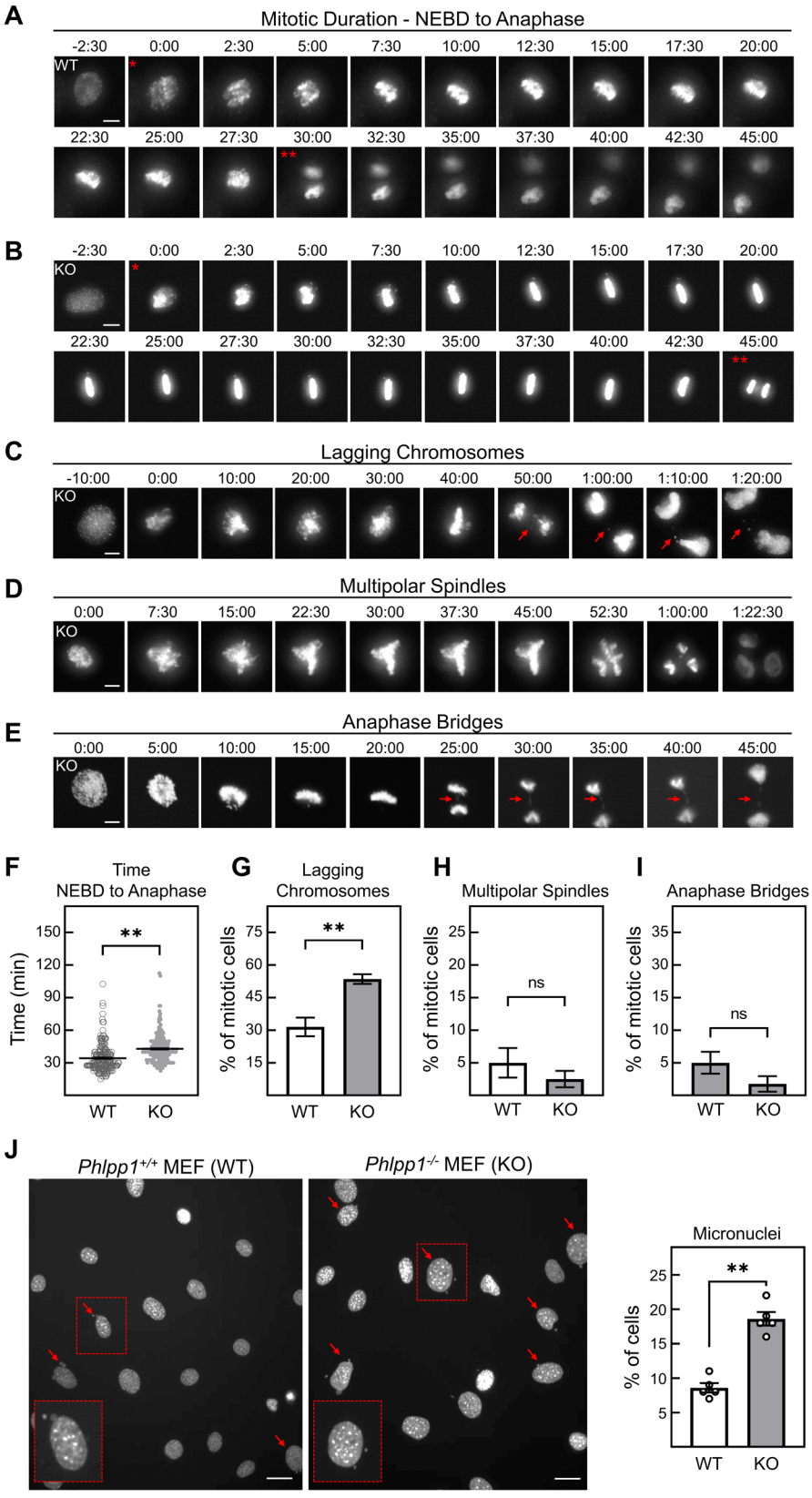
A
Mitotic Duration - NEBD to Anaphase
-2:30
0:00
2:30
5:00
7:30
10:00
12:30
15:00
17:30
20:00
WT
22:30
25:00
27:30
30:00
32:30
35:00
37:30
40:00
42:30
45:00
B
KO
C
Lagging Chromosomes
-10:00
0:00
10:00
20:00
30:00
40:00
50:00
1:00:00
1:10:00
1:20:00
D
Multipolar Spindles
0:00
7:30
15:00
22:30
30:00
37:30
45:00
52:30
1:00:00
1:22:30
E
Anaphase Bridges
F
Time
NEBD to Anaphase
Time (min)
G
Lagging
Chromosomes
% of mitotic cells
H
Multipolar Spindles
ns
I
Anaphase Bridges
J
Phlpp1+/+ MEF (WT)
Phlpp1-/- MEF (KO)
Micronuclei
% of cells

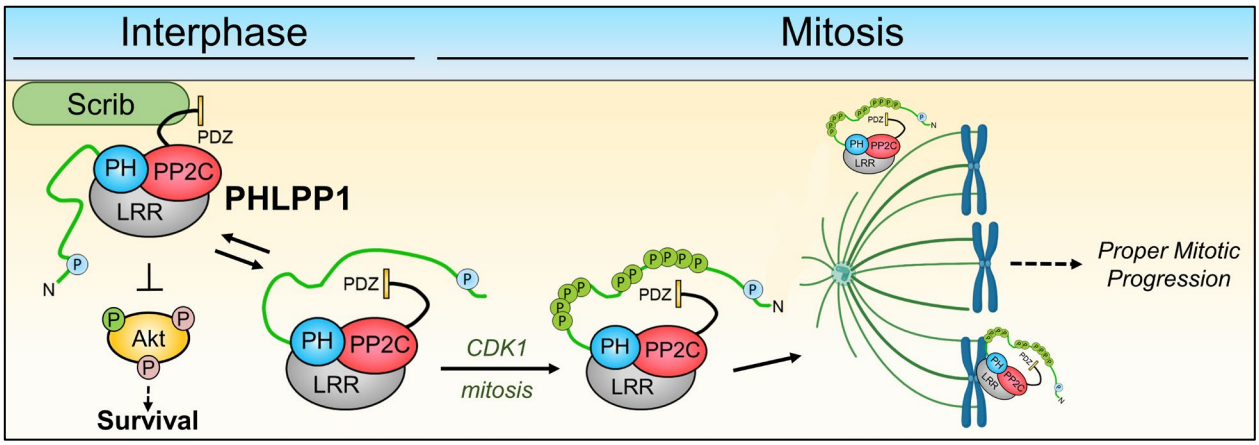

Figure 2.6: Proposed model of mitotic PHLPP1 regulation. During interphase, cytoplasmic unphosphorylated PHLPP1 functions to regulate substrates such as Akt. PHLPP1 is in close proximity to membrane-associated scaffolds such as Scrib. Upon entry into mitosis, the PHLPP1 NTE is hyperphosphorylated by Cdk1. Additionally, a diminished interaction with Scrib and an enhanced interaction with mitotic scaffolds are observed. Deletion of PHLPP1 results in mitotic defects, suggesting this pathway is important for proper mitotic progression.

Supplemental Dataset 1:
Phospho-mass spectrometry dataset.

Supplemental Dataset 2:
BioID MassIVE output files. MassIVE Table 1 describes the composition of the dataset. MassIVE Table 2 list the peptide idenfication evidence as per iProphet. MassIVE Table 3 lists the interactions identified by SAINTexpress. (128). The BioID data has been deposited as a complete submission to the MassIVE repository (https://massive.ucsd.edu/ProteoSAFe/static/massive.jsp) and assigned the accession number MSV000085628. The ProteomeXchange accession is PXD020003. The dataset is currently available for reviewers at ftp://MSV000085628@massive.ucsd.edu. Please login with username MSV000085628_reviewer; password: PHLPP1. The dataset will be made public upon acceptance of the manuscript.

Chapter 3 – PHLPP1 Counter-regulates STAT1-mediated Inflammatory Signaling

ABSTRACT

Inflammation is an essential aspect of innate immunity but also contributes to diverse human diseases. Although much is known about the kinases that control inflammatory signaling, less is known about the opposing phosphatases. Here we report that deletion of the gene encoding PH domain Leucine-rich repeat Protein Phosphatase 1 (PHLPP1) protects mice from lethal lipopolysaccharide (LPS) challenge and live *Escherichia coli* infection. Investigation of PHLPP1 function in macrophages reveals that it controls the magnitude and duration of inflammatory signaling by dephosphorylating the transcription factor STAT1 on Ser727 to inhibit its activity, reduce its promoter residency, and reduce the expression of target genes involved in innate immunity and cytokine signaling. This previously undescribed function of PHLPP1 depends on a bipartite nuclear localization signal in its unique N-terminal extension. Our data support a model in which nuclear PHLPP1 dephosphorylates STAT1 to control the magnitude and duration of inflammatory signaling in macrophages.

INTRODUCTION

Gene expression is an exquisitely regulated process that maintains cellular homeostasis and orchestrates appropriate responses to environmental stimuli such as hormones, cytokines, and pathogenic microbes (130, 131). Homeostatic control of inflammatory genes is particularly relevant to cancer since chronic inflammation promotes tumorigenesis and influences patient response to cancer therapeutics (132, 133). Dysregulated gene expression, a hallmark of cancer, can arise from mutations in transcription factors (exemplified by p53 (134)), alterations in signaling pathways controlling transcription factor function (for example, hormone-dependent transcription factors in prostate and breast cancers (135, 136)), or upregulation of oncogenic

transcription factors (notably c-myc, which regulates essential cell-cycle checkpoints (137)). Aberrant protein phosphorylation underpins all of these mechanisms, via dysregulation of signaling pathways, alterations in transcription factor machinery, and/or effects on the chromatin epigenetic landscape (138, 139). Thus, targeting phosphorylation mechanisms is of considerable therapeutic interest.

Macrophages are among the first responders to infection, engaging foreign pathogens via pattern recognition receptors, including the Toll-like receptors (TLRs). TLRs are a conserved family of cell surface or phagosome-associated receptors that discriminate distinct features of microbial and viral pathogens, including lipoproteins (TLR1/2/6), lipopolysaccharide (LPS) (TLR4), flagellin (TLR5), single-stranded RNA (TLR7/8), double-stranded RNA (TLR3), and double-stranded DNA (TLR9) (140, 141). Upon pathogen recognition by TLRs, a pro-inflammatory response is initiated that activates the signal-dependent transcription factors nuclear factor-κB (NF-κB), activator protein 1 (AP1), interferon response factors (IRFs), and, through secondary mechanisms, the signal transducer and activator of transcription (STAT) protein family (140). These activated transcription factors function in a combinatorial manner to drive expression of antimicrobial and inflammatory response genes that aid in elimination of foreign pathogens. However, while inflammation is required for protection against foreign microbes, it can lead to excessive cytokine production, chronic inflammation, and cancer if not properly resolved (132, 133, 142). Thus, macrophages have evolved regulatory mechanisms to resolve inflammatory responses in a timely manner, including shut down of STAT1 signaling pathways by the suppressor of cytokine signaling (SOCS) family of proteins (143), suppression of nitric oxide production by the enzyme arginase (144), and inhibition of a key subset of NFκB-dependent genes by anti-inflammatory omega-3 fatty acids, (145).

STAT1 is the founding member of the STAT transcription factor family and serves as a paradigm for how phosphorylation regulates transcription factor structure, function, and localization (146-148). In the canonical pathway, STATs are recruited from the cytosol to cytokine-bound and Tyr-phosphorylated receptors where they are phosphorylated on a key Tyr residue (Tyr701 for STAT1) by Janus Kinases (JAKs). This phosphorylation event promotes STAT dimerization and nuclear entry, allowing STAT binding to specific promoter sequences and thus initiating gene transcription. Upon promoter binding, STATs become additionally phosphorylated on a regulatory Ser residue at a MAPK consensus sequence (Ser727 for STAT1), a modification that enhances their transcriptional activity (138, 149-151). Importantly, STAT1 transduces signals from type I and II interferons (IFNs), resulting in binding to IFN-stimulated response elements (ISREs) and to IFN-gamma (IFNγ)-activated site (GAS) elements in the promoters of IFN-stimulated genes (ISGs), inducing their transcription and stimulating inflammation (152). While the kinases that phosphorylate Tyr701 and Ser727 on STAT1 have been extensively studied, as have been the phosphatases that dephosphorylate Tyr701, the phosphatases that oppose the Ser727 phosphorylation are unknown.

PH domain Leucine-rich Repeat Protein Phosphatase 1 (PHLPP1) is one of the newest members of the phosphatome (10, 81). Originally discovered for its function in suppressing growth factor signaling by dephosphorylating Akt on the hydrophobic motif site, Ser473 (10), the repertoire of PHLPP1 substrates is continually expanding (153). PHLPP1 is a bona fide tumor suppressor: its expression is frequently lost in cancer and its genetic ablation in a mouse model results in prostate neoplasia (50, 154). PHLPP1 is also involved in the immune response, where its dephosphorylation of Akt reduces the capacity of regulatory T cells to transduce T cell receptor signals, a key function in T cell development (58). Additionally, mice lacking PHLPP1 have

enhanced chondrocyte proliferation as a result of increased Akt2 activity, diminished FoxO1 levels, and increased *Fgf18* expression, suggesting PHLPP1 inhibition could be a strategy to promote cartilage regeneration and repair (7). PHLPP1 also suppresses receptor tyrosine kinase gene expression by a mechanism distinct from its effects on Akt, to influence growth factor signaling, including that mediated by the epidermal growth factor (EGF) receptor (14).

PHLPP1 is unusual among protein phosphatases in that its regulatory modules and catalytic domain are on the same polypeptide. Most notably, it has a PH domain essential for dephosphorylation of protein kinase C (PKC) (11), a PDZ ligand necessary for Akt recognition (10), and a leucine-rich repeat (LRR) segment required for transcriptional regulation of receptor tyrosine kinases (14). In addition, PHLPP1 possesses an approximately 60 kDa N-terminal extension (NTE) of unknown function. Stoichiometric association with substrates by direct binding to the protein-interaction domains on PHLPP or common scaffolds (e.g. PDZ domain proteins such as Scribble (155)) allows fidelity and specificity in PHLPP function, and may account for its >10-fold lower catalytic rate compared to the closely related phosphatase PP2Cα (4). Given its transcriptional regulation of at least one family of genes (14), PHLPP1 is an attractive pharmacological target for modulation of gene expression.

Here we report that nuclear-localized PHLPP1 opposes STAT1 Ser727 phosphorylation to inhibit its transcriptional activity and promote normal resolution of inflammatory signaling. We find that *Phlpp1*$^{-/-}$ mice have improved survival following infection with *Escherichia coli* (*E. coli*), indicating a role of the phosphatase in innate immunity. Since macrophages are key in the initial response to lipopolysaccharide (LPS) from Gram-negative bacteria such as *E. coli*, we further explored the role of PHLPP1 in controlling LPS-dependent signaling in this cell type. The STAT1 binding motif was identified from the most common promoter sequences of 199 genes that

remained elevated following LPS treatment of bone marrow-derived macrophages (BMDMs) from *Phlpp1*$^{-/-}$ mice compared to those from wild-type (WT) mice. We validated common transcriptional targets of PHLPP1 and STAT1, showing that loss of PHLPP1 upregulates the transcription of several genes including guanylate binding protein 5 (*Gbp5*), whereas loss of STAT1 downregulates them. Cellular studies revealed that dephosphorylation of STAT1 on Ser727 suppresses its transcriptional activity by a mechanism that depends both on the catalytic activity of PHLPP1 and a previously undescribed nuclear localization signal (NLS) in the NTE of PHLPP1. Taken together, our results identify PHLPP1 as a major player in the resolution of inflammatory signaling.

RESULTS

PHLPP1 regulates the innate immune response

To explore the role of PHLPP1 in acute inflammation, we examined the kinetics and outcome of sepsis-induced death caused by intraperitoneal (i.p.) injection of Gram-negative *E. coli* bacteria in WT and *Phlpp1*$^{-/-}$ mice. Surprisingly, absence of PHLPP1 provided a strong protective effect; at a dose where more than 50% of WT mice died within 12 h of *E. coli* challenge, 50% of the *Phlpp1*$^{-/-}$ mice remained alive after 10 days (Figure 3.1.A). Similarly, *Phlpp1*$^{-/-}$ mice were protected from toxicity induced by the purified Gram-negative bacterial cell wall component LPS, with nearly half of the *Phlpp1*$^{-/-}$ mice alive after 10 days compared to only 1 out of 16 of the WT mice (Figure 3.1.B). To understand the lower mortality rates in *Phlpp1*$^{-/-}$ mice, we measured levels of different cytokines in the serum of mice across a time course following LPS injection (Figure 3.1.C-E). Serum levels of pro-inflammatory cytokine interleukin 6 (IL-6) were significantly increased in WT mice within 5 h of LPS injection, returning to baseline within 12 h (Figure 3.1.C).

In contrast, the *Phlpp1*$^{-/-}$ mice had 2-fold lower IL-6 levels at 5 h post-infection, but these levels were sustained for up to 24 h, suggestive of improper resolution of inflammation. Levels of another pro-inflammatory cytokine, IL-1β, were likewise consistently higher in *Phlpp1*$^{-/-}$ mice compared with WT mice (Figure 3.1.D). By contrast, levels of the anti-inflammatory cytokine IL-10 did not differ significantly between the WT and *Phlpp1*$^{-/-}$ mice (Figure 3.1.E). Note that cytokine levels were measured up to 24 h post LPS injection, when the protective effect of PHLPP1 loss was not yet apparent. These findings indicate an essential role for PHLPP1 in regulation of the innate immune response at the whole organism level.

Loss of PHLPP1 results in increased STAT1-dependent transcription in macrophages

Since macrophages are a key cell type involved in the initial response to *E. coli* infection and LPS challenge, we analyzed the transcriptome of BMDMs isolated from WT or *Phlpp1*$^{-/-}$ mice before and after stimulation by the major LPS component, Kdo2-Lipid A (KLA), for 1, 6, or 24 h (Figure 3.2.A). RNA-Seq analysis identified 1,654 mRNA transcripts induced more than two-fold by KLA treatment, with a false discovery rate (FDR) less than 0.05 at any of the time points. Expression of approximately 12% of these genes (199 genes; **Supplemental Dataset 3**) was increased in macrophages from *Phlpp1*$^{-/-}$ mice compared to those from littermate control WT mice 6 h following KLA treatment; transcript levels of these genes remained significantly elevated (>two-fold) 24 h later. Another set of genes exhibited reduced expression 24 h following KLA treatment (144 genes; **Supplemental Dataset 4**). Gene ontology analysis revealed that many of the genes whose expression was elevated in the *Phlpp1*$^{-/-}$ macrophages are associated with inflammatory signaling: these included genes annotated for their involvement in the innate immune response, cytokine-cytokine receptor interactions, LPS signaling, interferon-β response,

and tumor necrosis factor (TNF) signaling-dependent pathways (Figure 3.2.B). Genes significantly decreased in *Phlpp1*$^{-/-}$ compared to WT macrophages were enriched most significantly in nodes related to central carbon metabolism, and to a lesser extent, chronic inflammatory responses and LPS signaling (Figure 3.2.B).

To gain insight into gene regulatory mechanisms affected by loss of PHLPP1, we performed *de novo* motif analysis of the promoters of upregulated genes in *Phlpp1*$^{-/-}$ macrophages using Hypergeometric Optimization of Motif EnRichment (HOMER), a suite of tools for motif discovery and Next Generation Sequencing (NGS) analysis (156). This algorithm defines motifs that are statistically enriched in a targeted promoter list compared to random promoter sequences with comparable GC content. The analysis revealed significant enrichment of STAT ($p<10^{-18}$) and IRF ($p<10^{-9}$) motifs (Figure 3.2.C) in the promoters of genes whose expression was statistically increased in *Phlpp1*$^{-/-}$ macrophages compared to WT macrophages. Of the 199 genes with elevated expression, 46% of the genes had promoters with a consensus STAT binding motif, 51% had promoters with a potential binding site for IRF family of transcription factors, and 26% had promoters with predicted binding sites for both STAT and IRF (Figure 3.2.D). We selected for further analysis three genes whose expression was elevated in the *Phlpp1*$^{-/-}$ compared to WT macrophages and which had proximal STAT1 binding motifs in their promoters: *Cd69*, *Ifit2*, and *Gbp5*. Normalized mRNA-Seq data for each of these three genes confirmed elevated mRNA levels in *Phlpp1*$^{-/-}$ macrophages compared to WT macrophages (Figure 3.2.E-G). Thus, loss of PHLPP1 leads to sustained KLA-induced expression of genes involved in inflammation, of which 46% have predicted STAT motifs in their proximal regulatory regions.

If PHLPP1 suppresses STAT-regulated gene transcription, we reasoned that 1] knockdown of a STAT family member should reduce transcription of the same genes affected by loss of

PHLPP1 and 2] knockdown of PHLPP1 should enhance STAT binding to its promoters. STAT1 is required for LPS-induced gene expression in macrophages (157) and implicated as a PHLPP1 target in iNOS regulation (158). STAT1 knockdown by siRNA in thioglycollate-elicited peritoneal macrophages resulted in a 2-fold reduction in KLA-induced transcription of *Cd69*, *Ifit2*, and *Gbp5* at 6 h compared to a control siRNA transfection, with transcript levels dropping to near baseline by 24 h (Figure 3.3.A-C). The effect of PHLPP1 knockdown on STAT1 promoter occupancy was examined by chromatin immunoprecipitation (ChIP) using STAT1-specific antibodies. KLA induced STAT1 binding to the promoters of *Cd69*, *Ifit2*, and *Gbp5*, with maximal binding observed 1 h post stimulation, followed by a decay in binding to near baseline after 24 h (Figure 3.3.D-F). In contrast, binding to these promoters was enhanced and sustained in *Phlpp1*$^{-/-}$ macrophages relative to WT cells. The degree of enhancement and the kinetics of activation/resolution varied depending on the gene examined: PHLPP1 loss had the most robust early effect (1 h) on the *Ifit2* promoter and at a later time (24 h) on the *Cd69* promoter. Thus, PHLPP1 suppresses KLA-stimulated binding of STAT1 to its promoters and thereby reduces transcription of its target genes.

PHLPP1 binds to STAT1 and dephosphorylates Ser727

We next examined whether PHLPP1 affects the phosphorylation state of the two regulatory STAT1 phosphorylation sites, Ser727 and Tyr701. Primary BMDMs were isolated from WT and *Phlpp1* $^{-/-}$ mice and the kinetics and magnitude of KLA-triggered phosphorylation at each of the two STAT1 sites were compared. Loss of PHLPP1 in BMDMs led to a robust increase in STAT1 phosphorylation on the regulatory site Ser727 but did not affect Tyr701 phosphorylation (Figure 3.4.A-B). PHLPP1 loss also resulted in an increase in Erk phosphorylation at its activation loop sites, as previously reported (14). Incubation of *in vitro* phosphorylated STAT1 with

immunoprecipitated FLAG-tagged PHLPP1 resulted in dephosphorylation at Ser727, suggesting that PHLPP1 directly dephosphorylates STAT1 (Figure 3.4.C). Furthermore, overexpression of PHLPP1 in HEK-293T cells reduced IFNγ-dependent phosphorylation of STAT1 on Ser727 but not on Tyr701 (Figure 3.4.D-E). Thus, PHLPP1 selectively dephosphorylates the Ser727 regulatory phosphorylation on STAT1 *in vitro* and in cells.

Because the abundance of PHLPP1 in the cell is much lower than other phosphatases such as PP2A (159), we next sought to determine whether regulation of STAT1 promoter activity was solely due to PHLPP1 phosphatase activity or occurred in combination with other phosphatases. Taking advantage of the insensitivity of PHLPP phosphatases to the PP1/PP2A inhibitor okadaic acid (OA) (10), we examined whether OA treatment affected KLA-dependent changes on Ser727 phosphorylation in primary BMDMs from WT mice. KLA-induced increase in Ser727 phosphorylation was relatively insensitive to OA, under conditions where the phosphorylation of Erk (at Thr202/Tyr204) and Akt (at Thr308) was significantly increased upon OA addition (Figure 3.5.A-B). These data are consistent with PHLPP1, a PP2C family member, being the primary regulator of phosphorylation on the activity-tuning Ser727 site of STAT1.

We next addressed whether enhanced promoter binding of STAT1 upon loss of PHLPP1 resulted in enhanced transcriptional activation using a luciferase reporter assay. WT or *Phlpp1*$^{-/-}$ mouse embryonic fibroblasts (MEFs) were co-transfected with a firefly luciferase reporter construct containing GAS promoter elements, as well as a renilla luciferase controlled by a constitutive CMV promoter as an internal control. STAT1 promoter activity was assessed by monitoring luminescence following IFNγ stimulation. STAT1 promoter activity was significantly higher in *Phlpp1*$^{-/-}$ MEFs compared to WT MEFs at both 6 h and 24 h (Figure 3.6.A). Pre-treatment of cells with okadaic acid, under conditions that increased the phosphorylation of PP2A-sensitive

substrates (Figure 3.5.A**,** Figure 3.7), had no effect on STAT1 promoter activity (Figure 3.6.A); note that treatment with a PKC inhibitor also had no effect on STAT1 promoter activity (Figure 3.8). Because STAT1 functions in the nucleus, we next asked whether PHLPP1 regulation of STAT1 occurs in the cytoplasm or nucleus. To this end, we assessed the effect of expressing either the PP2C domain of PHLPP1 or a nuclear-targeted (NLS) PP2C domain of PHLPP1 (Figure 3.6.B) on IFNγ-induced STAT1 promoter activity via the GAS luciferase assay. The overexpressed PP2C domain of PHLPP1 (Figure 3.6.C, blue) was considerably less effective in inhibiting STAT1 promoter activity compared to full-length PHLPP1 (Figure 3.6.C, red). However, forcing the PP2C domain into the nucleus by attaching an NLS to its N-terminus inhibited STAT1 promoter activity as effectively as overexpression of full-length PHLPP1 (Figure 3.6.C, orange). Analysis of the subcellular localization of the constructs used in this experiment revealed that full-length PHLPP1 was primarily cytosolic, the isolated PP2C domain had increased nuclear localization, and the NLS-PP2C was enriched in the nucleus (Figure 3.9.A-B). To address whether PHLPP1 catalytic activity is required for STAT1 regulation, we utilized a phosphatase-dead PP2C domain in which two active site residues, Asp1210 and Asp1413 (4) were mutated to Ala (DDAA). The catalytically-inactive NLS-PP2C was no longer able to suppress STAT1 activity (Figure 3.6.C, purple); immunohistochemistry confirmed its nuclear localization (Figure 3.9.A-B). Thus, both the catalytic activity and nuclear localization of PHLPP1 are necessary for it to regulate STAT1 transcriptional activity.

PHLPP1 has a bipartite Nuclear Localization Signal in its N-Terminal Extension

Bioinformatics analysis of the sequence of PHLPP1 using SeqNLS (160) revealed a potential Arg-rich bipartite NLS (^{92}RRRRR-X-^{122}RRGRLKR) in the N-terminal extension unique

to the PHLPP1 isozyme (Figure 3.6.D). To test whether these basic segments function as an NLS, we examined the subcellular localization in HeLa cells of the NTE alone or NTE in which the basic residues in each or both halves of the potential bipartite NLS were mutated to Ala (Figure 3.6.E). Immunocytochemistry revealed that the NTE localizes to the nucleus. Mutation of the first NLS or the second NLS increased the distribution of the NTE to the cytosol, and mutation of both decreased the nuclear:cytoplasmic ratio to be comparable to that of a construct of the NTE with a strong Nuclear Export Signal (NES) (LALKLAGLDI from PKI (161)) (Figure 3.6.F). Full-length PHLPP1 was primarily cytosolic, leading us to ask whether there may also be an NES. Bioinformatics analysis of the primary sequence identified a potential Leu-rich NES (162) immediately following the last LRR and preceding the phosphatase domain (Figure 3.10.A-B). Attachment of this 14-residue sequence to the N-terminus of the NTE resulted in distribution of the NTE to the cytosol (Figure 3.10.A-B). Thus, PHLPP1 nuclear localization is controlled by a bipartite NLS in the NTE and is opposed by an NES following the LRR. Lastly, we examined the effect of mutating the NLS on the ability of full-length PHLPP1 to reduce STAT1 transcriptional activity as assessed using the GAS promoter assay. The reduction in IFNγ-induced STAT1 activity resulting from PHLPP1 overexpression (Figure 3.6.G, red) was abolished upon mutation of NLS2 (Figure 3.6.G, brown) or both halves of the NLS (NLS1/2) (Figure 3.6.G, purple). Mutation of NLS1 had an intermediate effect (Figure 3.6.G, blue). These data reveal that a bipartite NLS in the NTE of PHLPP1 localizes PHLPP1 to the nucleus, where it suppresses the transcriptional activity of STAT1.

We next assessed which domain of PHLPP1 contributes to the observed regulation of STAT1 activity on the GAS promoter. Overexpression of full-length PHLPP1 in HEK-293T cells markedly reduced GAS promoter activity (Figure 3.11.A, red) compared to the vector only control

(Figure 3.11.A, black). A construct of PHLPP1 lacking the NTE (deletion of first 512 amino acids of its N-terminus; PHLPP1ΔNTE, blue) was less effective than full-length PHLPP1 in reducing STAT1 activity, whereas a construct comprised of just the NTE (amino acids 1-512, green) caused a significant increase in GAS promoter activity, suggesting a dominant-negative function of this segment. Co-immunoprecipitation assays revealed a robust interaction of STAT1 with the immunoprecipitated NTE of PHLPP1, in contrast to barely detectable binding of STAT1 to PHLPP1 lacking the NTE (Figure 3.11.B). Intermediate binding was observed between STAT1 and full-length PHLPP1. Quantification of three independent experiments revealed that the isolated NTE of PHLPP1 binds STAT1 approximately five times more strongly than full-length PHLPP1 and 26 times more strongly than PHLPP1 lacking the NTE (Figure 3.11.C). These data reveal that the NTE of PHLPP1 interacts with STAT1 and reduces its promoter activity.

DISCUSSION

The finding that *Phlpp1*$^{-/-}$ mice are protected from LPS-induced death allowed us to identify PHLPP1 as a physiologically relevant phosphatase in the overall innate immune response. It is likely that this immunoregulatory phenotype reflects roles of PHLPP1 in several immune cell types, and future studies of mice with cell-specific deletions of *Phlpp1* will be of great interest. Investigation of *Phlpp1*$^{-/-}$ macrophages indicates a significant role in counter-regulation of STAT1-dependent transcription that emerges as a secondary response to TLR4 ligation. Our mechanistic analyses show that PHLPP1 dephosphorylates STAT1 on a key regulatory site to suppress its transcriptional activity towards an array of genes involved in mounting an inflammatory response to IFNγ. Specifically, PHLPP1 directly dephosphorylates Ser727 on STAT1 *in vitro* and specifically suppresses phosphorylation of Ser727, but not Tyr701, on STAT1

in cells, correlating to decreased transcriptional activity of STAT1 at one of its major binding sites, the GAS promoter. The intrinsic catalytic activity and nuclear localization of PHLPP1 is required for this transcriptional regulation; while the isolated PP2C domain is not efficient in suppressing GAS promoter activity, forcing the PP2C domain into the nucleus is as effective as the full-length phosphatase in controlling transcriptional activity. Nuclear localization of the full-length enzyme is driven by a bipartite NLS we identify in the NTE. Elimination of PHLPP1 results in global changes in LPS-dependent transcriptional regulation, with 20% of the approximately 2,000 genes whose expression changes upon LPS stimulation differing by more than two-fold in BMDMs from *Phlpp1*$^{-/-}$ mice compared to WT mice.

Phosphorylation of STAT1 on Ser727 has been proposed to occur following the binding of the Tyr-phosphorylated STAT1 dimer to chromatin (150). Ser727 phosphorylation on the C-terminal transactivation domain of STAT1 is necessary for maximal transcriptional activity. Identification of PHLPP1 as a phosphatase that opposes this phosphorylation provides a mechanism to counter-regulate the activity of this key transcription factor. Several lines of evidence suggest that PHLPP1 may be the major phosphatase that controls this regulatory site. First, genetic depletion of PHLPP1 increases both STAT1 Ser727 phosphorylation and transcriptional activity at the GAS promoter, whereas PHLPP1 overexpression decreases both STAT1 Ser727 phosphorylation and transcriptional activity at the promoter. Second, both the IFNγ-induced phosphorylation of Ser727 and resulting increase in transcriptional activity at the GAS promoter are insensitive to OA, a phosphatase inhibitor that is ineffective towards PP2C family members but highly effective towards the abundant PP2A in cells. The insensitivity of STAT1 Ser727 phosphorylation to OA is consistent with PHLPP1 directly dephosphorylating this site in cells, a reaction it catalyzes *in vitro*. Furthermore, although PHLPP1 does suppress the

signaling output of Akt (by dephosphorylating Ser473 (10)) and Erk (by reducing the steady-state levels of RTKs (14)), its effect on STAT1 is unlikely to involve either of these targets because the activities of both kinases are sensitive to OA. Nor are the effects on Ser727 a result of PHLPP1 reducing PKC steady-state levels (11, 163), as the general PKC inhibitor Gö6983 did not alter GAS promoter activity (Figure 3.8). Third, genetic depletion of either PHLPP1 or STAT1 has opposing effects on transcriptional targets of STAT1: whereas KLA causes a larger increase in mRNA of *Cd69*, *Ifit2*, and *Gbp5* in BMDMs from *Phlpp1*$^{-/-}$ mice compared to WT mice, a reduction in these transcripts is observed upon STAT1 knockdown. Lastly, we have previously shown that PHLPP1 regulates transcription of genes and binds chromatin (14). Cumulatively, these data are consistent with PHLPP1 being the major phosphatase to oppose the activating phosphorylation of STAT1 on Ser727, thereby limiting its transcriptional activity.

The interaction of PHLPP1 with STAT1, mediated by its NTE, affords fidelity and specificity in its dephosphorylation of the transcription factor. PHLPP1 binding to STAT1 is consistent with this multi-valent protein utilizing its protein-interaction domains to position it near its substrates, either via direct interaction or by binding protein scaffolds, such as PDZ domain proteins that coordinate Akt signaling (155). Such coordination is essential for its dephosphorylation of relevant substrates, in part due to the low catalytic activity of the phosphatase (approximately 1 reaction per sec towards peptide substrates, over an order of magnitude lower than that of the related phosphatase PP2Cα (4)). The importance of enzyme proximity to its substrate is best illustrated with Akt, where deletion of the last 3 amino acids of PHLPP1 to remove the PDZ ligand abolishes the ability of PHLPP1 to dephosphorylate Akt in cells (10). Thus, binding of PHLPP1 via its NTE to STAT1 affords an efficient mechanism to restrict its activity by directly opposing its phosphorylation in the nucleus (Figure 3.12).

The regulation of STAT1 by PHLPP1 occurs in the nucleus, and we identify motifs in the phosphatase that control both the entry into (NLS) and exit from (NES) the nucleus. First, we identify a bipartite NLS in the NTE of PHLPP1 whose integrity is necessary for the phosphatase to regulate the transcriptional activity of STAT1. Second, we identify an NES in the segment between the LRR and PP2C domain that drives export out of the nucleus. Under the 'unstimulated' conditions of our immunocytochemistry, PHLPP1 localized primarily to the cytosol, suggesting masking of the NLS and exposure of the NES. Inputs that regulate the exposure of the NLS and NES are likely important regulators of PHLPP1 function.

Our transcriptomic data support a key role for PHLPP1 in the resolution of the inflammatory response specific to genes downstream of type II IFN signaling pathways. This suggests the possibility that PHLPP1 can selectively discriminate between inflammatory promoters that are differentially regulated by distinct transcription factor families. Surprisingly, over 50% of the inflammatory genes that fail to properly resolve in the macrophages from *Phlpp1*$^{-/-}$ mice contain a consensus STAT-binding motif in their proximal promoters. Our studies have demonstrated a direct interaction between PHLPP1 and STAT1, thus it is highly likely that PHLPP1 is recruited to gene promoters through its association with STAT1. Elevated STAT1 occupancy and delayed dismissal kinetics of STAT1 from its target promoters in *Phlpp1*$^{-/-}$ macrophages indicate a major function of PHLPP1-dependent dephosphorylation in termination of STAT1 signaling and its dismissal from chromatin.

Germline mutations that impair STAT1 function, by reducing either Tyr701 phosphorylation (L706S) or DNA binding (Q463H and E320Q), increase the susceptibility of otherwise healthy patients to mycobacterial and viral infection (164, 165). This increased susceptibility was proposed to arise because of reduced transcription of genes involved in bacterial

and viral immunity from the GAS and ISRE promoters, respectively. Similarly, genetic ablation of *Stat1* on the background of a mouse that has enhanced TLR4 signaling (because of deletion of *Il6st*, a key regulator of systemic inflammatory responses during LPS-mediated endotoxemia) provides protection against LPS-induced toxemic death compared to mice with normal STAT1 levels (166). Although the current study does not provide direct evidence that enhanced phosphorylation of STAT1 causes the protective effect of PHLPP1 loss on both *E. coli*-induced sepsis and LPS-induced endotoxemia in mice, our data indicate that PHLPP1 inhibitors could be explored as adjunctive therapies to antibiotics and supportive care of patients with Gram-negative sepsis, a leading cause of mortality in intensive care units.

MATERIALS AND METHODS

Materials and Antibodies

OA (459616) was purchased from Millipore. Gö6983 (365251) and staurosporine (569397) were purchased from Calbiochem. Antibody against HA (11867425001) was purchased from Roche; antibodies against GFP (2555), STAT1 (9172), phosphorylated Ser727 on STAT1 (9177), phosphorylated Tyr701 on STAT1 (7649), phosphorylated Thr202/Tyr204 on Erk1/2 (9101), total Erk1/2 (9102), and phosphorylated Thr308 on Akt (9275) were purchased from Cell Signaling. Antibody against total Akt (126811) was obtained from AbCam. Antibodies against PHLPP1 were purchased from Cosmo (KIAA0606) and Proteintech (22789-1-AP); antibodies against FLAG (F3165), β-Actin (A2228), and α-tubulin (T6074) were purchased from Sigma-Aldrich. The pcDNA3 HA-tagged PHLPP1 and PHLPP2 constructs for mammalian cell expression were described previously (10, 11, 56). Full-length PHLPP1 was cloned into pCMV 3xFLAG vector (Sigma-Aldrich, E4401). An NLS was cloned to the N-terminus of the PP2C domain of PHLPP1.

A double mutant of NLS-PP2C at residues D1210A and D1413A was cloned by site-directed mutagenesis. The HA-tagged PHLPP1 N-terminal extension (PHLPP1 NTE), residues 1-512, was cloned into pcDNA3 vector (Invitrogen). The NLS1 and NLS2 mutations were cloned by site-directed mutagenesis into HA-PHLPP1 NTE. The NES from PKI (LALKLALDI) was cloned into the N-terminus of HA-PHLPP1 NTE. The PHLPP1 NES (residues 1125-1134, LPPKLQELDL) was subcloned directly downstream of the HA-tag in HA-PHLPP1 NTE, to generate HA-^{PHLPP1}NES-NTE

Isolation and treatment of macrophages

Primary BMDM cells were isolated from male 6- to 8-week-old C57BL/6 mice (Charles River Laboratories). BMDMs were obtained by PBS flush of femurs and tibias (167), red blood cells lysed, and remaining cells plated in RPMI 1640 supplemented with 20% fetal bovine serum (FBS, Gibco, cat. 12657-029), 30% L-cell conditioned medium, 100 U/ml penicillin, 100 µg/ml streptomycin, and 2 mM L-glutamine. Cells were seeded in non-tissue culture treated Optilux Petri dishes (BD Biosciences), incubated at 37 °C in a 5% CO_2 atmosphere for 7 days, then treated with 100 ng/ml KLA (699500, Avanti Polar Lipids) for noted times. Peritoneal macrophages were collected by flushing mouse peritoneal cavities with PBS following 48 hours post peritoneal injection with 3 ml of thioglycolate (168).

Cell culture

MEFs from WT or *Phlpp1*$^{-/-}$ mice stably expressing shp53 were a kind gift from Lloyd Trotman (CSHL) and have been described previously (50); MEFs, HEK-293T, and HeLa (ATCC) cells were grown in Dulbecco's modified Eagle medium (DMEM, 10-013-CV, Corning)

supplemented with 10% fetal bovine serum (S11150, Atlanta biologicals) and 1% penicillin/streptomycin (15140-122, Gibco) at 37 °C in 5% (vol/vol) CO_2. Cells used were periodically tested for *Mycoplasma* contamination using a PCR-based protocol (169) and showed no evidence of contamination.

mRNA isolation and qPCR analysis:

RNA was purified using Direct-zol RNA Miniprep Kits (Zymo Research) from triplicate experiments and quantified using a NanoDrop Spectrophotometer (ThermoFisher Scientific). RNA was either reverse transcribed into cDNA for quantitative real-time PCR using gene-specific primers or used for next-generation library preparation. For cDNA generation, one □g of total mRNA was reverse transcribed using the SuperScript III Reverse Transcriptase (ThermoFisher Scientific). The resulting cDNA (25 ng) was used to perform real-time PCR using SYBR Green Master Mix (ThermoFisher Scientific) and 50 nM mix of forward and reverse primers. The real-time PCR values for individual genes were normalized to the house keeping gene, *36B4*, using the ΔΔCT method (170). The primer sequences used in this study are:

*36B4*_qPCR_F AATCTCCAGAGGCACCATTG

*36B4*_qPCR_R CCGATCTGCAGACACACACT

*Cd69*_qPCR_F CTATCCCTTGGGCTGTGTTAAT

*Cd69*_qPCR_R ACATGGTGGTCAGATGATTCC

*Ifit2*_qPCR_F GAGTTTGAGGACAGGGTGTTTA

*Ifit2*_qPCR_R AGACCTCTGCAGTGCTTTAC

*Gbp5*_qPCR_F GGAAGTGCTGCAGACCTATT

*Gbp5*_qPCR_R GCTCTTTCTTGTTCCGCTTTAC

Next-generation sequence library preparation and analysis

Libraries were prepared from 2 biological replicates per condition. RNA-Seq libraries were prepared as previously described (171). Sequencing libraries were prepared using magnetic beads similar to described previously using barcoded adapters (NextFlex, Bioo Scientific) (172). Libraries were sequenced for 36 or 50 cycles on an Illumina Genome Analyzer II or HiSeq 2000, respectively, according to the manufacturer's instructions. mRNA-Seq results were trimmed to remove A-stretches originating from the library preparation. Each sequence tag returned by the Illumina Pipeline was aligned to the mm10 assembly using ELAND allowing up to 2 mismatches. Only tags that mapped uniquely to the genome were considered for further analysis. Peak finding, MOTIF discovery, and downstream analysis was performed using HOMER, a software suite created for analysis of high-throughput sequencing data (156). Detailed instructions for analysis can be found at http://homer.ucsd.edu/homer/. Data visualization was performed using Microsoft Excel, JavaTreeGraph and software packages available in R.

RNA interference experiments

SMART siRNA pools for examined genes were purchased from Dharmacon (Control: D-001810-10-05, *Stat1*: L-058881). Thioglycollate-elicited peritoneal macrophages were transfected with 30 nM siRNA for 48 h using Deliver X (Affymetrix) according to the manufacturer's instructions prior to being stimulated with KLA for designated times.

Chromatin immunoprecipitation

ChIP assays were performed as described before (173). Cells were crosslinked with 2 mM disuccinimidyl glutarate for 30 min prior to 10 min treatment with 1% formaldehyde. The antibodies used in these studies were: STAT1 (sc-345, Santa Cruz Biotechnology). For the precipitations protein A Dynabeads (10003D, Invitrogen) were coated with antibody prior to pulldown and excess antibody was washed away. Pulldowns occurred while rotating for 16 h at 4 °C. Beads were then washed with TSE I (20 mMTris/HCl pH 7.4 at 20 °C, 150 mM NaCl, 0.1% SDS, 1% Triton X-100, 2 mM EDTA), twice with TSE III (10 mM Tris/HCl pH 7.4 at 20 °C, 250 mM LiCl, 1% IGEPAL CA-630, 0.7% Deoxycholate, 1 mM EDTA), and twice with TE followed by elution from the beads using elution buffer (0.1 M $NaHCO_3$, 1% SDS). Elutions were subsequently de-crosslinked overnight at 65 °C and DNA was purified using ChIP DNA Clean and Concentrator (Zymo Research) and DNA was used for qPCR. The primer sequences used in this study are:

*Cd69*_ChIP_F	TCCCTGCTGTCTGAAATGTG
*Cd69*_ChIP_R	GTGGAAGGATGTCTTCGATTCT
*Ifit2*_ChIP_F	GCATTGTGCAAGGAGAATTCTATG
*Ifit2*_ChIP_R	TTCCGGAATTGGGAGAGAGA
*Gbp5*_ChIP_F	TAAACAGCGCTTGAAACAATGA
*Gbp5*_ChIP_R	AGGCTTGAATGTCACTGAACTA

Luciferase assay

Cells were plated in a 96-well plate and transfected when approximately 80% confluent. Transfections of pRL-CMV encoding Renilla luciferase (156), together with a firefly luciferase

promoter-reporter construct containing eight GAS consensus sequences (174), control vector, or the indicated PHLPP constructs, were performed using Lipofectamine 3000 reagent (Invitrogen, L3000) for MEFs or Fugene 6 reagent (Promega, E269A) for HEK-293T cells. Cells were treated with murine or human IFNγ (PeproTech, 315-05, 300-02, respectively) for the indicated times at 37 °C and activity was measured using the Dual-Glo Luciferase Assay System (Promega, E2940) in a Tecan Infinite M200 Pro multi-well plate reader. Promoter activity was corrected for the luciferase activity of the internal control plasmid, pRL-CMV, and Relative Response Ratios (RRR) were calculated.

Immunoprecipitation and western blot

DNA was transfected into HEK-293T cells using FuGene 6. Cells were collected 24 h post-transfection and then lysed in a buffer containing 50 mM Na_2HPO_4 (pH 7.5), 1 mM sodium pyrophosphate, 20 mM NaF, 2 mM EDTA, 2 mM EGTA, 1% SDS, 1 mM DTT, 1 μM microcystin, 20 μM benzamidine, 40 μg/ml leupeptin, and 1 mM PMSF and then were sonicated briefly. For co-immunoprecipitation, cells were lysed and the detergent-solubilized cell lysates were incubated with an anti-HA antibody (BioLegend, 901503) at 4 °C overnight. Samples were incubated with protein A/G PLUS-Agarose (Santa Cruz Cat sc-2003) for 1 h at 4 °C and washed three times in lysis buffer containing 0.3 M NaCl and 0.1% Triton X 100. Bound proteins and lysates were separated by SDS/PAGE gel and analyzed by western blot.

Immunofluorescence

HeLa cells were plated on glass coverslips and transfected using FuGene 6. 24 h after transfection, cells were fixed with 4% paraformaldehyde for 20 min at room temperature, followed

by fixation with 100% methanol for 3 min at -20 °C. Cells were permeabilized and blocked in 0.3% Triton X 100 and 3% BSA for 30 min at room temperature, followed by three 5-min washes in PBS-T. Primary antibodies were diluted at the following dilutions: mouse anti-HA, 1:500; rabbit anti-α-tubulin (Cell Signaling, 2125), 1:200. Secondary antibodies were diluted at the following dilutions: Alexa647 anti-mouse (Life Technologies, A21235), 1:500; Alexa488 anti-rabbit (Life Technologies, A11034), 1:500. Coverslips were mounted onto slides with ProLong Diamond Antifade Mountant with DAPI (ThermoFisher, P36966). Images were acquired on a Zeiss Axiovert 200M microscope (Carl Zeiss Microimaging Inc.) using an iXon Ultra 888 EMCCD camera (ANDOR) controlled by MetaFluor software (Molecular Devices) and analyzed on ImageJ (NIH). The Nuclear to Cytoplasmic ratio was calculated as follows: the mean signal intensity was measured for a region of the nucleus and cytoplasm for each cell, and the mean signal intensity of the background was subtracted from these values. Then the Nuclear to Cytoplasmic ratio was calculated by dividing the background subtracted mean signal intensity for the nuclear signal by the background subtracted value for the cytoplasmic signal.

In vitro **phosphatase assay**

pCMV 3xFLAG PHLPP1 was transfected into HEK-293T cells plated in four 10 cm plates (approximately 9 x 10^6 cells per plate, 80% transfection efficiency) using Fugene 6. Cells were collected 48 h post-transfection and lysed in a buffer containing 20 mM Tris (pH 7.5), 150 mM NaCl, 1 mM EDTA, 1 mM EGTA, 1% Triton X 100, 2.5 mM sodium pyrophosphate, 1 mM Na_3VO_4, 1 mM DTT, 1 mM PMSF, 1 μM microcystin, 20 μM benzamidine, and 40 μg/ml leupeptin. The detergent-solubilized cell lysates were incubated with anti-FLAG M2 affinity gel (30 μl per plate, Sigma-Aldrich, A2220) for 1 h at 4 °C, washed four times in lysis buffer and the

beads were resuspended in 40 µl 200 mM Tris, 4 mM DTT, 20 mM $MnCl_2$ for use in *in vitro* phosphatase assay. STAT1 (0.3 µM) (Biosource, PHF0011) was phosphorylated *in vitro* by incubation with recombinant human cdk1/cyclinB (0.2 µM) (Millipore, 14-450) at 30 °C for 90 min in the presence of 1 mM ATP, and 1 X PK buffer (NEB, B6022) containing 50 mM Tris, 10 mM $MgCl_2$, 0.1 mM EDTA, 2 mM DTT, 0.01% Brij, pH 7.5, and the reaction was quenched by addition of 144 µM CDK1 inhibitor RO3306 (Enzo, ALX-270-463). Phosphorylated STAT1 substrate was added to 1/4 volume of beads with bound PHLPP1 (or to lysis buffer control) and reactions were allowed to proceed for an additional 120 min at 30 °C. For the zero minute time point, beads were added after the 120 min incubation and all reactions were immediately quenched with 4xSB (sample buffer). Samples were analyzed by western blot.

Mouse infection and endotoxin challenge

Bacterial sepsis in mice was induced by injection of *E. coli* K1 strain RS218 and LPS endotoxemia was induced by injection of purified *E. coli* O111:B4 LPS (Sigma-Aldrich). The *E. coli* culture was grown overnight in Luria broth (LB) medium (Hardy Diagnostics) at 37°C with shaking. The bacterial culture was diluted 1:50 in fresh LB, grown to mid-log phase, washed twice with PBS and reconstituted in PBS to yield the appropriate inoculum. For survival experiments, 10 to 14-week-old female C57BL/6 WT and littermate control *Phlpp1*$^{-/-}$ mice were injected i.p. with 5 x 10^7 colony forming units (cfu) *E. coli* or 15 mg/kg LPS and mouse survival recorded for 10 days following injection. For measurement of serum IL-6, IL-10 and IL-1β levels, mice were injected with 10 mg/kg LPS, and at 4, 8, 12 and 24 h after injection, 80 µl of blood was collected by submandibular bleeding using a lancet into a serum separating blood collection tubes (BD) that were spun at 1500 × *g* for 10 min to separate serum. Serum cytokines were quantified by specific

ELISA (R&D) following the manufacturer's protocol. All protocols for mouse experiments were conducted in accordance with the institutional guidelines and were approved by the Institutional Animal Care and Usage Committee (IACUC) at the University of California, San Diego.

Data Availability

Sequencing data have been deposited in GEO under accession code GSE116314, under the title "Transcriptomic changes in wild-type and Phlpp1-/- mice following KLA stimulation". All data generated or anaklysed during this study are included in the manuscript and supporting files.

ACKNOWLEDGMENTS

We thank Maya Kunkel for advice and Mira Sastri, Gregory Fonseca, and Ali Syed for assistance with reagents and methodologies. This work was supported by NIH R35 GM122523 (A.C.N.), NIH GM067946 (A.C.N.), NIH HL125352 (V.N.), NIH DK091183 (C.K.G.) and DK063491 (C.K.G.). K.C.-K. was supported in part by NIH/NCI T32 CA009523 and A.T.K. was supported in part by the University of California San Diego Graduate Training Grant in Cellular and Molecular Pharmacology through the National Institutes of Health Institutional Training Grant T32 GM007752 from the NIGMS.

Chapter 3, in full, is a reprint of material that appears in "PHLPP1 Counter-Regulates STAT1-mediated Inflammatory Signaling", as published by Ksenya Cohen-Katsenelson, Joshua D. Stender, Agnieszka T. Kawashima, Gema Lordén, Satoshi Uchiyama, Victor Nizet, Christopher K. Glass, and Alexandra C. Newton. The dissertation author was a co-first author, along with Ksenya Cohen-Katsenelson and Joshua D. Stender, on this publication. The dissertation authors

contributions specifically were: subcloning of the PHLPP1 NTE for use in multiple figures, Figure 3.6.D-G, Figure 3.9.A-B, and Figure 3.10.A-B.

FIGURES

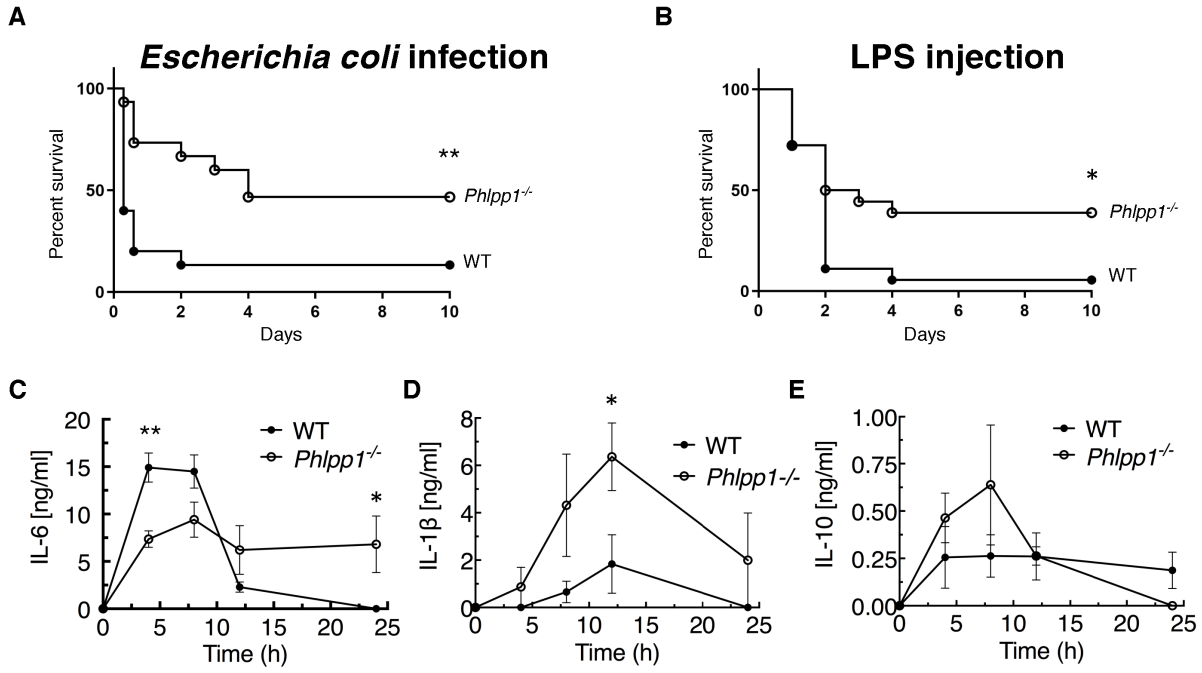

Figure 3.1: PHLPP1 knock-out mice are protected against sepsis-induced death. (A) Survival curve of WT and *Phlpp1*$^{-/-}$ mice i.p. infected with 1x10^{7} cfu of *E. coli*. Values are expressed as percent survival of 15 mice for each genotype. ** $p < 0.01$ by log-rank test. (**B**) Survival curve of WT and *Phlpp1*$^{-/-}$ mice i.p. injected with 15 mg/kg LPS. Values are expressed as percent survival of 16 mice for each genotype. * $p < 0.05$ by log-rank test. (**C-E**) ELISA showing IL-6 (**C**), IL-1β (**D**) and IL-10 (**E**) levels in serum at the indicated times after i.p. injection of 10 mg/kg LPS. Data represent mean ± SEM. Statistics analyzed by Student's *t*-test *$p < 0.05$, **$p < 0.01$.

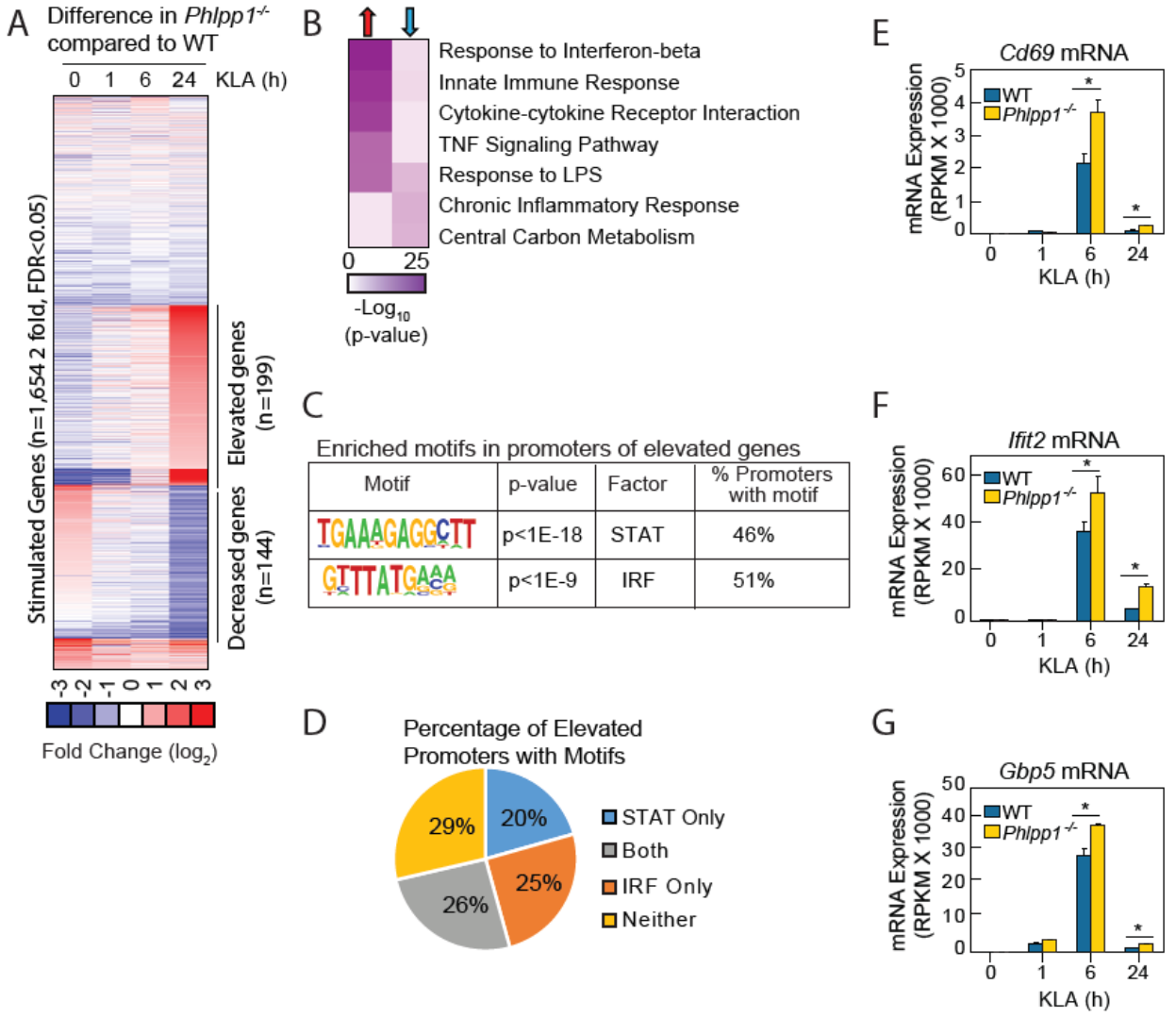

Figure 3.2: Loss of PHLPP1 modulates the expression of inflammatory genes in macrophages. (**A**) Heat map for mRNA-Seq expression of the 1,654 mRNA transcripts regulated greater than two-fold with a FDR < 0.05 in BMDMs isolated from WT or *Phlpp1*$^{-/-}$ animals treated with 100 ng/ml KLA for 1, 6 or 24 h. Data represent the $\log_2$ difference between the mRNA expression in *Phlpp1*$^{-/-}$ macrophages compared to wild-type macrophages. (**B**) Gene ontology analysis for the 199 elevated (red arrow) or 144 decreased (blue arrow) transcripts in *Phlpp1*$^{-/-}$ macrophages compared to wild-type macrophages. (**C**) *De novo* motif analysis using HOMER (Hypergeometric Optimization of Motif EnRichment) for the 199 promoters corresponding to the genes elevated in the *Phlpp1*$^{-/-}$ macrophages. (**D**) Pie graph showing the percentage of promoters of elevated genes that contain STAT or IRF binding motifs. (**E-G**) Normalized mRNA-Seq values for (**E**) *Cd69* (**F**) *Ifit2* and (**G**) *Gbp5* mRNA in BMDMs isolated from WT or *Phlpp1*$^{-/-}$ animals treated with 100 ng/ml KLA for 0, 1, 6, or 24 h. RPKM – Reads Per Kilobase Million. Values are expressed as mean ± SEM. *p < 0.05 (Student's *t*-test) compared to WT cells.

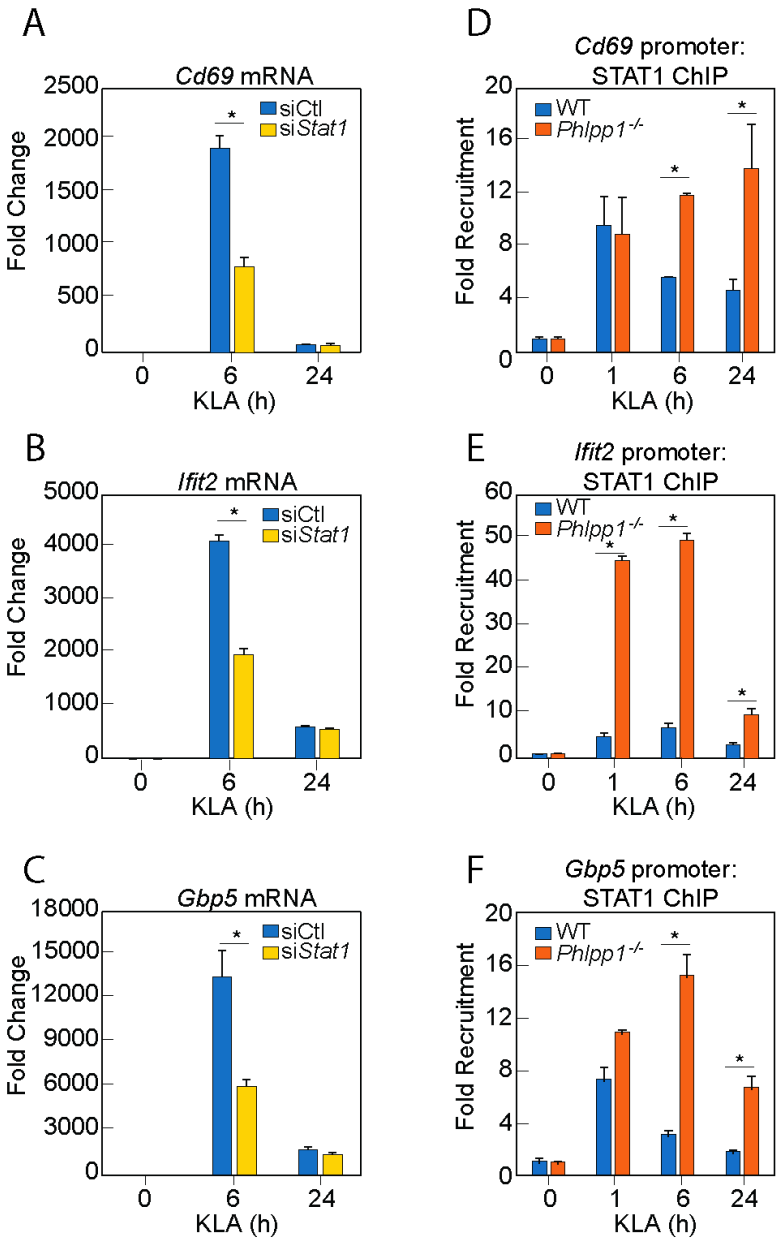

Figure 3.3: PHLPP1 controls STAT1 genomic recruitment and STAT1-dependent gene expression. (**A-C**) Quantitative PCR analysis for (**A**) *Cd69* (**B**) *Ifit2* and (**C**) *Gbp5* mRNA isolated from thioglycollate-elicited peritoneal macrophages treated with control siRNA (siCtl) or siRNA specifically targeting *Stat1* (si*Stat1*) and subsequently treated with vehicle or 100 ng/ml KLA for 6 or 24 h. Values are expressed as mean ± SEM from replicate experiments. *$p < 0.05$ (Student's *t*-test) compared to siCtl treated cells. (**D-F**) Quantitative PCR analysis of ChIPs for STAT1 at the (**D**) *Cd69* (**E**) *Ifit2* and (**F**) *Gbp5* promoter in BMDMs isolated from WT or *Phlpp1*$^{-/-}$ animals and treated with 100 ng/ml KLA for 0, 1, 6 or 24 h. Values are expressed as mean ± SEM. *$p < 0.05$ (Student's *t*-test) compared to WT cells.

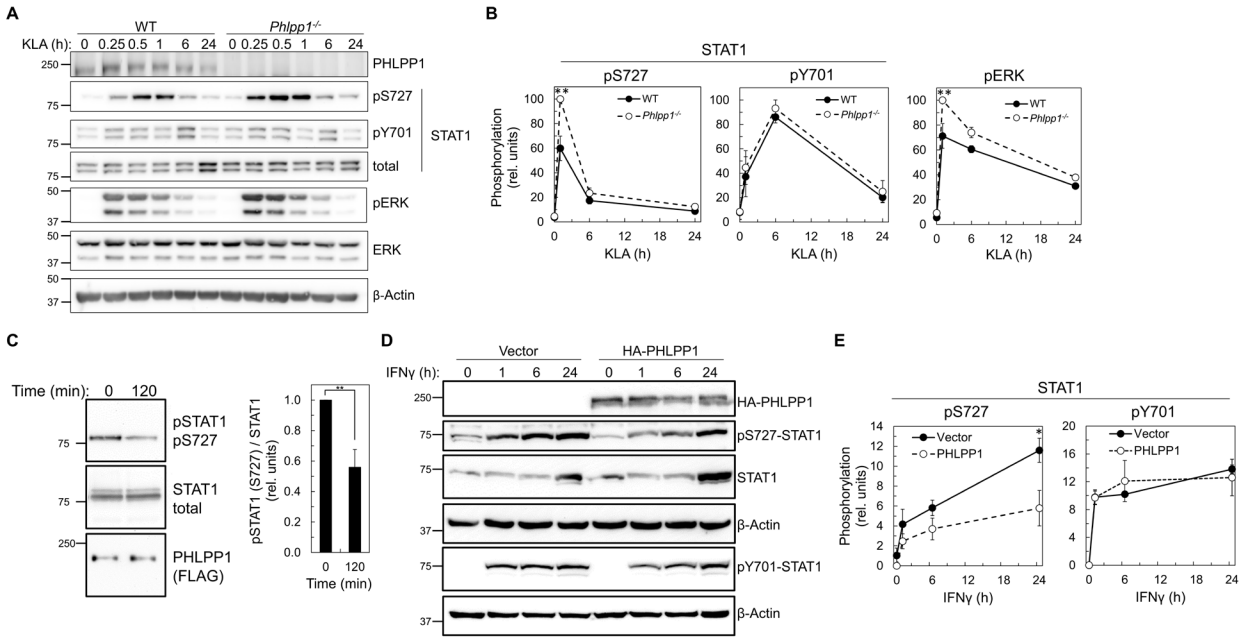

Figure 3.4: PHLPP1 regulates STAT1 phosphorylation on Ser727. (**A**) Western blot analysis of primary BMDM from WT or *Phlpp1*$^{-/-}$ mice treated with 100 ng/ml KLA for the indicated times and probed with the indicated antibodies. (**B**) Ratio of pSTAT1 (S727):total STAT1, pSTAT1 (Y701):total STAT1 or phosphoERK (T202/Y204):total ERK normalized to the highest value; data represent the mean ± SEM of five independent experiments as in (A). ** $p < 0.01$ (Student's *t*-test) compared to WT cells. (**C**) Western blot analysis of an *in vitro* phosphatase assay of purified and phosphorylated STAT1 and immunoprecipitated FLAG-PHLPP1, incubated for 0 or 120 min at 30 °C (on the left). On the right, quantification of pSTAT1 (S727) divided by total STAT1 and normalized to 0 time point. Values are expressed as mean ± SEM of three independent experiments. ** $p < 0.01$ (Student's *t*-test). (**D**) Western blot analysis of HEK-293T cells over-expressing vector control (Vector) or HA-tagged PHLPP1 and treated with 10 ng/ml IFNγ for 0, 1, 6, or 24 h. (**E**) Graphs represent the quantification of three independent experiments as presented in (D). Values are expressed as mean relative units of pSTAT1 (S727) or (Y701) divided by β-Actin and normalized to vector 0 h ± SEM. * $p < 0.05$ (Student's *t*-test) compared to vector control expressing cells.

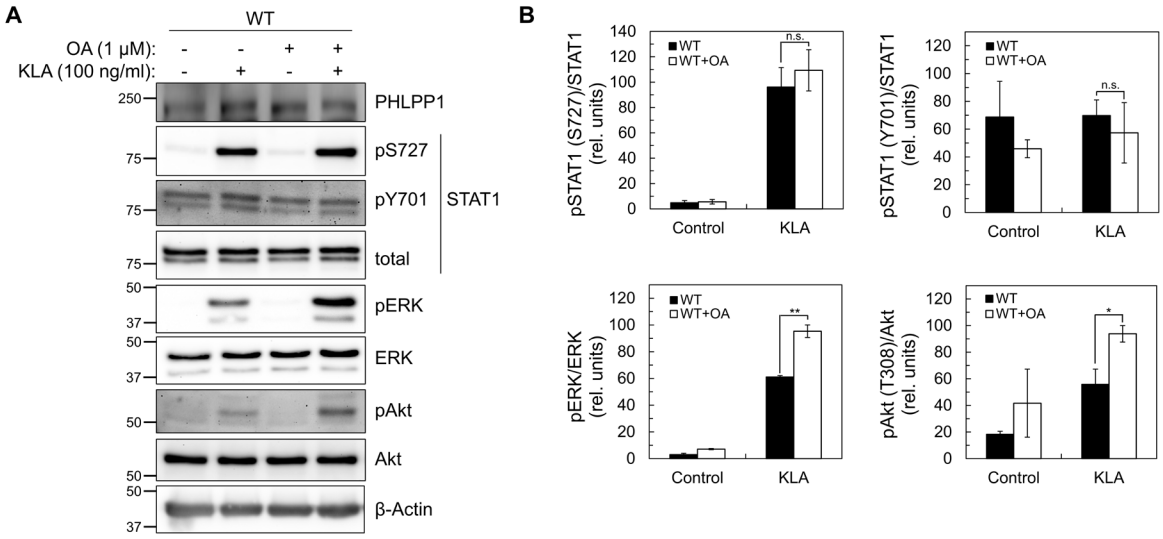

Figure 3.5: STAT1 Ser727 phosphorylation and transcriptional activity are insensitive to okadaic acid. (**A**) Western blot analysis of primary BMDMs from WT or *Phlpp1*$^{-/-}$ mice treated with 100 ng/ml KLA for 0 or 30 min followed by treatment with 1 μM OA or DMSO control for an additional 15 min. and probed with the indicated antibodies; pAkt antibody recognizes phosphorylated Thr308 (**B**) Graph represents the quantification of three independent experiments as presented in (A). Values are expressed as the mean ± SEM of the ratio of pSTAT1 (S727) to total STAT1 normalized to the highest value; * $p<0.05$, ** $p<0.01$ and n.s.- non-significant (Student's *t*-test).

Figure 3.6: PHLPP1 suppresses STAT1 transcriptional activity by a mechanism that depends on its catalytic activity and an NLS in its N-Terminal Extension (**A**) Luciferase reporter assay in WT (+/+) and *Phlpp1*$^{-/-}$ (-/-) MEFs over-expressing GAS luciferase reporter and treated with 10 ng/ml IFNγ for 0, 1, 6, or 24 h in combination with 1 μM OA or DMSO control treatment for 15 minutes. Values are expressed as mean of relative light units (RLU) ± SEM of three independent experiments. *p < 0.05 (Student's *t*-test). See also **Figure 6-figure supplement 1**. (**B**) Schematic of HA-tagged PHLPP1 constructs used in this study: the PP2C domain of PHLPP1 (PP2C), nuclear targeted PP2C with NLS (NLS- PP2C), NLS-PP2C with active site residues Asp1210 and Asp1413 residues mutated to Ala (NLS-PP2C DDAA), and full-length PHLPP1 (PHLPP1). (**C**) Luciferase reporter assay in HEK-293T cells over-expressing GAS luciferase reporter in combination with either vector control (vector, black) or the constructs described in (B) and treated with 10 ng/ml IFNγ for 0, 1, 6, or 24 h. Values are expressed as mean RLU ± SEM of four independent experiments. All data points at 24 h were significant against each other except for vector to PP2C, vector to NLS-PP2C DDAA, P1 to NLS-PP2C, and PP2C to NLS-PP2C DDAA. * p < 0.05, ** p < 0.01 (Student's *t*-test). (**D**) Schematic showing position and sequence of bipartite NLS in the NTE, and NLS mutants used in this study. (**E**) HeLa cells over-expressing the constructs used in Figure 6D were stained for HA (green), α-Tubulin (red), and DAPI (blue). Scale bar indicates 15 μm. (**F**) The Nuclear to Cytoplasmic ratio was calculated for each construct (300 cells per construct) and values are expressed as mean ± SEM. All data points were significant against each other except for NLS1 to NLS2, and NLS2 to NLS1/2. ** p < 0.01, n.s. – non-significant (Student's *t*-test). (**G**) Luciferase reporter assay in HEK-293T cells over-expressing a GAS luciferase reporter in combination with either vector control (vector, black) or the constructs described in (D) however in the context of a full-length PHLPP1 and treated with 10 ng/ml IFNγ for 0, 1, 6, or 24 h. Values are expressed as mean RLU ± SEM of eight independent experiments. *p < 0.05, **p < 0.01, n.s. - non-significant (Student's *t*-test).

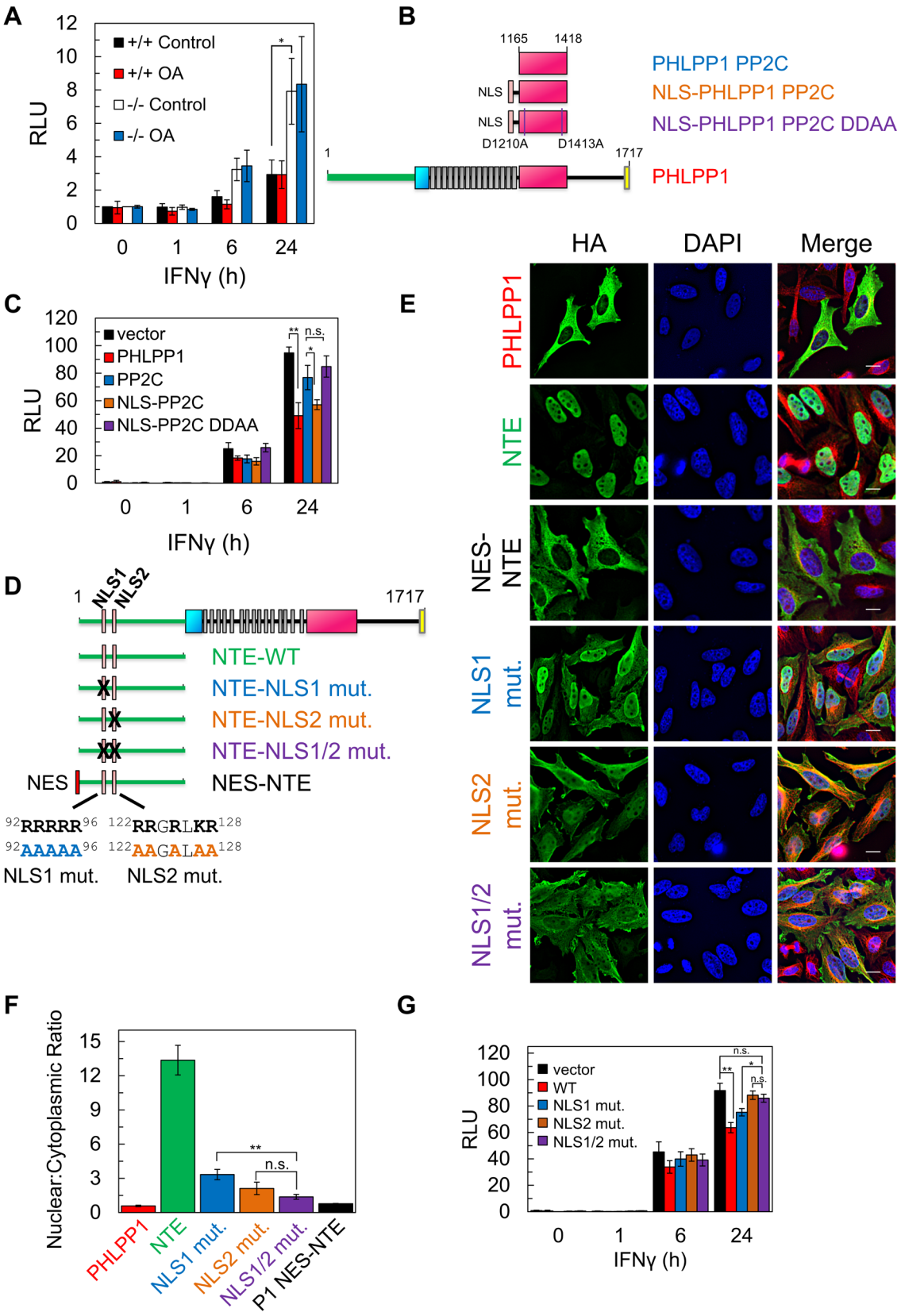
A
RLU
+/+ Control
+/+ OA
-/- Control
-/- OA
IFNγ (h)
B
1165
1418
NLS
NLS
D1210A
D1413A
1
1717
PHLPP1 PP2C
NLS-PHLPP1 PP2C
NLS-PHLPP1 PP2C DDAA
PHLPP1
C
vector
PHLPP1
PP2C
NLS-PP2C
NLS-PP2C DDAA
RLU
IFNγ (h)
D
NLS1
NLS2
1717
NTE-WT
NTE-NLS1 mut.
NTE-NLS2 mut.
NTE-NLS1/2 mut.
NES
NES-NTE
92RRRRR96 122RRGRLKR128
92AAAAA96 122AAGALAA128
NLS1 mut.
NLS2 mut.
E
HA
DAPI
Merge
PHLPP1
NTE
NES-NTE
NLS1 mut.
NLS2 mut.
NLS1/2 mut.
F
Nuclear:Cytoplasmic Ratio
PHLPP1
NTE
NLS1 mut.
NLS2 mut.
NLS1/2 mut.
P1 NES-NTE
G
RLU
vector
WT
NLS1 mut.
NLS2 mut.
NLS1/2 mut.
IFNγ (h)

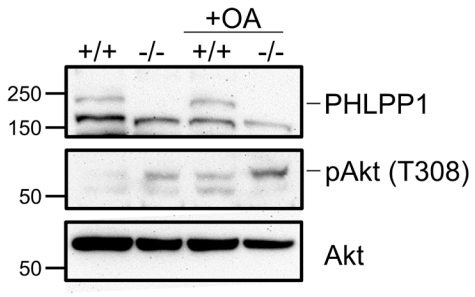

Figure 3.7: STAT1 phosphorylation and transcriptional activity are insensitive to okadaic acid. Western blot analysis of extracts used in the luciferase reporter assay in WT (+/+) and *Phlpp1*$^{-/-}$ (-/-) MEFs over-expressing GAS luciferase reporter and treated with 10 ng/ml IFNγ for 0 or 24 h in combination with 1 μM OA or DMSO control treatment for 15 minutes. Phosphorylation of the PP2A target site on Akt (Thr308) was increased upon OA treatment.

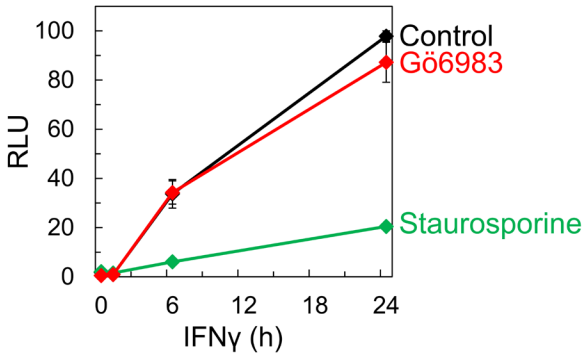

Figure 3.8: Inhibition of PKC does not affect STAT1 activity. Luciferase reporter assay in HEK-293T cells over-expressing GAS luciferase reporter and treated with 10 ng/ml IFNγ for 0, 1, 6, or 24 h followed by 250 nM Gö6983 for 10 min, 1 μM staurosporine for 30 min, or DMSO control. Values are expressed as mean of RLU ± SEM of three independent experiments.

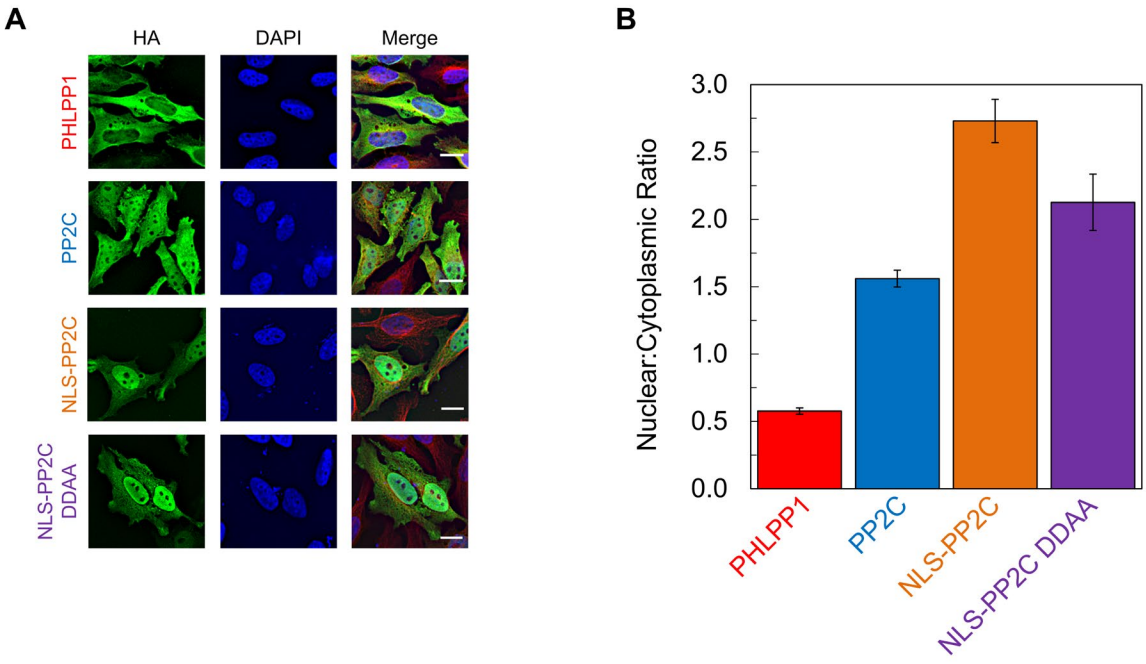

Figure 3.9: The phosphatase activity of PHLPP1 is important for the regulation of STAT1 activity. (**A**) HeLa cells over-expressing the HA-tagged constructs used in Figure 6B were stained for HA (green), α-Tubulin (red), and DAPI (blue). Scale bar indicates 15 μm. (**B**) The Nuclear to Cytoplasmic ratio was calculated for each construct and values are expressed as mean ± SEM of: 169 cells for P1, 101 cells for PP2C, 100 cells for NLS-PP2C, and 101 cells for NLS-PP2C DDAA.

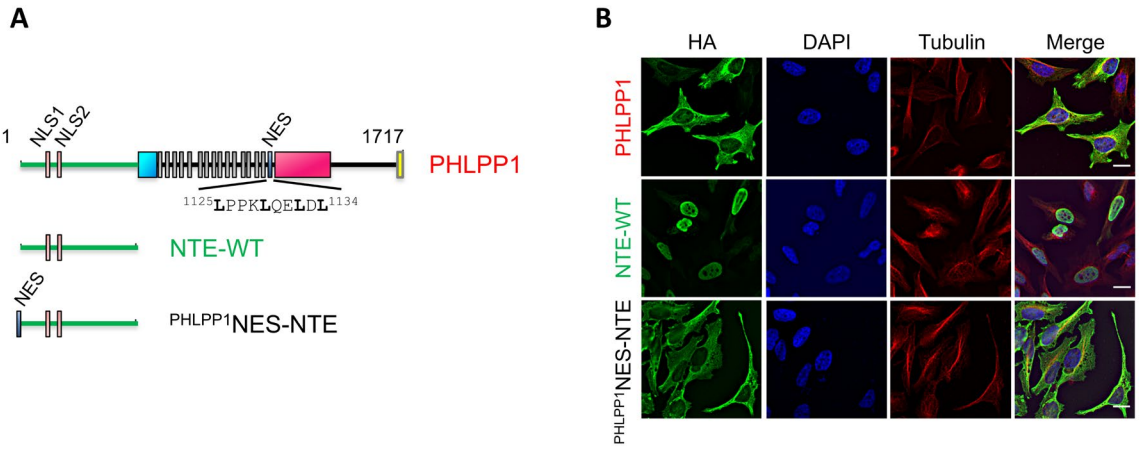

Figure 3.10: PHLPP1 has a nuclear export signal (NES). (**A**) Schematic showing position of NES (residues 1125-1134) immediately following the last LRR. (**B**) HeLa cells over-expressing PHLPP1, the NTE from WT PHLPP1 (NTE-WT) or the NTE-WT in which the PHLPP1 NES was fused to the N-terminus (^{PHLPP1}NES-NTE) were stained for HA (green), α-Tubulin (red), and DAPI (blue). Scale bar indicates 15 μm.

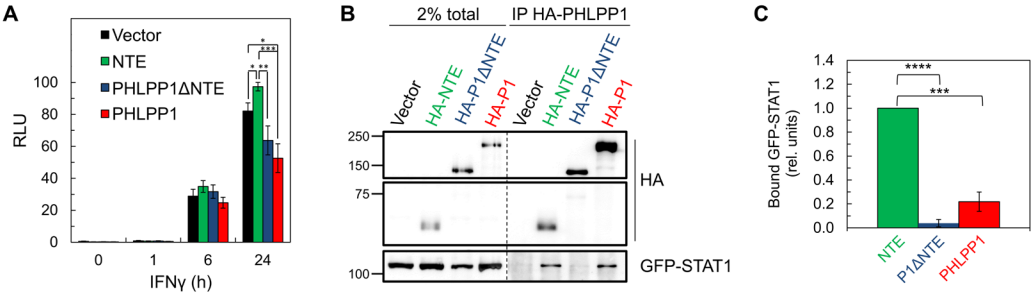

Figure 3.11: STAT1 associates with the N-terminal extension of PHLPP1 (**A**) Luciferase reporter assay in HEK-293T cells over-expressing GAS luciferase reporter in combination with either vector control (Vector, black), PHLPP1 NTE (NTE, green), PHLPP1ΔNTE (blue), or PHLPP1 (red) and treated with 10 ng/ml IFNγ for 0, 1, 6, or 24 h. Values are expressed as mean of RLU ± SEM of five independent experiments. All data points at 24 h were significant against each other except for vector to PHLPP1ΔNTE, and PHLPP1ΔNTE to PHLPP1. * $p < 0.05$, ** $p < 0.01$, *** $p < 0.001$ (Student's *t*-test). (**B**) Western blot analysis of detergent-solubilized lysate of HEK-293T cells transfected with vector control (Vector), HA-tagged NTE of PHLPP1, PHLPP1 with the NTE deleted (P1ΔNTE) or full-length PHLPP1 (HA-P1) and immunoprecipitated (IP) using HA antibody; blots were probed for co-IP of STAT1 tag using GFP antibody. (**C**) Quantification of GFP-STAT1 IP divided by HA IP and normalized to HA-NTE IP. Values are expressed as mean ± SEM of three independent experiments. *** $p < 0.001$, **** $p < 0.0001$ (Student's *t*-test).

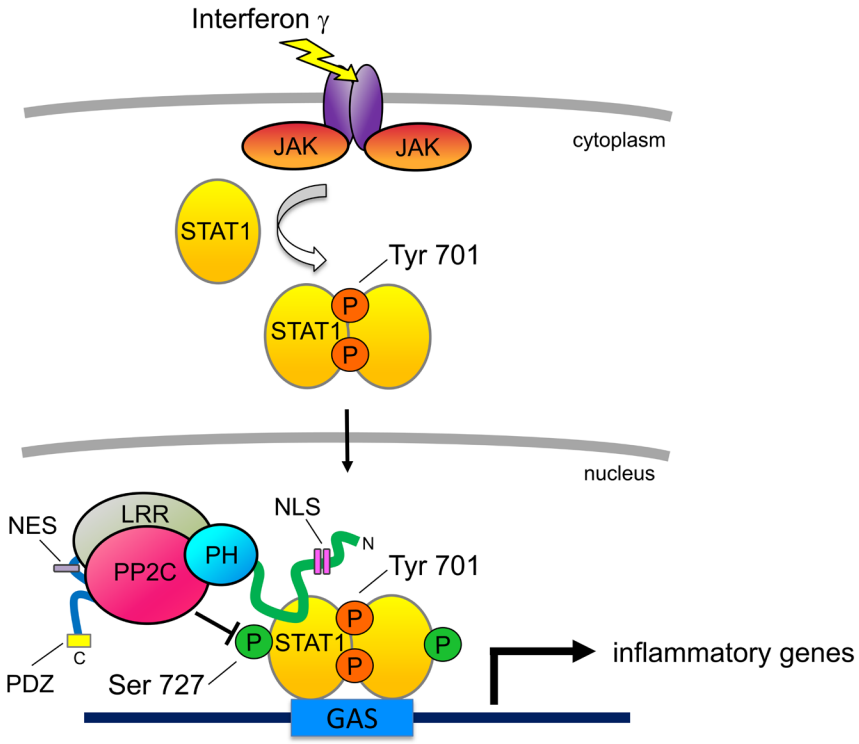

Figure 3.12: Proposed model for PHLPP1-dependent suppression of STAT1 activity. Binding of IFNγ to IFN receptors results in their dimerization and phosphorylation, promoting the recruitment of JAK, which phosphorylates STAT1 on Tyr701 by JAK. This promotes the dimerization of STAT1 and its translocation into the nucleus where it binds the GAS promoter to allow the transcription of inflammatory response genes. Activity of STAT1 is enhanced by phosphorylation on Ser727. However, nuclear-localized PHLPP1, which binds STAT1 via its N-terminal extension, tunes the activity of STAT1 by directly dephosphorylating this site to keep activity finely controlled. Loss of PHLPP1 results in poor resolution of inflammatory response. The nuclear localization of PHLPP1 is controlled by a bipartite NLS (pink rectangles) in the NTE (green line) and an NES (purple rectangle) in the segment between the LRR (grey oval) and the PP2C domain (red oval).

Supplemental Dataset 3 – Related to Figure 2.2
List of 199 KLA-induced genes that are elevated in *Phlpp1*$^{-/-}$ BMDMs compared to WT cells.

Supplemental Dataset 4 – Related to Figure 2.2
List of 144 KLA-induced genes that are reduced in *Phlpp1*$^{-/-}$ BMDMs compared to WT cells.

Chapter 4 – PHLPP1 Expression is Sensitive to Extracellular Glutamine Levels

ABSTRACT

Glutamine plays a critical role in a variety of metabolic pathways, such as the Krebs cycle, nucleotide synthesis, and the generation of antioxidants. A growing body of evidence suggests that changes in glutamine levels can affect gene expression. Here we report that the expression of the tumor suppressor phosphatase PH domain Leucine-rich repeat Protein Phosphatase 1 (PHLPP1) is sensitive to changes in extracellular glutamine levels. Specifically, we show that in two-dimensional cell culture systems, PHLPP1 expression and activity against histone substrates are decreased as cells reach confluency, a condition where extracellular glutamine is depleted. When cells are seeded at a low confluency and cultured in the presence of either media from high confluency cells or media lacking glutamine, the dilution-triggered increase in PHLPP1 expression is abolished, and PHLPP1 expression remains low. This suggests that PHLPP1 expression is sensitive to glutamine levels. As glutamine metabolism is severely altered in cancer cells, this finding can provide a potential mechanism to explain how the expression of this tumor suppressor is altered during tumorigenesis.

INTRODUCTION

Nutrients derived from the environment play an essential role in regulating cellular metabolism. The uptake of key nutrients, such as glucose and glutamine, are needed for cells to grow and divide. Irregularities in the metabolism of these nutrients are key hallmarks of cancer and other metabolic diseases (175, 176). Cancer cells frequently exhibit the Warburg effect (177), a critical metabolic shift from utilizing mitochondrial respiration for the breakdown of glucose to generate ATP to relying primarily on aerobic glycolysis as a more rapid means to generate ATP;

this shift is a key factor for any cancer cell that wants to survive and thrive. Deregulated glutamine metabolism occurs in a large variety of cancers (178). Additionally, high extracellular glutamine levels result in increased tumor growth and cellular transformation, and glutamine breakdown occurs at higher rates in tumor cells (178, 179). Thus, proper regulation of glucose and glutamine metabolism in the cell are critical to maintain cellular homeostasis.

The metabolism of both glucose and glutamine converge in the Krebs cycle, where a series of reactions occur within the mitochondria that result in the generation of ATP, NADH, and CO_2. Glucose is shuttled into the cell following insulin stimulation via glucose transporters, such as GLUT4 (180), and converted to pyruvate in the cytoplasm during glycolysis. Once in the mitochondria, pyruvate is decarboxylated to generate acetyl coenzyme A (acetyl-CoA), the initial substrate of the Krebs cycle. Glutamine metabolism feeds into this cycle via the intermediate alpha-ketoglutarate. Extracellular glutamine transport is facilitated through the function of two transmembrane amino acid transporters found at the plasma membrane, ASCT2 (SLC1A5) (181) and LAT1 (SLC7A5) (182). While glutamine is imported into the cell via ASCT2, excess cellular glutamine is exported via the LAT1 transporter; this function is coupled to cellular leucine intake (183). Both of these transporters are up-regulated in a variety of different cancers (184, 185). Thus, both of these key nutrients, which are often supplemented into mammalian tissue culture media, are critical for maintaining cellular growth and proliferation.

Glucose and glutamine metabolism contribute to other cellular signaling pathways as well. For example, various byproducts of the Krebs cycle function as co-factors for enzymes that post-translationally modify histone proteins. Acetyl-CoA is a substrate of histone acetyltransferases whose activity results in the acetylation of histone lysine residues, a mark of "active" transcriptional regions (186). NAD^+ is a co-factor of the Sirtuin family of histone deacetylases

(187), while alpha-ketoglutarate is a co-factor of demethylases which function to remove methyl groups from histone lysine residues (188). Disruption in epigenetic regulation, and the subsequent effects on downstream transcription, have been implicated in many different cancers (189). The coupled activity of the glutamine transporters ASCT2 and LAT1 results in the activation of mTOR signaling due to increased leucine uptake, resulting in increased cellular proliferation and growth (183). Inhibition of these enzymes with small molecules can suppress tumor growth *in vivo*. Moreover, depletion of either glucose or glutamine results in global changes in gene expression (190). In this study, we identify that the expression of the tumor suppressor phosphatase PH domain Leucine-rich repeat Protein Phosphatase 1 (PHLPP1) is sensitive to the levels of extracellular glutamine.

PHLPP1 was originally discovered during the search for the phosphatase that negatively regulates Akt at the hydrophobic motif, Ser473. By dephosphorylating this residue directly, PHLPP1 is able to suppress pro-survival signaling through Akt. Thus, loss of PHLPP1 would promote cellular growth and proliferation through increased Akt signaling. Not only is the gene encoding *PHLPP1* frequently deleted in a multitude of cancers (47, 48, 83, 84), but various mouse models have shown that the deletion of PHLPP1 results in increased tumor growth and metastasis (51, 85). Other substrates of PHLPP1 have since been identified, including kinases such as protein kinase C (PKC) (11), ribosomal protein S6 kinase 1 (S6K1) (12), and Mst1 (13, 191). Recently, PHLPP1 has been implicated in two separate signaling pathways that converge on gene expression regulation. Namely, PHLPP1 controls receptor tyrosine kinase transcription by suppressing histone phosphorylation (14), and it suppresses inflammatory signaling in macrophages by dephosphorylating the transcription factor STAT1 (64). This same study also identified a nuclear

localization signal (NLS) within the previously uncharacterized PHLPP1 N-terminal extension (64).

In addition to the identification of downstream targets of PHLPP1, there have been interesting findings regarding the regulation of PHLPP1 itself; increasing evidence suggests that PHLPP1 expression is dynamically regulated on the transcriptional, translational, and post-translational levels. In the context of bone development, stimulation with transforming growth factor beta (TFGβ) results in deacetylation of the *PHLPP1* promoter by HDAC3, causing a decrease in PHLPP1 expression (29). A follow up study also identified a decrease in *PHLPP1* promoter methylation and increased PHLPP1 expression in human articular cartilage and chondrocyte cell lines (31). Other extracellular factors have been identified as controlling PHLPP1 expression as well. The chemokine CXCL13 stimulates PHLPP1 expression in NIH-3T3-L1 cells (192), while leptin and LPS appear to reduce PHLPP1 expression in bone marrow-derived macrophages (62, 63, 65). PHLPP1 expression and phosphorylation are also dynamically regulated during the cell cycle, peaking during mitosis (see Chapter 2). Additionally, a vast number of studies have identified many micro RNAs that impact the levels of PHLPP1 transcripts in the cell (33-36). Lastly, phosphorylation and ubiquitination of a phospho-degron motif within the PP2C catalytic domain of PHLPP1 results in the degradation of PHLPP1 following Akt inactivation (41); this negative feedback loop is uncoupled in glioblastoma (121). These studies all suggest that PHLPP1 expression is regulated by both extracellular and intracellular cues.

In this study, we propose that PHLPP1 expression is regulated by the levels of extracellular glutamine. We specifically show that cultures grown at high confluency have depleted levels of PHLPP1 protein and mRNA. Using conditioned media, we were able to determine that this is due to the depletion of glutamine from the extracellular environment rather than the downstream action

of a secreted protein. We also show that histone modifications that are suppressed by PHLPP1 – specifically histone H3 acLys9, acLys27, and pSer10 – are also sensitive to changes in cellular confluency in a PHLPP1-dependent manner. These data provide novel insight into how PHLPP1 expression is regulated by changes in nutrient levels, a link that could explain loss of PHLPP1 expression during cancer.

RESULTS

PHLPP1 protein and mRNA levels are sensitive to cellular confluency.

To explore the effects of the extracellular environment on PHLPP1 expression in cell culture, we examined PHLPP1 protein levels in cells grown at varying levels of confluency. Wild-type mouse embryonic fibroblasts (WT MEFs) were seeded at various levels of confluency and lysed 24 hours later, after which PHLPP1 and PHLPP2 levels were analyzed by western blot. As the number of cells in two-dimensional cell culture increased, the amount of total PHLPP1 protein was reduced (Figure 4.1.A); levels of the closely related family member PHLPP2 were unchanged. A five-fold reduction in PHLPP1 protein was observed in high confluency cells compared to low confluency cells (Figure 4.1.B). We performed this same experiment in other cell lines and found that while some lines exhibited this effect (NIH-3T3, HEK-293A, Figure 4.1.C lanes 1-3), others did not (SF-268, U-251) (Figure 4.1.C lanes 4-6). To determine if this effect occurred on the transcriptional level, we performed RT-qPCR and assessed whether mRNA levels of *Phlpp1* were affected by changes in cellular confluency. *Phlpp1* mRNA levels were reduced by three-fold at higher cellular confluency levels relative to the low confluency condition (Figure 4.1.D). To determine how quickly PHLPP1 protein steady-state levels increased following dilution, cells grown at a high confluency were re-seeded at a low confluency and lysed at various time points

(Figure 4.1.E). PHLPP1 levels began to increase 8 hours after dilution, a time frame that fits with a transcriptional response. These data suggest that PHLPP1 transcription is up-regulated during conditions of low cellular confluency in a cell-type dependent manner.

Next, we sought to determine if downstream targets of PHLPP1 were affected by changes in cellular confluency as well. First, we examined histone phosphorylation and acetylation on key residues of histone H3 as a previous study identified that PHLPP1 suppresses histone acetylation and phosphorylation at these sites (14). Histone modifications on H3 – acLys9, acLys27, and pSer10 – increased in WT MEFs as cellular confluency increased (Figure 4.2, lanes 1-3). To determine if this confluency-dependent effect was due to changes in PHLPP1 expression, we repeated this analysis in *Phlpp1*$^{-/-}$ (KO) MEFs (Figure 4.2, lanes 4-6). While the confluency-dependent effects on acLys9 and acLys27 were lost, no effect was observed on pSer10 (Figure 4.2). Although these results were not statistically significant, the trend suggests that PHLPP1 suppression of histone acetylation is sensitive to cellular confluency levels.

Deprivation of extracellular glutamine explains why PHLPP1 expression declines in confluent cell cultures.

We next sought to determine why PHLPP1 expression is sensitive to changes in confluency. We reasoned that either changes in the extracellular environment or increased cell-cell contacts result in the activation of signaling pathways that lead to down-regulation of PHLPP1. To answer this question, low confluency cells were grown in conditioned media from high confluency cells. Specifically, 24 hours after WT MEFs were seeded at a high confluency, conditioned media from these cells was removed and filtered to remove any debris and dead cells (Figure 4.3.A). These high confluency cells were re-seeded at a low confluency with either fresh

media (Figure 4.3.B, lane 2) or the high confluency-conditioned media. (Figure 4.3.B, lane 3). Low confluency cells grown in conditioned media (Figure 4.3.B lane 3) were not able to up-regulate PHLPP1 expression compared to the cells grown in fresh media (Figure 4.3.B, lane 2). Rather, the level of PHLPP1 in these cells was more similar to that of high confluency cells (Figure 4.3.B, lane 1). This suggests that a component of the extracellular environment plays a role in the down-regulation of PHLPP1 during conditions of high cellular confluency.

Next, we asked what component in the extracellular environment was required to down-regulate PHLPP1 expression at high levels of cellular confluency. We hypothesized that a secreted protein that either accumulates in the media or is specifically excreted when cells reach a high confluency may be critical. To this end, high confluency-conditioned media was heat-treated to denature any secreted proteins. Low confluency WT MEFs were grown in either fresh media (Figure 4.3.C lane 2-3), high confluency-conditioned media (Figure 4.3.C lane 4-5), or heat-treated high confluency-conditioned media (Figure 4.3.C lane 6-7). Dilution of cells with heat-treated media resulted in no change in PHLPP1 protein levels (Figure 4.3.C, lane 6,7) compared to the non-heat-treated conditioned media (Figure 4.3.C, lane 4,5). Since the heat-treated conditioned media was not able to rescue the expression of PHLPP1, we concluded that a secreted protein was not a critical factor in this pathway.

We next tested whether depletion of a key nutrient, such as glucose and glutamine, accounted for the inability of conditioned media to trigger the expression of PHLPP1 (Figure 4.3.D-E). WT MEFs were seeded at a low confluency in either fresh complete media (Figure 4.3.D, lane 2), high confluency-conditioned media (Figure 4.3.D, lane 3), complete media lacking glucose (Figure 4.3.D, lane 4), complete media lacking glutamine (Figure 4.3.D, lane 5), or complete media lacking both glucose and glutamine (Figure 4.3.D, lane 6); levels of PHLPP1 were then assessed

by western blot. As fetal bovine serum, a common additive to cell culture media, naturally contains glucose and glutamine, dialyzed fetal bovine serum (FBS) was used in these experiments. We observed that while there was a moderate, but not statistically significant, decrease in PHLPP1 expression following depletion of glucose (Figure 4.3.D-E, lane 4), depletion of glutamine resulted in a significant drop in PHLPP1 levels (Figure 4.3.D-E, lane 5), similar to that observed in both high confluency cells (Figure 4.3.D-E, lane 1) and low confluency cells grown in high-confluency conditioned media (Figure 4.3.D-E, lane 3). Depletion of both glucose and glutamine did not result in a greater depletion in PHLPP1 levels compared to glutamine depletion alone (Figure 4.3.D-E, lane 6). Therefore, these results suggest that PHLPP1 levels are sensitive to extracellular levels of glutamine.

DISCUSSION

The studies in this chapter establish that PHLPP1 expression is sensitive to the levels of glutamine in the extracellular environment (Figure 4.4). Specifically, cells grown at a low confluency, where extracellular glutamine is abundant, have higher levels of PHLPP1 compared to cells grown at a high confluency. Furthermore, re-seeding of high confluency cells at a low confluency can rescue PHLPP1 levels, but only if the cells are grown in fresh complete media containing glutamine; conditioned media from high confluency cells or media lacking additional glutamine was ineffective. Moreover, the nutrient-sensitive regulation of PHLPP1 levels impacts PHLPP1 nuclear signaling as assessed by effects on two histone marks that are regulated by PHLPP1: H3 acLys9 and H3 acLys27. The acetylation on these two lysine residues is sensitive to cellular confluency in WT, but not *Phlpp1*$^{-/-}$, MEFs.

The mechanism by which low glutamine levels lead to a down-regulation in PHLPP1 expression has yet to be determined, but several possibilities exist. One potential mechanism is through alpha-ketoglutarate, a byproduct of glutamine metabolism and a co-factor of the Jumonji domain containing histone demethylases (193). Chromatin methylation is generally, but not exclusively, considered a mark of transcriptional silencing (194), and removal of methylation marks is facilitated by demethylases, resulting in the activation of gene expression. Therefore, increased glutamine levels could result in demethylation of the PHLPP1 promoter, and thus increase gene expression. Furthermore, DNA demethylation is regulated by the Ten-Eleven Translocation (TET) family of demethylases (195), which also utilize alpha-ketoglutarate as a co-factor. Depletion of glutamine levels has been linked with activation of transcription factors such as c-jun (196, 197), Hypoxia-Inducible Factor 1α (HIF-1α) (198, 199), and Heat Shock Factor 1 (HSF-1) (200-202). Interestingly, two studies have indicated the existence of a Cell Density Response Element (CDRE) in the promoters of genes regulated by cell confluency, specifically Transferring Receptor 1 (Tfr1) (203) and Insulin-Like Growth Factor 1 (IGF-1) (204), but whether these are activated specifically following glutamine depletion has not been determined. Further studies will be needed to identify the specific mechanism by which PHLPP1 is down-regulated following glutamine deprivation.

Work from this dissertation has identified that PHLPP1 is in proximity to three amino acid transport proteins that are required for the movement of glutamine across the plasma membrane (see Chapter 2). Specifically, a proximity-dependent biotin identification (BioID) screen was utilized to identify novel PHLPP1 protein interactors. PHLPP1 was tagged with *E.coli* biotin ligase that harbors a mutation (BirA-R118G), allowing it to indiscriminately biotinylate nearby proteins. By adding biotin to cells expressing this biotin ligase-tagged PHLPP1, any proteins in close

proximity to PHLPP1 are biotinylated, allowing for simple purification and analysis by mass spectrometry. This screen identified three amino acid transporters – ASCT2 (SLC1A5), CD98hc (SLC3A2), and LAT1 (SLC7A5) – as top hits. Glutamine can enter the cell through the amino acid transporter ASCT2 (SLC1A5) (184). LAT1 (SLC7A5) and CD98hc (SLC3A2) function to export intracellular glutamine, a process which fuels leucine uptake (182). Additionally, PHLPP1 (10), ASCT2 (205), and CD98hc (206) all contain PDZ-binding ligands that allow them to scaffold on PDZ domain-containing proteins, further suggesting that an interaction in the cell could be relevant. This is pertinent to this study as glutamine metabolism appears to play a role in regulating PHLPP1 expression. The expression of these transporters is frequently increased during cancer (182, 207-211), while PHLPP1 expression is generally down-regulated (80). A tantalizing hypothesis is that PHLPP1 phosphatase activity can regulate the function or stability of these transporters in a negative feedback loop. During conditions of glutamine starvation, loss of PHLPP1 expression could boost the activity or expression of these transporters, resulting in an increase in glutamine uptake. An increase in intracellular glutamine levels would result in an increase in PHLPP1 expression and thus shut off transporter activity. Further experimentation and analysis are required to better tease apart this potential mechanism.

A better understanding of the interplay between glutamine metabolism and PHLPP1 expression can provide novel insight into how PHLPP1 functions as a tumor suppressor. A large volume of research has indicated that glutamine metabolism is increased in cancer cells. In order to culture most cancer cell lines; additional glutamine must be supplemented into the cellular media. As PHLPP1 expression is frequently down-regulated in cancer (80), the fact that our studies identified that high levels of glutamine-stimulated PHLPP1 expression is paradoxical. One possible mechanism to explain this disconnect is that the feedback mechanism between glutamine

metabolism and PHLPP1 transcriptional regulation may be uncoupled in certain cell types. PHLPP1 expression was not confluency-dependent in all cell lines tested, as two cancer cell lines (U-251 and SF-268 cells) had PHLPP1 levels unchanged at various levels of confluency, while three other cell lines (MEFs, HEK-293A, and NIH-3T3) were sensitive to changes in confluency. A previous study identified a similar phenomenon in glioblastoma cell lines, where the mechanism to regulate PHLPP1 stability was decoupled in cancer cells compared to normal cells. The authors found that the E3 ubiquitin ligase, β-TrCP, was mis-localized to the nucleus in various glioblastoma cell lines, thus making it unable to mark its cytoplasmic substrate, PHLPP1, for degradation. Thus, if PHLPP1 expression and glutamine metabolism are uncoupled in cancer cells, the increased breakdown of glutamine would not result in greater levels of the tumor suppressor PHLPP1.

The high consumption rate of glutamine in cancer cells can result in a depletion of glutamine in the tumor microenvironment (212). While tumor cells find ways to scavenge for glutamine, such as through micropinocytosis (213), other cell types are not able to as easily adapt to the depletion of this key nutrient. This affects the activity and function of cells found in the microenvironment, including cancer-associated fibroblasts (214) and lymphocytes. A recent study identified that pharmacological inhibition of glutamine metabolism in cancer cells results in increased activation of tumor infiltrating lymphocytes in the tumor microenvironment. How glutamine depletion affects the levels of PHLPP1 in both cancer cells but also the nearby cells in the stroma, and how that promotes tumor progression, is an interesting question that required more analysis.

In conclusion, this study unveils a novel mechanism to control PHLPP1 expression, showing that gene expression is sensitive to the levels of glutamine in the extracellular

environment. This finding may be relevant to better understanding PHLPP1 signaling in the context of cancer, where suppression of PHLPP1 function may be important in the tumor microenvironment when nutrients are low. The sensitivity of PHLPP1 levels to cellular confluency in the two-dimensional tissue culture setting, in a cell line-dependent manner, also identifies a key parameter in cellular studies of this enzyme. On a practical level, this is a significant finding as it underscores the importance of taking confluency into account during the experimental design of studies analyzing PHLPP1. For example, if cells are harvested at a high confluency in MEFs, a PHLPP1-dependent effect may be masked due to down-regulation of PHLPP1 protein. Therefore, this study provides multiple facets of insight into PHLPP1 biology.

MATERIALS AND METHODS

Cell Culture

MEFs from WT or *Phlpp1*$^{-/-}$ mice stably expressing shp53 and GFP were a kind gift from the group of Dr. Lloyd Trotman (CSHL) and have been previously described (85). MEFs, HEK-293A (a kind gift from the laboratory of Dr. Kun-Liang Guan, UCSD), NIH-3T3, U-251, and SF-268 cells were grown in Dulbecco's modified Eagle medium (DMEM, 10-013-CV, Corning) – this media contains 4.5 g/L glucose, 584 mg/L L-Glutamine, and 110 mg/L sodium pyruvate. Cell lines were grown in 100 mm polystyrene tissue culture dishes (83.3902, Sarstedt). Media was supplemented with 10% fetal bovine serum (S11150, Atlanta Biologicals) and 1% penicillin/streptomycin (15140-122, Gibco), and all cell lines were cultured at 37°C in 5% (vol/vol) CO_2. For experiments analyzing effects of glucose and glutamine (Figure 2D), dialyzed FBS was used (S12850, Atlanta Biologicals). Cells were periodically tested for *Mycoplasma* contamination using a PCR-based protocol (123) and showed no evidence of contamination.

Antibodies

Antibodies used in this study are as listed: β-actin (A2066, Sigma), H3 total (39163, Active Motif), H3 acK9 (39917, Active Motif), H3 acK27 (39685, Active Motif), H3 pS10 (39253, Active Motif), Hsp90 (610418, BD Transductions), PHLPP1 (22789-1-AP, Proteintech), PHLPP2 (A300-661A, Bethyl Laboratories) Tubulin (T6074, Sigma-Aldrich), Vinculin (13901, Cell Signaling).

Cell Lysis and Western Blot

Cells were lysed in buffer containing 20 mM Tris (pH 7.5), 150 mM NaCl, 1 mM EDTA, 1 mM EGTA, 1% Triton X-100, 2.5 mM sodium pyrophosphate, 1 mM Na_3VO_4, 1 mM DTT, 1 mM PMSF, 1 μM microcystin, 20 μM benzamidine, and 40 μg/mL leupeptin and sonicated briefly. Cells were lysed for 10 min at 4°C. Soluble lysates were separated by SDS-PAGE gel, transferred to PVDF membranes (BioRad), and analyzed by western blot. Detection and quantification were done using chemiluminescence on a FluorChem Q imaging system (ProteinSimple).

Cellular Confluency Analysis

For analysis of PHLPP1 at varying levels of confluency, cells were seeded in 100 mm polystyrene tissue culture dishes (83.3902, Sarstedt) as listed in the table below. Unless otherwise stated, cells were lysed 24 h after re-plating.

Table 1 – Initial Seeding Confluency for Cellular Confluency Analysis

	Confluency (# cells seeded / 100mm plate)		
	LOW	MED	HIGH
MEF (WT & KO)	0.3×10^5	1.2×10^5	5.0×10^5
U-251	2.2×10^5	8.8×10^5	35×10^5
SF-268	0.8×10^5	3.0×10^5	12×10^5
HEK-293A	3.0×10^5	12×10^5	50×10^5
NIH-3T3	2.5×10^5	5.0×10^5	10×10^5

For experiments utilizing conditioned media, cells were seeded at a high confluency. 24 h after seeding, the media was removed from the cells, passed through a 0.22 μm filter (SCGP00525, EMD Millipore), and incubated at 37°C. For heat-treated conditioned media, filtered media was incubated at 75°C for 30 min. Immediately following removal of media, high confluency cells were trypsinized, centrifuged, and the pellet was resuspended in 1 mL of high confluency conditioned media. Cells were counted using a Countess cell counter (Invitrogen) and re-seeded at a low confluency with either fresh regular growth media or the conditioned media. The remainder of the cells were lysed to include as a control. 24 h after re-seeding, cells were lysed and analyzed by western blot.

For experiments utilizing glucose- and glutamine-free media, a similar protocol was used. To analyze glucose depletion, a glucose-free media was created. Commercially available glucose- and pyruvate- free media (11966-025, Life) was used as a base media. This media was supplemented with 1 mM sodium pyruvate (25-000-CI, Corning), 1% penicillin/streptomycin (15140-122, Gibco), and 10% dialyzed FBS (S12850, Atlanta Biologicals). To analyze glutamine depletion, a glutamine-free media was created. Commercially available glutamine- and pyruvate-free media (11966-025, Life) was used as a base media. This media was supplemented with 1 mM sodium pyruvate (25-000-CI, Corning), 1% penicillin/streptomycin (15140-122, Gibco), and 10% dialyzed FBS (S12850, Atlanta Biologicals). To analyze both glucose and glutamine depletion in combination, a glucose- and glutamine-free media was created. Commercially available glucose-, glutamine-, and pyruvate- free media (A1443001, ThermoFisher Scientific) was used as a base media. This media was supplemented with 1 mM sodium pyruvate (25-000-CI, Corning), 1% penicillin/streptomycin (15140-122, Gibco), and 10% dialyzed FBS (S12850, Atlanta Biologicals).

RT-qPCR

Total RNA from *Phlpp1*$^{+/+}$ and *Phlpp1*$^{-/-}$ mouse embryonic fibroblasts was isolated using the RNeasy Mini kit (74104, Qiagen). 2.5 μg of total mRNA was reverse transcribed using the Superscript III First Strand Synthesis System (18080-051, Invitrogen). The resulting cDNA (20 ng) was used to perform real-time PCR using SYBR Premix Ex Taq II (RR820A, Takara Bio) and a 100 nm mix of forward and reverse primers for either *Phlpp1* (mouse) or *Actin* (mouse). Real-time PCR was performed on an ABI-7500 real-time PCR system (Applied Biosystems). The real-time PCR values for *Phlpp1* were normalized to the housekeeping gene, *Actin*, using the ΔΔCT method (170). The primer sequences used in this study are:

*mActin*_qPCR_F_TGTAGTTTCATGGATGCCACAG

*mActin*_qPCR_R_GAAATCGTGCGTGACATCAAAG

*mPhlpp1*_qPCR_F_CGTGAAAGACAGCGTGAGTG

*mPhlpp1*_qPCR_R_ ACGCTAAACAGTGCTGGTGC

ACKNOWLEDGMENTS

We thank members of the Newton laboratory for helpful discussion. We thank the laboratory of Dr. Jack Dixon (UCSD) for help with the ABI-7500 Real Time PCR System.

FIGURES:

Figure 4.1: PHLPP1 protein and mRNA levels are depleted as cellular confluency increases. **(A)** Western blot of WT mouse embryonic fibroblasts (MEFs) plated at varying levels of confluency. Graph in **(B)** represents the quantification of four independent experiments. Values expressed as the mean relative (rel.) units ± SEM of the ratio of total PHLPP1 to loading control (tubulin), normalized to the LOW condition. **(C)** Similar analysis as in (A) performed using different immortalized cell lines. Number of independent experiments for each cell line are as follows: SF-268 n=1, U-251 n=2, HEK-293A n=3, and NIH-3T3 n=2. **(D)** RT-qPCR of WT and *Phlpp1* KO MEF samples seeded at varying levels of cellular confluency as described in (A). Represents the quantification of four independent experiments. Values expressed as the mean ± SEM of the ratio of PHLPP1 to the internal loading control (actin), normalized to the LOW condition in WT MEFs. **(E)** Time course of high confluency WT MEFs re-seeded at a low confluency. Blot represents an n=1. Blots for all gels are probing for endogenous protein. *$p<0.05$, **$p<0.005$ (Student's t-test). Numbers below each blot refer to the lane number. Media used for all experiments in Figure 4 is standard DMEM supplemented with 584 mg/L L-glutamine, 4.5 g/L D-glucose, 110 mg/L sodium pyruvate, 10% fetal bovine serum, and 1% penicillin/streptomycin.

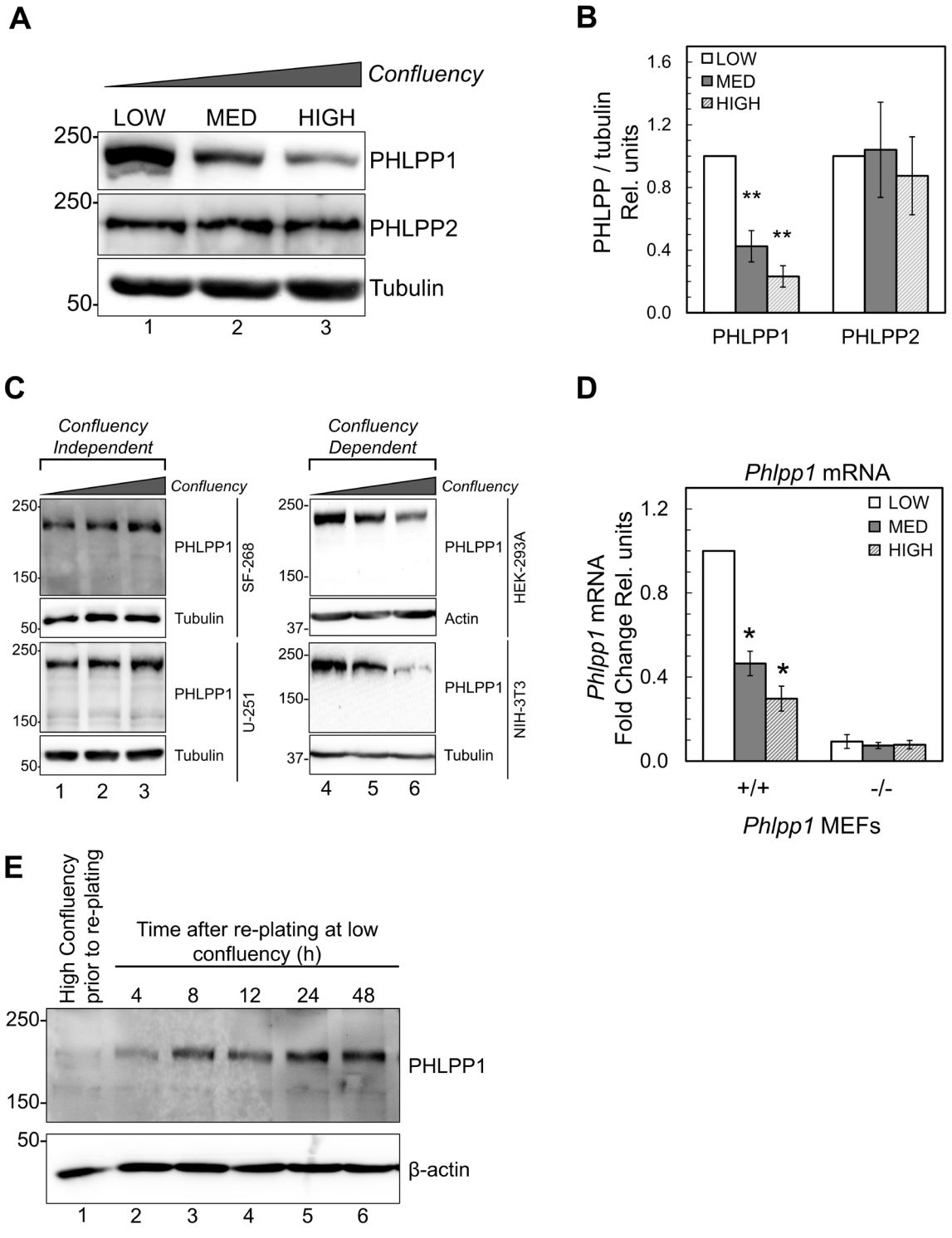
A
Confluency
LOW
MED
HIGH
250
PHLPP1
250
PHLPP2
50
Tubulin
1
2
3
B
LOW
MED
HIGH
PHLPP / tubulin
Rel. units
1.6
1.2
0.8
0.4
0.0
**
**
PHLPP1
PHLPP2
C
Confluency
Independent
Confluency
Dependent
Confluency
Confluency
250
150
PHLPP1
Tubulin
SF-268
50
250
150
PHLPP1
Tubulin
U-251
250
150
PHLPP1
Actin
HEK-293A
37
250
150
PHLPP1
Tubulin
NIH-3T3
37
1
2
3
4
5
6
D
Phlpp1 mRNA
Phlpp1 mRNA
Fold Change Rel. units
LOW
MED
HIGH
1.2
0.8
0.4
0.0
*
*
+/+
-/-
Phlpp1 MEFs
E
High Confluency
prior to re-plating
Time after re-plating at low
confluency (h)
4
8
12
24
48
250
150
PHLPP1
50
β-actin
1
2
3
4
5
6

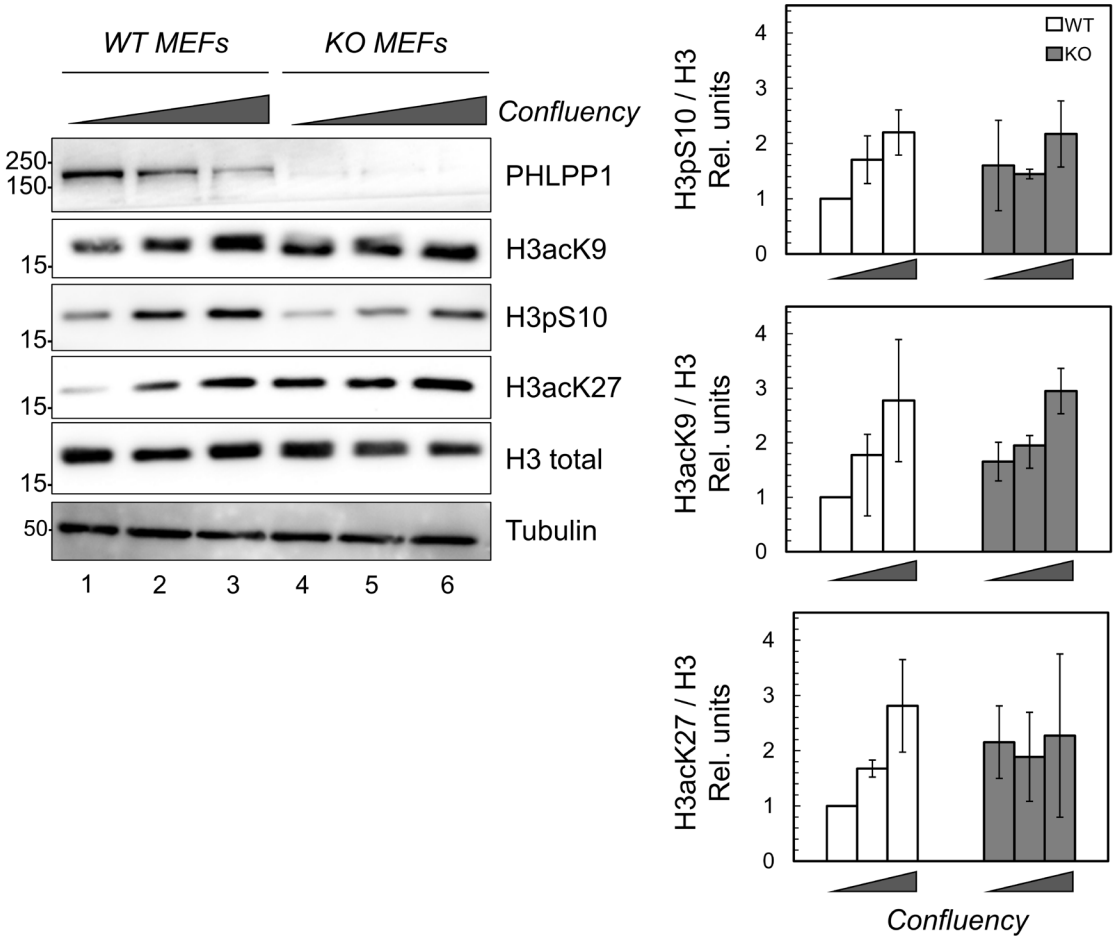

Figure 4.2: Histone acetylation is sensitive to changes in cellular confluency in a PHLPP1-dependent manner. Western blot and quantification of WT and *Phlpp1*KO MEFs seeded at varying levels of confluency. Graphs represent the quantification of four independent experiments. Values expressed as the mean relative (rel.) units ± SEM of the ratio of each histone modification to total H3, normalized to the LOW condition in WT MEFs. Blots for all gels are probing for endogenous protein. *$p<0.05$, **$p<0.005$ (Student's t-test). Numbers below each blot refer to the lane number. Media used for all experiments in Figure 4 is standard DMEM supplemented with 584 mg/L L-glutamine, 4.5 g/L D-glucose, 110 mg/L sodium pyruvate, 10% fetal bovine serum, and 1% penicillin/streptomycin.

Figure 4.3: Removal of glutamine from extracellular media results in a down-regulation of PHLPP1 in low confluency cells. (A) Schematic of media swap experiment used in **(B).** WT MEFs are seeded at a high confluency. 24 hours after seeding, conditioned media is removed and filtered, and cells are re-seeded at a low confluency in either fresh media or high confluency conditioned media. **(B)** WT MEFs grown at a high confluency (lane 1) are re-seeded at a low confluency in either fresh media or high confluency conditioned media. Cells are harvested 4 and 8 hours after re-seeding. **(C)** High confluency WT MEFs are re-seeded at a low confluency in either fresh media, high confluency conditioned media, or high confluency conditioned media that has been heat treated. Time refers to the number of hours after re-seeding that cells were lysed. Blot represents an n=1. **(D)** High confluency WT MEFs are re-seeded at a low confluency in either fresh media, high confluency conditioned media, or fresh media lacking glucose, glutamine (Gln), or both glucose and glutamine. For this experiment, media was supplemented with dialyzed 10% fetal bovine serum to ensure no additional glucose or glutamine is present in the media. **(E)** Quantification of (D). Graph represents the quantification of four independent experiments. Values expressed as the mean relative (rel.) units ± SEM of the ratio of total PHLPP1 to loading control (tubulin), normalized to the HIGH confluency condition. Blots for all gels are probing for endogenous protein. *$p<0.05$, **$p<0.005$ (Student's t-test). Numbers below each blot refer to the lane number.

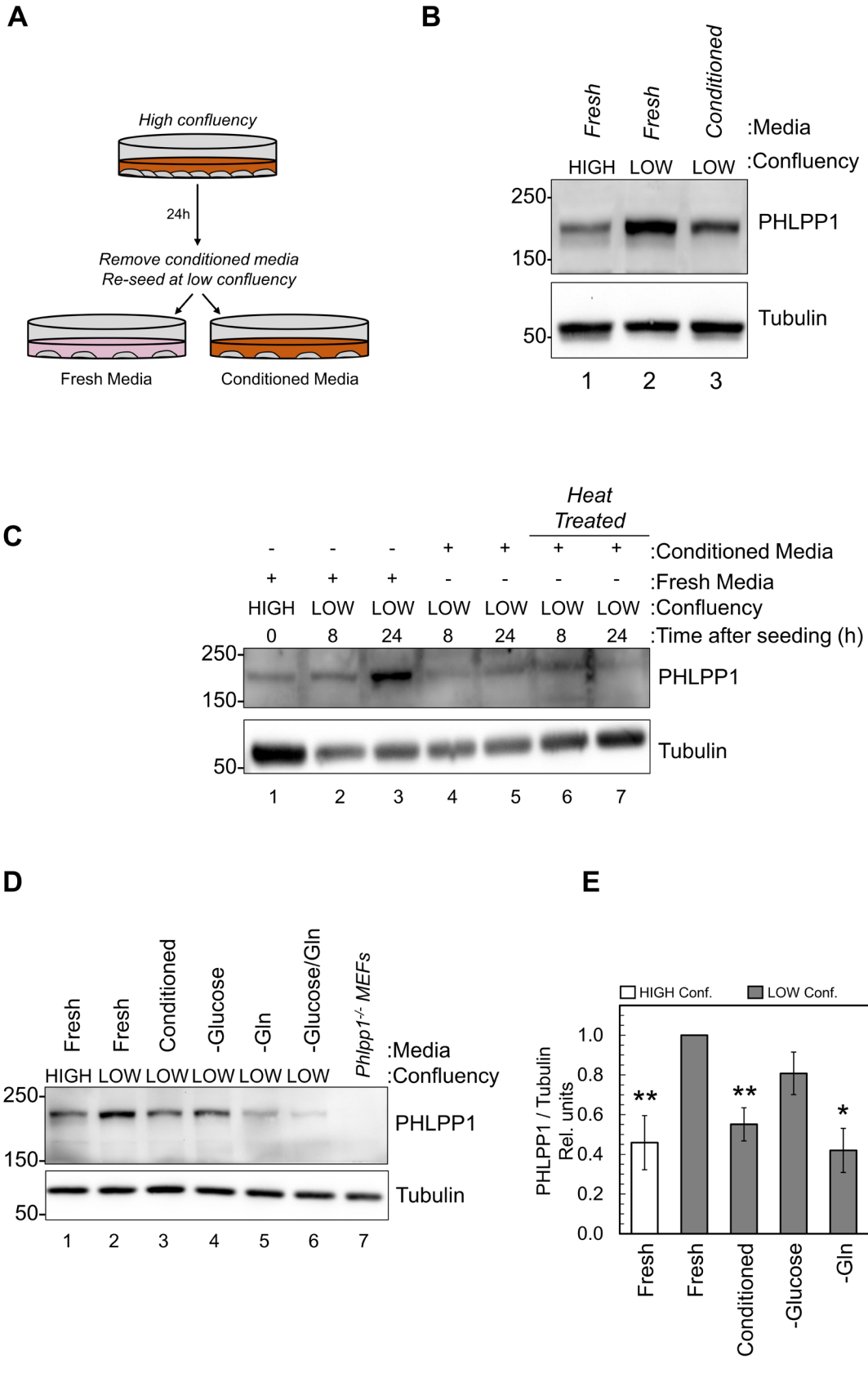
A
High confluency
24h
Remove conditioned media
Re-seed at low confluency
Fresh Media
Conditioned Media
B
Fresh
Fresh
Conditioned
:Media
HIGH LOW LOW :Confluency
250
150
PHLPP1
50
Tubulin
1 2 3
C
Heat Treated
- - - + + + + :Conditioned Media
+ + + - - - - :Fresh Media
HIGH LOW LOW LOW LOW LOW LOW :Confluency
0 8 24 8 24 8 24 :Time after seeding (h)
250
150
PHLPP1
50
Tubulin
1 2 3 4 5 6 7
D
Fresh
Fresh
Conditioned
-Glucose
-Gln
-Glucose/Gln
Phlpp1-/- MEFs
:Media
HIGH LOW LOW LOW LOW LOW :Confluency
250
150
PHLPP1
50
Tubulin
1 2 3 4 5 6 7
E
HIGH Conf.
LOW Conf.
PHLPP1 / Tubulin Rel. units
1.0
0.8
0.6
0.4
0.2
0.0
**
**
*
Fresh
Fresh
Conditioned
-Glucose
-Gln
-Glucose/Gln

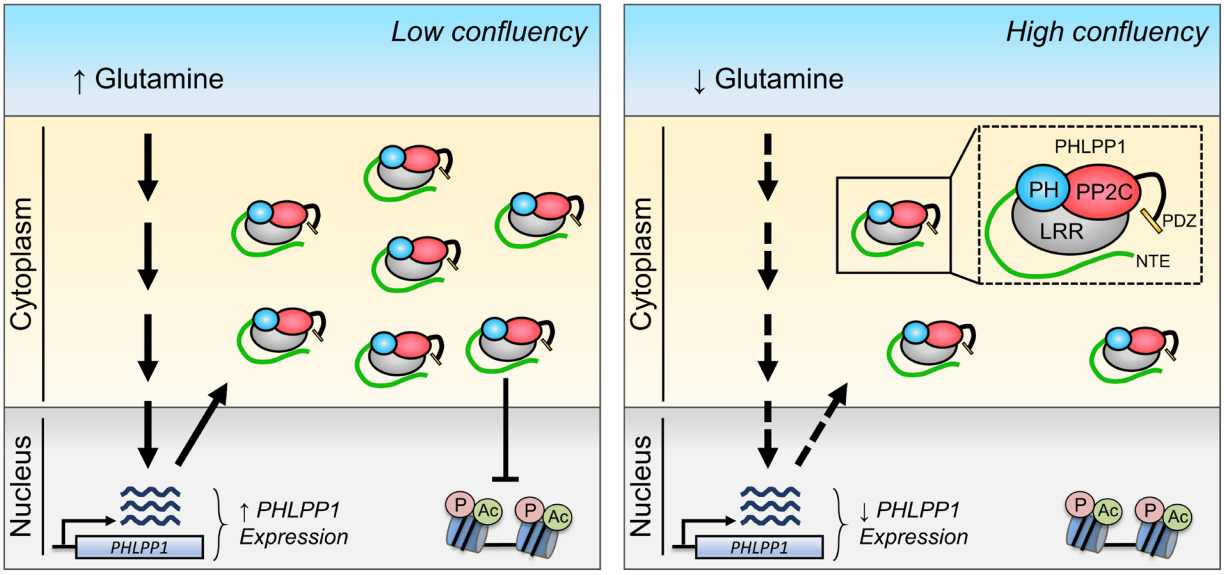

Figure 4.4: Proposed model of PHLPP1 regulation by extracellular glutamine levels. When cells are grown at a low confluency in two-dimensional tissue culture, glutamine levels are high, resulting in the up-regulation of PHLPP1 transcription and translation. The resulting increase in PHLPP1 protein levels results in a greater suppression of histone phosphorylation and acetylation. As cells reach confluency, glutamine is depleted, resulting in PHLPP1 expression being turned off. This decrease in PHLPP1 protein levels results in a loss of PHLPP1-mediated histone regulation.

Chapter 5 – Conclusions and Future Directions

The work presented in this dissertation describes various new mechanisms of how the tumor suppressor phosphatase PHLPP1 is regulated in the cell (Figure 5.1). It provides novel insight into how a previously uncharacterized region of this enzyme, the NTE, plays a critical role in regulating PHLPP1 localization, interactions and function. This work uncovered that the NTE utilizes both reversible and intrinsic modes of regulation. Prior to this work there had be no studies that specifically characterized this large region of the enzyme. Additionally, we unveiled how PHLPP1 expression is regulated by changes in the extracellular environment, namely depletion of key nutrients such as glutamine. These findings provide a new layer of understanding about how this enzyme functions in the context of a healthy cell, but also sheds new insight into how PHLPP1 biology may be deregulated in disease.

In Chapter 2, we demonstrate that the PHLPP1 NTE is hyperphosphorylated during mitosis by Cdk1, and that this NTE is also responsible for disrupting PHLPP1 interactions with plasma membrane scaffolds during mitosis. In this present study, we show that the NTE has the capacity to be heavily modified by phosphorylation, as 13 various phosphorylated residues were identified via phospho-mass spectrometry. Whether all of these phosphorylation events are present and required outside of a synchronized mitotic population is an interesting question that needs to be determined. But, there is precedent suggesting that several down-stream substrates of Cdk1 are hyper-phosphorylated in this manner, and that the large increase in negative charge is more important than the specific residues being phosphorylated (112). In addition to showing that Cdk1 phosphorylates the NTE during mitosis, we performed a proximity-dependent biotin identification (BioID) screen to identify the PHLPP1 interactome in both the presence and absence of the NTE. This screen identified that during interphase, PHLPP1 is in proximity to a number of protein complexes localized at the plasma membrane, and these interactions are lost when cells are

synchronized in mitosis; deletion of the NTE resulted in an even greater pull down of these prey proteins in both asynchronous and mitotic cells. Interestingly, two of these prey protein, Scrib and WDR48, are known to interact with PHLPP1 through its CTE (23, 24), suggesting that the NTE can prohibit the binding of interaction partners at the CTE. Thus, this study brings up a variety of new questions about the folding of PHLPP1 and how the CTE and NTE interact. As there are no structures of PHLPP1 available, neither full length nor of individual domains, the answer to this question remains elusive. It would be of interest to determine the interaction between the CTE and NTE, and how hyperphosphorylation of the NTE during mitosis affects the interplay between the two unstructured tails.

Chapter 2 also highlights a potentially new role for PHLPP1 in the cell cycle. Not only is PHLPP1 in proximity to key mitotic signaling hubs, the mitotic spindles and the kinetochore, and loss of PHLPP1 results in subtle defects in mouse embryonic fibroblasts. As deletion of the *Phlpp1* locus in mice is not embryonic lethal like critical cell cycle genes such as the Cdk1-endcoding gene *Cdc2*, it is not surprising that the defect observed in cells is subtle. Interestingly, siRNA knock-down of PHLPP1 in human RPE1 cells had no impact on mitotic fidelity or timing. As RPE1 cells have generally low levels of genomic instability compared to human cancer cell lines, like HeLa cells, or MEFs (as observed by the high levels of chromosomal segregation errors observed in our WT MEFs), it suggests that PHLPP1 may function during mitosis when cells have incurred DNA damage or other genomic insults. This would be an interesting direction to follow as it could shed greater insight into how PHLPP1 suppresses tumorigenesis, as aneuploidy and genomic instability is a hallmark of cancer (176).

The data presented in Chapter 3 again focuses on the function of the NTE but in the context of inflammatory signaling. In this study, we show that the NTE directs PHLPP1 to the inflammatory

transcription factor STAT1 in two ways: 1) by bringing PHLPP1 to the nucleus, and 2) by directly binding to STAT1. This study revealed that the NTE houses an arginine-rich bipartite NLS, providing a concrete mechanism to understand how PHLPP1 can get into and signal in the nucleus. We also found an NES directly proceeding the catalytic PP2C domain, suggesting that PHLPP1 localization between the cytoplasm and nucleus can occur bi-directionally. By binding to and dephosphorylating STAT1, PHLPP1 is able to dampen the transcription of inflammatory genes. Bone marrow derived macrophages from PHLPP1 knock-out mice have prolonged expression of STAT1-targets, such as *Cd69,* suggesting that the cells are not able to properly resolve their inflammatory response following stimulation by LPS. Interestingly, *in vivo* mouse studies suggest that deletion of PHLPP1 is protective against bacterial sepsis, which would suggest that PHLPP1 promotes a pro-inflammatory state. This paradoxical finding suggests that PHLPP1 may have varied roles in different immune cells. Our studies focused on macrophages, but other studies have shown PHLPP functions in other immune cell types, like Tregs (58, 59) and neutrophils (215). Therefore, a pressing new direction is to determine how PHLPP1 protects mice from bacterial sepsis in the context of the entire immune response. This could have massive clinical implications as there are currently no effective therapeutics to treat septic patients.

Finally, we presented in Chapter 4 that PHLPP1 expression is down-regulated as cells become confluent in culture, most likely due to a depletion in extracellular glutamine. This study is relevant not only to better understand how PHLPP1 transcription is regulated, but also on a more practical level. We found that some, but not all, cell lines exhibited this confluency-dependent effect; thus, confluency needs to be taken into account when using these specific cell lines in the studies of a PHLPP1-dependent effect. For example, the difference in H3 Lys27 acetylation may not be as dramatic in high confluency compared to low confluency MEFs.

These new data open up various new windows into the world of PHLPP1 signaling. In the fifteen years since its discovery, PHLPP1 has been implicated in a variety of different disease states, indicating that maintaining PHLPP1 homeostasis is required to prevent pathophysiologies (Figure 5.2). While a number of these connections are attributed to the negative regulation of Akt, this dissertation provides potentially novel connections. For example, we showed that through regulation of STAT1, PHLPP1 plays a role in resolution of the inflammatory response in macrophages. Whether the involvement of PHLPP1 in mitosis is to regulate Akt signaling is still unclear. While PHLPP inhibitors tdo exist and have been used successfully in mouse models of osteoarthritis (32), there is still a long way to go before these inhibitors could be useful in a clinical setting. Furthermore, several studies have successfully used small molecule PP2A activators (SMAPs) to restore PP2A function and inhibit cancer progression in cell lines and transgenic mouse models (216, 217). Pharmacological activators of PHLPP1 could also provide this type of therapeutic benefit. Thus, the data presented here can provide novel directions for future work to better understand the therapeutic potential of PHLPP1.

FIGURES:

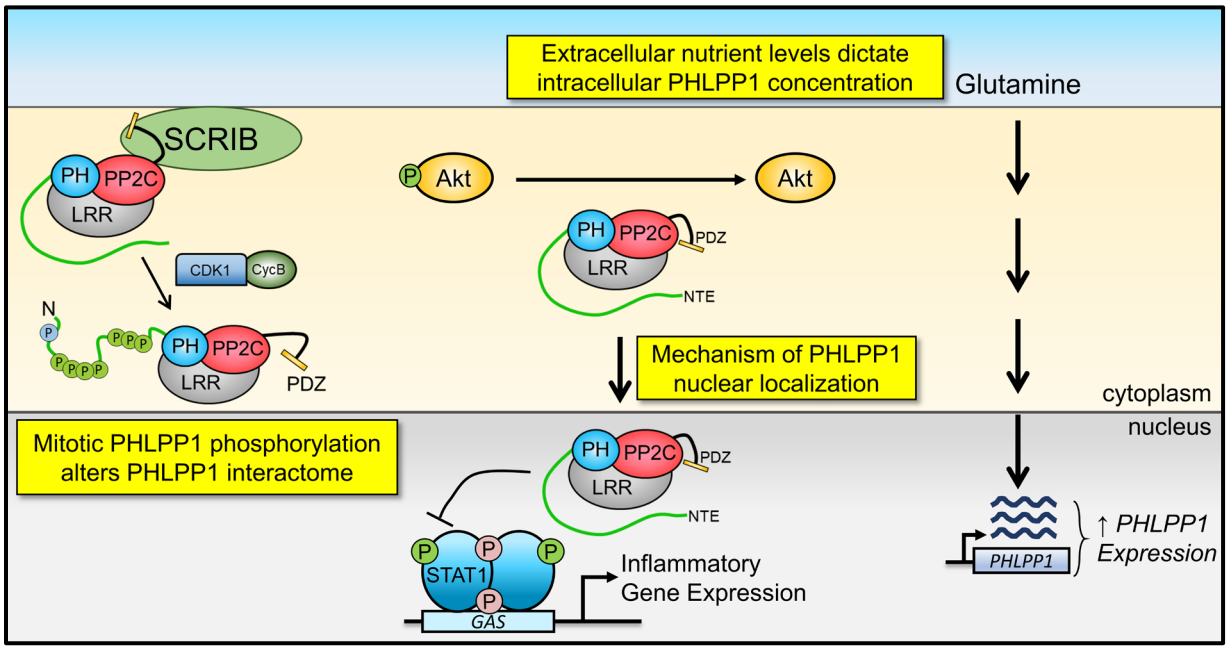

Figure 5.1: Novel PHLPP1 signaling pathways reveal insight into PHLPP1 regulation. This dissertation unveiled three novel PHLPP1 regulatory pathways. First, it showed that the PHLPP1 N-terminal extension (NTE) is hyper-phosphorylated by Cdk1 during mitosis, and that the NTE is required for a PHLPP1 interactome switch between interphase and mitosis. Second, it revealed that the PHLPP1 NTE houses a nuclear localization signal, providing a mechanism to how PHLPP1 targets nuclear STAT1 and histones. Third, it determined that PHLPP1 expression is sensitive to glutamine deprivation in certain cells lines.

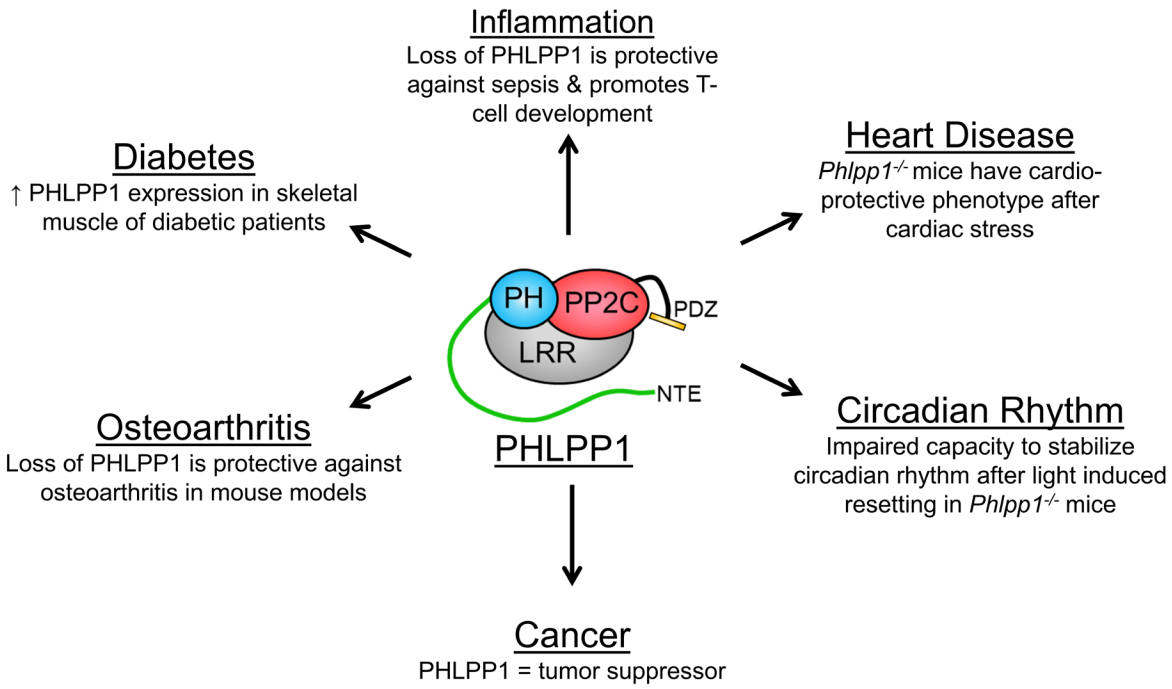

Figure 5.2: PHLPP1 biology is linked to various disease states. De-regulation of PHLPP1 signaling has been linked to various different diseases, including cancer, osteoarthritis, diabetes, and heart disease. Additionally, PHLPP1 has been implicated in proper resolution of the inflammatory response and in regulating the circadian rhythm.

REFERENCES

1. Hornbeck PV, Kornhauser JM, Tkachev S, Zhang B, Skrzypek E, Murray B, Latham V, Sullivan M. 2012. PhosphoSitePlus: a comprehensive resource for investigating the structure and function of experimentally determined post-translational modifications in man and mouse. Nucleic Acids Res 40:D261-70.

2. Ubersax JA, Ferrell Jr JE. 2007. Mechanisms of specificity in protein phosphorylation. Nat Rev Mol Cell Biol 8:530-541.

3. Shi Y. 2009. Serine/threonine phosphatases: mechanism through structure. Cell 139:468-84.

4. Sierecki E, Newton AC. 2014. Biochemical characterization of the phosphatase domain of the tumor suppressor PH domain leucine-rich repeat protein phosphatase. Biochemistry 53:3971-81.

5. Mumby MC, Walter G. 1993. Protein serine/threonine phosphatases: structure, regulation, and functions in cell growth. Physiol Rev 73:673-99.

6. Sierecki E, Sinko W, McCammon JA, Newton AC. 2010. Discovery of small molecule inhibitors of the PH domain leucine-rich repeat protein phosphatase (PHLPP) by chemical and virtual screening. J Med Chem 53:6899-911.

7. Bradley EW, Carpio LR, Newton AC, Westendorf JJ. 2015. Deletion of the PH-domain and Leucine-rich Repeat Protein Phosphatase 1 (Phlpp1) Increases Fibroblast Growth Factor (Fgf) 18 Expression and Promotes Chondrocyte Proliferation. J Biol Chem 290:16272-80.

8. Arias E, Koga H, Diaz A, Mocholi E, Patel B, Cuervo Ana M. 2015. Lysosomal mTORC2/PHLPP1/Akt Regulate Chaperone-Mediated Autophagy. Molecular Cell 59:270-284.

9. Jackson TC, Verrier JD, Drabek T, Janesko-Feldman K, Gillespie DG, Uray T, Dezfulian C, Clark RS, Bayir H, Jackson EK, Kochanek PM. 2013. Pharmacological inhibition of pleckstrin homology domain leucine-rich repeat protein phosphatase is neuroprotective: differential effects on astrocytes. J Pharmacol Exp Ther 347:516-28.

10. Gao T, Furnari F, Newton AC. 2005. PHLPP: a phosphatase that directly dephosphorylates Akt, promotes apoptosis, and suppresses tumor growth. Mol Cell 18:13-24.

11. Gao T, Brognard J, Newton AC. 2008. The phosphatase PHLPP controls the cellular levels of protein kinase C. J Biol Chem 283:6300-11.

12. Liu J, Stevens PD, Li X, Schmidt MD, Gao T. 2011. PHLPP-mediated dephosphorylation of S6K1 inhibits protein translation and cell growth. Mol Cell Biol 31:4917-27.

13. Qiao M, Wang Y, Xu X, Lu J, Dong Y, Tao W, Stein J, Stein GS, Iglehart JD, Shi Q, Pardee AB. 2010. Mst1 is an interacting protein that mediates PHLPPs' induced apoptosis. Mol Cell 38:512-23.

14. Reyes G, Niederst M, Cohen-Katsenelson K, Stender JD, Kunkel MT, Chen M, Brognard J, Sierecki E, Gao T, Nowak DG, Trotman LC, Glass CK, Newton AC. 2014. Pleckstrin homology domain leucine-rich repeat protein phosphatases set the amplitude of receptor tyrosine kinase output. Proc Natl Acad Sci U S A 111:E3957-65.

15. Sawan C, Herceg Z. 2010. Histone modifications and cancer. Adv Genet 70:57-85.

16. Hynes NE, Lane HA. 2005. ERBB receptors and cancer: the complexity of targeted inhibitors. Nat Rev Cancer 5:341-54.

17. Li X, Stevens PD, Liu J, Yang H, Wang W, Wang C, Zeng Z, Schmidt MD, Yang M, Lee EY, Gao T. 2014. PHLPP is a negative regulator of RAF1, which reduces colorectal cancer cell motility and prevents tumor progression in mice. Gastroenterology 146:1301-12 e1-10.

18. Wellbrock C, Karasarides M, Marais R. 2004. The RAF proteins take centre stage. Nat Rev Mol Cell Biol 5:875-885.

19. Newton AC, Trotman LC. 2014. Turning off AKT: PHLPP as a drug target. Annu Rev Pharmacol Toxicol 54:537-58.

20. Matsumoto K, Uno I, Oshima Y, Ishikawa T. 1982. Isolation and characterization of yeast mutants deficient in adenylate cyclase and cAMP-dependent protein kinase. Proc Natl Acad Sci U S A 79:2355-9.

21. Tamanoi F. 2011. Ras signaling in yeast. Genes Cancer 2:210-5.

22. Russell M, Bradshaw-Rouse J, Markwardt D, Heideman W. 1993. Changes in gene expression in the Ras/adenylate cyclase system of Saccharomyces cerevisiae: correlation with cAMP levels and growth arrest. Mol Biol Cell 4:757-65.

23. Li X, Yang H, Liu J, Schmidt MD, Gao T. 2011. Scribble-mediated membrane targeting of PHLPP1 is required for its negative regulation of Akt. EMBO reports 12:818-824.

24. Gagnon D, Lehoux M, Archambault J. 2015. Artificial Recruitment of UAF1-USP Complexes by a PHLPP1-E1 Chimeric Helicase Enhances Human Papillomavirus DNA Replication. J Virol 89:6227-39.

25. Gangula NR, Maddika S. 2013. WD repeat protein WDR48 in complex with deubiquitinase USP12 suppresses Akt-dependent cell survival signaling by stabilizing PH domain leucine-rich repeat protein phosphatase 1 (PHLPP1). J Biol Chem 288:34545-54.

26. Goldbraikh D, Neufeld D, Eid-Mutlak Y, Lasry I, Gilda JE, Parnis A, Cohen S. 2020. USP1 deubiquitinates Akt to inhibit PI3K-Akt-FoxO signaling in muscle during prolonged starvation. EMBO Rep 21:e48791.

27. Zhiqiang Z, Qinghui Y, Yongqiang Z, Jian Z, Xin Z, Haiying M, Yuepeng G. 2012. USP1 regulates AKT phosphorylation by modulating the stability of PHLPP1 in lung cancer cells. J Cancer Res Clin Oncol 138:1231-8.

28. Kita K, Kimura T, Nakamura N, Yoshikawa H, Nakano T. 2008. PI3K/Akt signaling as a key regulatory pathway for chondrocyte terminal differentiation. Genes Cells 13:839-50.

29. Bradley EW, Carpio LR, Westendorf JJ. 2013. Histone deacetylase 3 suppression increases PH domain and leucine-rich repeat phosphatase (Phlpp)1 expression in chondrocytes to suppress Akt signaling and matrix secretion. J Biol Chem 288:9572-82.

30. Bradley EW, Carpio LR, McGee-Lawrence ME, Castillejo Becerra C, Amanatullah DF, Ta LE, Otero M, Goldring MB, Kakar S, Westendorf JJ. 2015. Phlpp1 facilitates post-traumatic osteoarthritis and is induced by inflammation and promoter demethylation in human osteoarthritis. Osteoarthritis Cartilage doi:10.1016/j.joca.2015.12.014.

31. Bradley EW, Carpio LR, McGee-Lawrence ME, Castillejo Becerra C, Amanatullah DF, Ta LE, Otero M, Goldring MB, Kakar S, Westendorf JJ. 2016. Phlpp1 facilitates post-traumatic osteoarthritis and is induced by inflammation and promoter demethylation in human osteoarthritis. Osteoarthritis Cartilage 24:1021-8.

32. Hwang SM, Feigenson M, Begun DL, Shull LC, Culley KL, Otero M, Goldring MB, Ta LE, Kakar S, Bradley EW, Westendorf JJ. 2018. Phlpp inhibitors block pain and cartilage degradation associated with osteoarthritis. J Orthop Res 36:1487-1497.

33. Beezhold K, Liu J, Kan H, Meighan T, Castranova V, Shi X, Chen F. 2011. miR-190-mediated downregulation of PHLPP contributes to arsenic-induced Akt activation and carcinogenesis. Toxicol Sci 123:411-20.

34. Chang RM, Yang H, Fang F, Xu JF, Yang LY. 2014. MicroRNA-331-3p promotes proliferation and metastasis of hepatocellular carcinoma by targeting PH domain and leucine-rich repeat protein phosphatase. Hepatology 60:1251-63.

35. Jiang J, Zhang Y, Guo Y, Yu C, Chen M, Li Z, Tian S, Sun C. 2015. MicroRNA-3127 promotes cell proliferation and tumorigenicity in hepatocellular carcinoma by disrupting of PI3K/AKT negative regulation. Oncotarget 6:6359-72.

36. Cai J, Fang L, Huang Y, Li R, Yuan J, Yang Y, Zhu X, Chen B, Wu J, Li M. 2013. miR-205 targets PTEN and PHLPP2 to augment AKT signaling and drive malignant phenotypes in non-small cell lung cancer. Cancer Res 73:5402-15.

37. Jiang L, Wang C, Lei F, Zhang L, Zhang X, Liu A, Wu G, Zhu J, Song L. 2015. miR-93 promotes cell proliferation in gliomas through activation of PI3K/Akt signaling pathway. Oncotarget 6:8286-99.

38. Efeyan A, Sabatini DM. 2010. mTOR and cancer: many loops in one pathway. Curr Opin Cell Biol 22:169-76.

39. Liu J, Stevens PD, Gao T. 2011. mTOR-dependent regulation of PHLPP expression controls the rapamycin sensitivity in cancer cells. J Biol Chem 286:6510-20.

40. Kim K, Qiang L, Hayden MS, Sparling DP, Purcell NH, Pajvani UB. 2016. mTORC1-independent Raptor prevents hepatic steatosis by stabilizing PHLPP2. Nat Commun 7:10255.

41. Li X, Liu J, Gao T. 2009. beta-TrCP-mediated ubiquitination and degradation of PHLPP1 are negatively regulated by Akt. Mol Cell Biol 29:6192-205.

42. Gao G, Kun T, Sheng Y, Qian M, Kong F, Liu X, Yu Z, Zhang H, Zhang Q, Gu J, Zhang X. 2013. SGT1 regulates Akt signaling by promoting beta-TrCP-dependent PHLPP1 degradation in gastric cancer cells. Mol Biol Rep 40:2947-53.

43. Vera J, Lartigue L, Vigneron S, Gadea G, Gire V, Del Rio M, Soubeyran I, Chibon F, Lorca T, Castro A. 2015. Greatwall promotes cell transformation by hyperactivating AKT in human malignancies. Elife 4.

44. Sowa ME, Bennett EJ, Gygi SP, Harper JW. 2009. Defining the human deubiquitinating enzyme interaction landscape. Cell 138:389-403.

45. Li X, Stevens PD, Yang H, Gulhati P, Wang W, Evers BM, Gao T. 2013. The deubiquitination enzyme USP46 functions as a tumor suppressor by controlling PHLPP-dependent attenuation of Akt signaling in colon cancer. Oncogene 32:471-8.

46. Goel A, Arnold CN, Niedzwiecki D, Chang DK, Ricciardiello L, Carethers JM, Dowell JM, Wasserman L, Compton C, Mayer RJ, Bertagnolli MM, Boland CR. 2003. Characterization of Sporadic Colon Cancer by Patterns of Genomic Instability. Cancer Research 63:1608-1614.

47. Johnson-Pais TL, Nellissery MJ, Ammerman DG, Pathmanathan D, Bhatia P, Buller CL, Leach RJ, Hansen MF. 2003. Determination of a minimal region of loss of heterozygosity on chromosome 18q21.33 in osteosarcoma. Int J Cancer 105:285-8.

48. Rakha EA, Green AR, Powe DG, Roylance R, Ellis IO. 2006. Chromosome 16 tumor-suppressor genes in breast cancer. Genes Chromosomes Cancer 45:527-35.

49. Torring N, Borre M, Sorensen KD, Andersen CL, Wiuf C, Orntoft TF. 2007. Genome-wide analysis of allelic imbalance in prostate cancer using the Affymetrix 50K SNP mapping array. Br J Cancer 96:499-506.

50. Chen M, Pratt CP, Zeeman ME, Schultz N, Taylor BS, O'Neill A, Castillo-Martin M, Nowak DG, Naguib A, Grace DM, Murn J, Navin N, Atwal GS, Sander C, Gerald WL, Cordon-Cardo C, Newton AC, Carver BS, Trotman LC. 2011. Identification of PHLPP1 as a tumor suppressor reveals the role of feedback activation in PTEN-mutant prostate cancer progression. Cancer Cell 20:173-86.

51. Li X, Stevens PD, Liu J, Yang H, Wang W, Wang C, Zeng Z, Schmidt MD, Yang M, Lee EY, Gao T. 2014. PHLPP is a negative regulator of RAF1, which reduces colorectal cancer cell motility and prevents tumor progression in mice. Gastroenterology 146:1301-1312.e10.

52. Shimizu K, Okada M, Takano A, Nagai K. 1999. SCOP, a novel gene product expressed in a circadian manner in rat suprachiasmatic nucleus. FEBS Lett 458:363-9.

53. Masubuchi S, Gao T, O'Neill A, Eckel-Mahan K, Newton AC, Sassone-Corsi P. 2010. Protein phosphatase PHLPP1 controls the light-induced resetting of the circadian clock. Proc Natl Acad Sci U S A 107:1642-7.

54. Andreozzi F, Procopio C, Greco A, Mannino GC, Miele C, Raciti GA, Iadicicco C, Beguinot F, Pontiroli AE, Hribal ML, Folli F, Sesti G. 2011. Increased levels of the Akt-specific phosphatase PH domain leucine-rich repeat protein phosphatase (PHLPP)-1 in obese participants are associated with insulin resistance. Diabetologia 54:1879-87.

55. Cozzone D, Frojdo S, Disse E, Debard C, Laville M, Pirola L, Vidal H. 2008. Isoform-specific defects of insulin stimulation of Akt/protein kinase B (PKB) in skeletal muscle cells from type 2 diabetic patients. Diabetologia 51:512-21.

56. Brognard J, Sierecki E, Gao T, Newton AC. 2007. PHLPP and a second isoform, PHLPP2, differentially attenuate the amplitude of Akt signaling by regulating distinct Akt isoforms. Mol Cell 25:917-31.

57. Miyamoto S, Purcell NH, Smith JM, Gao T, Whittaker R, Huang K, Castillo R, Glembotski CC, Sussman MA, Newton AC, Brown JH. 2010. PHLPP-1 negatively regulates Akt activity and survival in the heart. Circ Res 107:476-84.

58. Patterson SJ, Han JM, Garcia R, Assi K, Gao T, O'Neill A, Newton AC, Levings MK. 2011. Cutting edge: PHLPP regulates the development, function, and molecular signaling pathways of regulatory T cells. J Immunol 186:5533-7.

59. Chen HH, Händel N, Ngeow J, Muller J, Hühn M, Yang HT, Heindl M, Berbers RM, Hegazy AN, Kionke J, Yehia L, Sack U, Bläser F, Rensing-Ehl A, Reifenberger J, Keith J, Travis S, Merkenschlager A, Kiess W, Wittekind C, Walker L, Ehl S, Aretz S, Dustin ML, Eng C, Powrie F, Uhlig HH. 2017. Immune dysregulation in patients with PTEN hamartoma tumor syndrome: Analysis of FOXP3 regulatory T cells. J Allergy Clin Immunol 139:607-620.e15.

60. Etemire E, Krull M, Hasenberg M, Reichardt P, Gunzer M. 2013. Transiently reduced PI3K/Akt activity drives the development of regulatory function in antigen-stimulated Naïve T-cells. PloS one 8:e68378-e68378.

61. Teng DC, Sun J, An YQ, Hu ZH, Liu P, Ma YC, Han B, Shi Y. 2016. Role of PHLPP1 in inflammation response: Its loss contributes to gliomas development and progression. Int Immunopharmacol 34:229-234.

62. Fischer J, Gutièrrez S, Ganesan R, Calabrese C, Ranjan R, Cildir G, Hos NJ, Rybniker J, Wolke M, Fries JWU, Tergaonkar V, Plum G, Antebi A, Robinson N. 2019. Leptin signaling impairs macrophage defenses against Salmonella Typhimurium. Proceedings of the National Academy of Sciences of the United States of America 116:16551-16560.

63. Alamuru-Yellapragada NP, Vundyala S, Behera S, Parsa KVL. 2017. LPS depletes PHLPP levels in macrophages through the inhibition of SP1 dependent transcriptional regulation. Biochemical and Biophysical Research Communications 486:533-538.

64. Cohen Katsenelson K, Stender JD, Kawashima AT, Lordén G, Uchiyama S, Nizet V, Glass CK, Newton AC. 2019. PHLPP1 counter-regulates STAT1-mediated inflammatory signaling. Elife 8.

65. Alamuru NP, Behera S, Butchar JP, Tridandapani S, Kaimal Suraj S, Babu PP, Hasnain SE, Ehtesham NZ, Parsa KVL. 2014. A novel immunomodulatory function of PHLPP1: inhibition of iNOS via attenuation of STAT1 ser727 phosphorylation in mouse macrophages. Journal of Leukocyte Biology 95:775-783.

66. Naylor RM, van Deursen JM. 2016. Aneuploidy in Cancer and Aging. Annual Review of Genetics 50:45-66.

67. Kettenbach AN, Schweppe DK, Faherty BK, Pechenick D, Pletnev AA, Gerber SA. 2011. Quantitative phosphoproteomics identifies substrates and functional modules of Aurora and Polo-like kinase activities in mitotic cells. Science signaling 4:rs5-rs5.

68. Dephoure N, Zhou C, Villén J, Beausoleil SA, Bakalarski CE, Elledge SJ, Gygi SP. 2008. A quantitative atlas of mitotic phosphorylation. Proceedings of the National Academy of Sciences of the United States of America 105:10762-10767.

69. Wurzenberger C, Gerlich DW. 2011. Phosphatases: providing safe passage through mitotic exit. Nat Rev Mol Cell Biol 12:469-82.

70. King RW, Peters JM, Tugendreich S, Rolfe M, Hieter P, Kirschner MW. 1995. A 20S complex containing CDC27 and CDC16 catalyzes the mitosis-specific conjugation of ubiquitin to cyclin B. Cell 81:279-88.

71. Sudakin V, Ganoth D, Dahan A, Heller H, Hershko J, Luca FC, Ruderman JV, Hershko A. 1995. The cyclosome, a large complex containing cyclin-selective ubiquitin ligase activity, targets cyclins for destruction at the end of mitosis. Mol Biol Cell 6:185-97.

72. Irniger S, Piatti S, Michaelis C, Nasmyth K. 1995. Genes involved in sister chromatid separation are needed for B-type cyclin proteolysis in budding yeast. Cell 81:269-78.

73. Dou Z, von Schubert C, Körner R, Santamaria A, Elowe S, Nigg EA. 2011. Quantitative mass spectrometry analysis reveals similar substrate consensus motif for human Mps1 kinase and Plk1. PloS one 6:e18793-e18793.

74. Hayward D, Alfonso-Pérez T, Cundell MJ, Hopkins M, Holder J, Bancroft J, Hutter LH, Novak B, Barr FA, Gruneberg U. 2019. CDK1-CCNB1 creates a spindle checkpoint-permissive state by enabling MPS1 kinetochore localization. The Journal of cell biology 218:1182-1199.

75. Gharbi-Ayachi A, Labbé J-C, Burgess A, Vigneron S, Strub J-M, Brioudes E, Van-Dorsselaer A, Castro A, Lorca T. 2010. The Substrate of Greatwall Kinase, Arpp19, Controls Mitosis by Inhibiting Protein Phosphatase 2A. Science 330:1673.

76. Blake-Hodek KA, Williams BC, Zhao Y, Castilho PV, Chen W, Mao Y, Yamamoto TM, Goldberg ML. 2012. Determinants for Activation of the Atypical AGC Kinase Greatwall during M Phase Entry. Molecular and Cellular Biology 32:1337.

77. Vigneron S, Gharbi-Ayachi A, Raymond A-A, Burgess A, Labbé J-C, Labesse G, Monsarrat B, Lorca T, Castro A. 2011. Characterization of the Mechanisms Controlling Greatwall Activity. Molecular and Cellular Biology 31:2262.

78. Mailand N, Podtelejnikov AV, Groth A, Mann M, Bartek J, Lukas J. 2002. Regulation of G(2)/M events by Cdc25A through phosphorylation-dependent modulation of its stability. Embo j 21:5911-20.

79. Wu Z, Jiang Q, Clarke PR, Zhang C. 2013. Phosphorylation of Crm1 by CDK1–cyclin-B promotes Ran-dependent mitotic spindle assembly. Journal of Cell Science 126:3417.

80. Grzechnik AT, Newton AC. 2016. PHLPPing through history: a decade in the life of PHLPP phosphatases. Biochemical Society Transactions 44:1675-1682.

81. Chen MJ, Dixon JE, Manning G. 2017. Genomics and evolution of protein phosphatases. Sci Signal 10.

82. Brognard J, Sierecki E, Gao T, Newton AC. 2007. PHLPP and a Second Isoform, PHLPP2, Differentially Attenuate the Amplitude of Akt Signaling by Regulating Distinct Akt Isoforms. Molecular Cell 25:917-931.

83. Goel A, Arnold CN, Niedzwiecki D, Chang DK, Ricciardiello L, Carethers JM, Dowell JM, Wasserman L, Compton C, Mayer RJ, Bertagnolli MM, Boland CR. 2003. Characterization of sporadic colon cancer by patterns of genomic instability. Cancer Res 63:1608-14.

84. Tørring N, Borre M, Sørensen KD, Andersen CL, Wiuf C, Ørntoft TF. 2007. Genome-wide analysis of allelic imbalance in prostate cancer using the Affymetrix 50K SNP mapping array. Br J Cancer 96:499-506.

85. Chen M, Pratt Christopher P, Zeeman Martha E, Schultz N, Taylor Barry S, O'Neill A, Castillo-Martin M, Nowak Dawid G, Naguib A, Grace Danielle M, Murn J, Navin N, Atwal Gurinder S, Sander C, Gerald William L, Cordon-Cardo C, Newton Alexandra C, Carver Brett S, Trotman Lloyd C. 2011. Identification of PHLPP1 as a Tumor Suppressor Reveals the Role of Feedback Activation in PTEN-Mutant Prostate Cancer Progression. Cancer Cell 20:173-186.

86. Baffi TR, Van AN, Zhao W, Mills GB, Newton AC. 2019. Protein Kinase C Quality Control by Phosphatase PHLPP1 Unveils Loss-of-Function Mechanism in Cancer. Mol Cell 74:378-392.e5.

87. Bradley EW, Carpio LR, Newton AC, Westendorf JJ. 2015. Deletion of the PH-domain and Leucine-rich Repeat Protein Phosphatase 1 (Phlpp1) Increases Fibroblast Growth Factor (Fgf) 18 Expression and Promotes Chondrocyte Proliferation. The Journal of biological chemistry 290:16272-16280.

88. Gangula NR, Maddika S. 2017. Interplay between the phosphatase PHLPP1 and E3 ligase RNF41 stimulates proper kinetochore assembly via the outer-kinetochore protein SGT1. The Journal of biological chemistry 292:13947-13958.

89. Mészáros B, Erdős G, Dosztányi Z. 2018. IUPred2A: context-dependent prediction of protein disorder as a function of redox state and protein binding. Nucleic Acids Research 46:W329-W337.

90. Malumbres M. 2014. Cyclin-dependent kinases. Genome Biol 15:122.

91. Songyang Z, Blechner S, Hoagland N, Hoekstra MF, Piwnica-Worms H, Cantley LC. 1994. Use of an oriented peptide library to determine the optimal substrates of protein kinases. Current Biology 4:973-982.

92. Mok J, Kim PM, Lam HYK, Piccirillo S, Zhou X, Jeschke GR, Sheridan DL, Parker SA, Desai V, Jwa M, Cameroni E, Niu H, Good M, Remenyi A, Ma J-LN, Sheu Y-J, Sassi HE, Sopko R, Chan CSM, De Virgilio C, Hollingsworth NM, Lim WA, Stern DF, Stillman B, Andrews BJ, Gerstein MB, Snyder M, Turk BE. 2010. Deciphering Protein Kinase Specificity Through Large-Scale Analysis of Yeast Phosphorylation Site Motifs. Science Signaling 3:ra12.

93. Shang C, Hazbun TR, Cheeseman IM, Aranda J, Fields S, Drubin DG, Barnes G. 2003. Kinetochore Protein Interactions and their Regulation by the Aurora Kinase Ipl1p. Molecular Biology of the Cell 14:3342-3355.

94. Roux KJ, Kim DI, Burke B, May DG. 2018. BioID: A Screen for Protein-Protein Interactions. Current protocols in protein science 91:19.23.1-19.23.15.

95. Choi-Rhee E, Schulman H, Cronan JE. 2004. Promiscuous protein biotinylation by Escherichia coli biotin protein ligase. Protein Sci 13:3043-50.

96. Teo G, Liu G, Zhang J, Nesvizhskii AI, Gingras AC, Choi H. 2014. SAINTexpress: improvements and additional features in Significance Analysis of INTeractome software. J Proteomics 100:37-43.

97. Wan S, Meyer AS, Weiler SME, Rupp C, Tóth M, Sticht C, Singer S, Thomann S, Roessler S, Schorpp-Kistner M, Schmitt J, Gretz N, Angel P, Tschaharganeh DF, Marquardt J, Schirmacher P, Pinna F, Breuhahn K. 2018. Cytoplasmic localization of the cell polarity factor scribble supports liver tumor formation and tumor cell invasiveness. Hepatology 67:1842-1856.

98. Zhang X, Lu X, Akhter S, Georgescu MM, Legerski RJ. 2016. FANCI is a negative regulator of Akt activation. Cell Cycle 15:1134-43.

99. McClurg UL, Summerscales EE, Harle VJ, Gaughan L, Robson CN. 2014. Deubiquitinating enzyme Usp12 regulates the interaction between the androgen receptor and the Akt pathway. Oncotarget 5:7081-7092.

100. Reimand J, Kull M, Peterson H, Hansen J, Vilo J. 2007. g:Profiler--a web-based toolset for functional profiling of gene lists from large-scale experiments. Nucleic Acids Res 35:W193-200.

101. Kalsbeek D, Golsteyn RM. 2017. G2/M-Phase Checkpoint Adaptation and Micronuclei Formation as Mechanisms That Contribute to Genomic Instability in Human Cells. Int J Mol Sci 18.

102. Santamaría D, Barrière C, Cerqueira A, Hunt S, Tardy C, Newton K, Cáceres JF, Dubus P, Malumbres M, Barbacid M. 2007. Cdk1 is sufficient to drive the mammalian cell cycle. Nature 448:811-5.

103. Szmyd R, Niska-Blakie J, Diril MK, Renck Nunes P, Tzelepis K, Lacroix A, van Hul N, Deng L-W, Matos J, Dreesen O, Bisteau X, Kaldis P. 2019. Premature activation of Cdk1 leads to mitotic events in S phase and embryonic lethality. Oncogene 38:998-1018.

104. Piao J, Zhu L, Sun J, Li N, Dong B, Yang Y, Chen L. 2019. High expression of CDK1 and BUB1 predicts poor prognosis of pancreatic ductal adenocarcinoma. Gene 701:15-22.

105. Ravindran Menon D, Luo Y, Arcaroli JJ, Liu S, KrishnanKutty LN, Osborne DG, Li Y, Samson JM, Bagby S, Tan A-C, Robinson WA, Messersmith WA, Fujita M. 2018. CDK1 interacts with Sox2 and promotes tumor initiation in human melanoma. Cancer Research doi:10.1158/0008-5472.CAN-18-0330:canres.0330.2018.

106. Yasukawa M, Ando Y, Yamashita T, Matsuda Y, Shoji S, Morioka MS, Kawaji H, Shiozawa K, Machitani M, Abe T, Yamada S, Kaneko MK, Kato Y, Furuta Y, Kondo T, Shirouzu M, Hayashizaki Y, Kaneko S, Masutomi K. 2020. CDK1 dependent phosphorylation of hTERT contributes to cancer progression. Nat Commun 11:1557.

107. Heo J, Noh B-J, Lee S, Lee H-Y, Kim Y, Lim J, Ju H, Yu HY, Ryu C-M, Lee PCW, Jeong H, Oh Y, Kim K, Kim S-Y, Son J, Hong B, Kim JS, Cho YM, Shin D-M. 2020. Phosphorylation of TFCP2L1 by CDK1 is required for stem cell pluripotency and bladder carcinogenesis. EMBO Molecular Medicine 12:e10880.

108. Dong S, Huang F, Zhang H, Chen Q. 2019. Overexpression of BUB1B, CCNA2, CDC20, and CDK1 in tumor tissues predicts poor survival in pancreatic ductal adenocarcinoma. Bioscience Reports 39.

109. Vassilev LT, Tovar C, Chen S, Knezevic D, Zhao X, Sun H, Heimbrook DC, Chen L. 2006. Selective small-molecule inhibitor reveals critical mitotic functions of human CDK1. Proceedings of the National Academy of Sciences of the United States of America 103:10660-10665.

110. Voets E, Marsman J, Demmers J, Beijersbergen R, Wolthuis R. 2015. The lethal response to Cdk1 inhibition depends on sister chromatid alignment errors generated by KIF4 and isoform 1 of PRC1. Scientific Reports 5:14798.

111. McCloy RA, Rogers S, Caldon CE, Lorca T, Castro A, Burgess A. 2014. Partial inhibition of Cdk1 in G2 phase overrides the SAC and decouples mitotic events. Cell Cycle 13:1400-1412.

112. Holt LJ, Tuch BB, Villén J, Johnson AD, Gygi SP, Morgan DO. 2009. Global Analysis of Cdk1 Substrate Phosphorylation Sites Provides Insights into Evolution. Science 325:1682.

113. Cukier IH, Li Y, Lee JM. 2007. Cyclin B1/Cdk1 binds and phosphorylates Filamin A and regulates its ability to cross-link actin. FEBS Letters 581:1661-1672.

114. Foisner R, Malecz N, Dressel N, Stadler C, Wiche G. 1996. M-phase-specific phosphorylation and structural rearrangement of the cytoplasmic cross-linking protein plectin involve p34cdc2 kinase. Mol Biol Cell 7:273-88.

115. Blethrow JD, Glavy JS, Morgan DO, Shokat KM. 2008. Covalent capture of kinase-specific phosphopeptides reveals Cdk1-cyclin B substrates. Proceedings of the National Academy of Sciences of the United States of America 105:1442-1447.

116. Koffa MD, Casanova CM, Santarella R, Köcher T, Wilm M, Mattaj IW. 2006. HURP is part of a Ran-dependent complex involved in spindle formation. Curr Biol 16:743-54.

117. Kandel ES, Skeen J, Majewski N, Di Cristofano A, Pandolfi PP, Feliciano CS, Gartel A, Hay N. 2002. Activation of Akt/protein kinase B overcomes a G(2)/m cell cycle checkpoint induced by DNA damage. Mol Cell Biol 22:7831-41.

118. Shtivelman E, Sussman J, Stokoe D. 2002. A Role for PI 3-Kinase and PKB Activity in the G2/M Phase of the Cell Cycle. Current Biology 12:919-924.

119. Dangi S, Cha H, Shapiro P. 2003. Requirement for phosphatidylinositol-3 kinase activity during progression through S-phase and entry into mitosis. Cell Signal 15:667-75.

120. Liu X, Shi Y, Woods KW, Hessler P, Kroeger P, Wilsbacher J, Wang J, Wang JY, Li C, Li Q, Rosenberg SH, Giranda VL, Luo Y. 2008. Akt inhibitor a-443654 interferes with mitotic progression by regulating aurora a kinase expression. Neoplasia (New York, NY) 10:828-837.

121. Warfel NA, Niederst M, Stevens MW, Brennan PM, Frame MC, Newton AC. 2011. Mislocalization of the E3 ligase, β-transducin repeat-containing protein 1 (β-TrCP1), in glioblastoma uncouples negative feedback between the pleckstrin homology domain leucine-rich repeat protein phosphatase 1 (PHLPP1) and Akt. J Biol Chem 286:19777-88.

122. Kean MJ, Couzens AL, Gingras A-C. 2012. Mass spectrometry approaches to study mammalian kinase and phosphatase associated proteins. Methods 57:400-408.

123. Uphoff CC, Drexler HG. 2004. Detecting Mycoplasma contamination in cell cultures by polymerase chain reaction. Methods Mol Med 88:319-26.

124. Liu G, Knight JD, Zhang JP, Tsou CC, Wang J, Lambert JP, Larsen B, Tyers M, Raught B, Bandeira N, Nesvizhskii AI, Choi H, Gingras AC. 2016. Data Independent Acquisition analysis in ProHits 4.0. J Proteomics 149:64-68.

125. Perkins DN, Pappin DJ, Creasy DM, Cottrell JS. 1999. Probability-based protein identification by searching sequence databases using mass spectrometry data. Electrophoresis 20:3551-67.

126. Eng JK, Jahan TA, Hoopmann MR. 2013. Comet: an open-source MS/MS sequence database search tool. Proteomics 13:22-4.

127. Shteynberg D, Deutsch EW, Lam H, Eng JK, Sun Z, Tasman N, Mendoza L, Moritz RL, Aebersold R, Nesvizhskii AI. 2011. iProphet: multi-level integrative analysis of shotgun proteomic data improves peptide and protein identification rates and error estimates. Mol Cell Proteomics 10:M111.007690.

128. Knight JDR, Choi H, Gupta GD, Pelletier L, Raught B, Nesvizhskii AI, Gingras AC. 2017. ProHits-viz: a suite of web tools for visualizing interaction proteomics data. Nat Methods 14:645-646.

129. Meitinger F, Anzola JV, Kaulich M, Richardson A, Stender JD, Benner C, Glass CK, Dowdy SF, Desai A, Shiau AK, Oegema K. 2016. 53BP1 and USP28 mediate p53 activation and G1 arrest after centrosome loss or extended mitotic duration. The Journal of cell biology 214:155-166.

130. Flavahan WA, Gaskell E, Bernstein BE. 2017. Epigenetic plasticity and the hallmarks of cancer. Science 357.

131. Dawson MA, Kouzarides T. 2012. Cancer epigenetics: from mechanism to therapy. Cell 150:12-27.

132. Coussens LM, Werb Z. 2002. Inflammation and cancer. Nature 420:860-7.

133. Grivennikov SI, Greten FR, Karin M. 2010. Immunity, inflammation, and cancer. Cell 140:883-99.

134. Sabapathy K, Lane DP. 2018. Therapeutic targeting of p53: all mutants are equal, but some mutants are more equal than others. Nat Rev Clin Oncol 15:13-30.

135. Jernberg E, Bergh A, Wikstrom P. 2017. Clinical relevance of androgen receptor alterations in prostate cancer. Endocr Connect 6:R146-R161.

136. Pejerrey SM, Dustin D, Kim JA, Gu G, Rechoum Y, Fuqua SAW. 2018. The Impact of ESR1 Mutations on the Treatment of Metastatic Breast Cancer. Horm Cancer doi:10.1007/s12672-017-0306-5.

137. Kalkat M, De Melo J, Hickman KA, Lourenco C, Redel C, Resetca D, Tamachi A, Tu WB, Penn LZ. 2017. MYC Deregulation in Primary Human Cancers. Genes (Basel) 8.

138. Whitmarsh AJ, Davis RJ. 2000. Regulation of transcription factor function by phosphorylation. Cell Mol Life Sci 57:1172-83.

139. Rossetto D, Avvakumov N, Cote J. 2012. Histone phosphorylation: a chromatin modification involved in diverse nuclear events. Epigenetics 7:1098-108.

140. O'Neill LA, Golenbock D, Bowie AG. 2013. The history of Toll-like receptors - redefining innate immunity. Nat Rev Immunol 13:453-60.

141. Karin M, Lawrence T, Nizet V. 2006. Innate immunity gone awry: linking microbial infections to chronic inflammation and cancer. Cell 124:823-35.

142. Fullerton JN, Gilroy DW. 2016. Resolution of inflammation: a new therapeutic frontier. Nat Rev Drug Discov 15:551-67.

143. O'Shea JJ, Murray PJ. 2008. Cytokine signaling modules in inflammatory responses. Immunity 28:477-87.

144. Wynn TA, Vannella KM. 2016. Macrophages in Tissue Repair, Regeneration, and Fibrosis. Immunity 44:450-462.

145. Oishi Y, Spann NJ, Link VM, Muse ED, Strid T, Edillor C, Kolar MJ, Matsuzaka T, Hayakawa S, Tao J, Kaikkonen MU, Carlin AF, Lam MT, Manabe I, Shimano H, Saghatelian A, Glass CK. 2017. SREBP1 Contributes to Resolution of Pro-inflammatory TLR4 Signaling by Reprogramming Fatty Acid Metabolism. Cell Metab 25:412-427.

146. Darnell JE, Jr., Kerr IM, Stark GR. 1994. Jak-STAT pathways and transcriptional activation in response to IFNs and other extracellular signaling proteins. Science 264:1415-21.

147. Stark GR, Darnell JE, Jr. 2012. The JAK-STAT pathway at twenty. Immunity 36:503-14.

148. Morris R, Kershaw NJ, Babon JJ. 2018. The molecular details of cytokine signaling via the JAK/STAT pathway. Protein Sci 27:1984-2009.

149. Darnell JE, Jr. 1997. STATs and gene regulation. Science 277:1630-5.

150. Sadzak I, Schiff M, Gattermeier I, Glinitzer R, Sauer I, Saalmuller A, Yang E, Schaljo B, Kovarik P. 2008. Recruitment of Stat1 to chromatin is required for interferon-induced serine phosphorylation of Stat1 transactivation domain. Proc Natl Acad Sci U S A 105:8944-9.

151. Wen Z, Zhong Z, Darnell JE, Jr. 1995. Maximal activation of transcription by Stat1 and Stat3 requires both tyrosine and serine phosphorylation. Cell 82:241-50.

152. Platanias LC. 2005. Mechanisms of type-I- and type-II-interferon-mediated signalling. Nat Rev Immunol 5:375-86.

153. Grzechnik AT, Newton AC. 2016. PHLPPing through history: a decade in the life of PHLPP phosphatases. Biochem Soc Trans 44:1675-1682.

154. Liu J, Weiss HL, Rychahou P, Jackson LN, Evers BM, Gao T. 2009. Loss of PHLPP expression in colon cancer: role in proliferation and tumorigenesis. Oncogene 28:994-1004.

155. Li X, Yang H, Liu J, Schmidt MD, Gao T. 2011. Scribble-mediated membrane targeting of PHLPP1 is required for its negative regulation of Akt. EMBO Rep 12:818-24.

156. Heinz S, Benner C, Spann N, Bertolino E, Lin YC, Laslo P, Cheng JX, Murre C, Singh H, Glass CK. 2010. Simple combinations of lineage-determining transcription factors prime cis-regulatory elements required for macrophage and B cell identities. Mol Cell 38:576-89.

157. Ohmori Y, Hamilton TA. 2001. Requirement for STAT1 in LPS-induced gene expression in macrophages. J Leukoc Biol 69:598-604.

158. Alamuru NP, Behera S, Butchar JP, Tridandapani S, Kaimal Suraj S, Babu PP, Hasnain SE, Ehtesham NZ, Parsa KV. 2014. A novel immunomodulatory function of PHLPP1: inhibition of iNOS via attenuation of STAT1 ser727 phosphorylation in mouse macrophages. J Leukoc Biol 95:775-783.

159. Hein MY, Hubner NC, Poser I, Cox J, Nagaraj N, Toyoda Y, Gak IA, Weisswange I, Mansfeld J, Buchholz F, Hyman AA, Mann M. 2015. A human interactome in three quantitative dimensions organized by stoichiometries and abundances. Cell 163:712-23.

160. Lin JR, Hu J. 2013. SeqNLS: nuclear localization signal prediction based on frequent pattern mining and linear motif scoring. PLoS One 8:e76864.

161. Wen W, Meinkoth JL, Tsien RY, Taylor SS. 1995. Identification of a signal for rapid export of proteins from the nucleus. Cell 82:463-73.

162. Xu D, Marquis K, Pei J, Fu SC, Cagatay T, Grishin NV, Chook YM. 2015. LocNES: a computational tool for locating classical NESs in CRM1 cargo proteins. Bioinformatics 31:1357-65.

163. Baffi TR, Van AN, Zhao W, Mills GB, Newton AC. 2019. Protein Kinase C Quality Control by Phosphatase PHLPP1 Unveils Loss-of-Function Mechanism in Cancer. Mol Cell doi:10.1016/j.molcel.2019.02.018.

164. Chapgier A, Boisson-Dupuis S, Jouanguy E, Vogt G, Feinberg J, Prochnicka-Chalufour A, Casrouge A, Yang K, Soudais C, Fieschi C, Santos OF, Bustamante J, Picard C, de Beaucoudrey L, Emile JF, Arkwright PD, Schreiber RD, Rolinck-Werninghaus C, Rosen-Wolff A, Magdorf K, Roesler J, Casanova JL. 2006. Novel STAT1 alleles in otherwise healthy patients with mycobacterial disease. PLoS Genet 2:e131.

165. Dupuis S, Dargemont C, Fieschi C, Thomassin N, Rosenzweig S, Harris J, Holland SM, Schreiber RD, Casanova JL. 2001. Impairment of mycobacterial but not viral immunity by a germline human STAT1 mutation. Science 293:300-3.

166. Luu K, Greenhill CJ, Majoros A, Decker T, Jenkins BJ, Mansell A. 2014. STAT1 plays a role in TLR signal transduction and inflammatory responses. Immunol Cell Biol 92:761-9.

167. Weischenfeldt J, Porse B. 2008. Bone Marrow-Derived Macrophages (BMM): Isolation and Applications. CSH Protoc 2008:pdb prot5080.

168. Ray A, Dittel BN. 2010. Isolation of mouse peritoneal cavity cells. J Vis Exp doi:10.3791/1488.

169. Uphoff CC, Drexler HG. 2011. Detecting mycoplasma contamination in cell cultures by polymerase chain reaction. Methods Mol Biol 731:93-103.

170. Livak KJ, Schmittgen TD. 2001. Analysis of relative gene expression data using real-time quantitative PCR and the 2(-Delta Delta C(T)) Method. Methods 25:402-8.

171. Kaikkonen MU, Spann NJ, Heinz S, Romanoski CE, Allison KA, Stender JD, Chun HB, Tough DF, Prinjha RK, Benner C, Glass CK. 2013. Remodeling of the enhancer landscape during macrophage activation is coupled to enhancer transcription. Mol Cell 51:310-25.

172. Garber M, Yosef N, Goren A, Raychowdhury R, Thielke A, Guttman M, Robinson J, Minie B, Chevrier N, Itzhaki Z, Blecher-Gonen R, Bornstein C, Amann-Zalcenstein D, Weiner A, Friedrich D, Meldrim J, Ram O, Cheng C, Gnirke A, Fisher S, Friedman N, Wong B, Bernstein BE, Nusbaum C, Hacohen N, Regev A, Amit I. 2012. A high-throughput chromatin immunoprecipitation approach reveals principles of dynamic gene regulation in mammals. Mol Cell 47:810-22.

173. Stender JD, Nwachukwu JC, Kastrati I, Kim Y, Strid T, Yakir M, Srinivasan S, Nowak J, Izard T, Rangarajan ES, Carlson KE, Katzenellenbogen JA, Yao XQ, Grant BJ, Leong HS, Lin CY, Frasor J, Nettles KW, Glass CK. 2017. Structural and Molecular Mechanisms of Cytokine-Mediated Endocrine Resistance in Human Breast Cancer Cells. Mol Cell 65:1122-1135 e5.

174. Horvai AE, Xu L, Korzus E, Brard G, Kalafus D, Mullen TM, Rose DW, Rosenfeld MG, Glass CK. 1997. Nuclear integration of JAK/STAT and Ras/AP-1 signaling by CBP and p300. Proc Natl Acad Sci U S A 94:1074-9.

175. Pavlova NN, Thompson CB. 2016. The Emerging Hallmarks of Cancer Metabolism. Cell Metab 23:27-47.

176. Hanahan D, Weinberg RA. 2011. Hallmarks of cancer: the next generation. Cell 144:646-74.

177. Diaz-Ruiz R, Rigoulet M, Devin A. 2011. The Warburg and Crabtree effects: On the origin of cancer cell energy metabolism and of yeast glucose repression. Biochim Biophys Acta 1807:568-76.

178. Jin L, Alesi GN, Kang S. 2016. Glutaminolysis as a target for cancer therapy. Oncogene 35:3619-3625.

179. Newsholme EA, Crabtree B, Ardawi MS. 1985. Glutamine metabolism in lymphocytes: its biochemical, physiological and clinical importance. Q J Exp Physiol 70:473-89.

180. Huang S, Czech MP. 2007. The GLUT4 glucose transporter. Cell Metab 5:237-52.

181. Utsunomiya-Tate N, Endou H, Kanai Y. 1996. Cloning and functional characterization of a system ASC-like Na+-dependent neutral amino acid transporter. J Biol Chem 271:14883-90.

182. Yanagida O, Kanai Y, Chairoungdua A, Kim DK, Segawa H, Nii T, Cha SH, Matsuo H, Fukushima J, Fukasawa Y, Tani Y, Taketani Y, Uchino H, Kim JY, Inatomi J, Okayasu I, Miyamoto K, Takeda E, Goya T, Endou H. 2001. Human L-type amino acid transporter 1 (LAT1): characterization of function and expression in tumor cell lines. Biochim Biophys Acta 1514:291-302.

183. Nicklin P, Bergman P, Zhang B, Triantafellow E, Wang H, Nyfeler B, Yang H, Hild M, Kung C, Wilson C, Myer VE, MacKeigan JP, Porter JA, Wang YK, Cantley LC, Finan PM, Murphy LO. 2009. Bidirectional transport of amino acids regulates mTOR and autophagy. Cell 136:521-534.

184. Jiang H, Zhang N, Tang T, Feng F, Sun H, Qu W. 2020. Target the human Alanine/Serine/Cysteine Transporter 2(ASCT2): Achievement and Future for Novel Cancer Therapy. Pharmacol Res 158:104844.

185. Lu JJ, Li P, Yang Y, Wang L, Zhang Y, Zhu JY, Zhu XR, Chen MB. 2020. Prognostic value of LAT-1 status in solid cancer: A systematic review and meta-analysis. PLoS One 15:e0233629.

186. Roth SY, Denu JM, Allis CD. 2001. Histone acetyltransferases. Annu Rev Biochem 70:81-120.

187. Imai S-i, Armstrong CM, Kaeberlein M, Guarente L. 2000. Transcriptional silencing and longevity protein Sir2 is an NAD-dependent histone deacetylase. Nature 403:795-800.

188. Anand R, Marmorstein R. 2007. Structure and mechanism of lysine-specific demethylase enzymes. J Biol Chem 282:35425-9.

189. Zhao Z, Shilatifard A. 2019. Epigenetic modifications of histones in cancer. Genome Biology 20:245.

190. Qie S, Liang D, Yin C, Gu W, Meng M, Wang C, Sang N. 2012. Glutamine depletion and glucose depletion trigger growth inhibition via distinctive gene expression reprogramming. Cell Cycle 11:3679-3690.

191. Jung S, Kang JG, Lee JH, Song KJ, Ko JH, Kim YS. 2014. PHLPP1 regulates contact inhibition by dephosphorylating Mst1 at the inhibitory site. Biochem Biophys Res Commun 443:1263-9.

192. Kusuyama J, Bandow K, Ohnishi T, Amir MS, Shima K, Semba I, Matsuguchi T. 2019. CXCL13 is a differentiation- and hypoxia-induced adipocytokine that exacerbates the inflammatory phenotype of adipocytes through PHLPP1 induction. Biochemical Journal 476:3533-3548.

193. Tsukada Y, Fang J, Erdjument-Bromage H, Warren ME, Borchers CH, Tempst P, Zhang Y. 2006. Histone demethylation by a family of JmjC domain-containing proteins. Nature 439:811-6.

194. Bannister AJ, Schneider R, Kouzarides T. 2002. Histone methylation: dynamic or static? Cell 109:801-6.

195. Tahiliani M, Koh KP, Shen Y, Pastor WA, Bandukwala H, Brudno Y, Agarwal S, Iyer LM, Liu DR, Aravind L, Rao A. 2009. Conversion of 5-methylcytosine to 5-hydroxymethylcytosine in mammalian DNA by MLL partner TET1. Science 324:930-5.

196. Kandil HM, Argenzio RA, Chen W, Berschneider HM, Stiles AD, Westwick JK, Rippe RA, Brenner DA, Rhoads JM. 1995. L-glutamine and L-asparagine stimulate ODC activity and proliferation in a porcine jejunal enterocyte line. Am J Physiol 269:G591-9.

197. Meng Q, Epler MJ, Lin C, Karinch AM, Vary TC, Pan M. 2004. Insulin-like growth factor-2 activation of intestinal glutamine transport is mediated by mitogen-activated protein kinases. J Gastrointest Surg 8:40-7.

198. Kwon SJ, Lee YJ. 2005. Effect of low glutamine/glucose on hypoxia-induced elevation of hypoxia-inducible factor-1alpha in human pancreatic cancer MiaPaCa-2 and human prostatic cancer DU-145 cells. Clin Cancer Res 11:4694-700.

199. Drogat B, Bouchecareilh M, North S, Petibois C, Déléris G, Chevet E, Bikfalvi A, Moenner M. 2007. Acute L-glutamine deprivation compromises VEGF-a upregulation in A549/8 human carcinoma cells. J Cell Physiol 212:463-72.

200. Peng ZY, Hamiel CR, Banerjee A, Wischmeyer PE, Friese RS, Wischmeyer P. 2006. Glutamine attenuation of cell death and inducible nitric oxide synthase expression following inflammatory cytokine-induced injury is dependent on heat shock factor-1 expression. JPEN J Parenter Enteral Nutr 30:400-6; discussion 406-7.

201. Ropeleski MJ, Riehm J, Baer KA, Musch MW, Chang EB. 2005. Anti-apoptotic effects of L-glutamine-mediated transcriptional modulation of the heat shock protein 72 during heat shock. Gastroenterology 129:170-84.

202. Morrison AL, Dinges M, Singleton KD, Odoms K, Wong HR, Wischmeyer PE. 2006. Glutamine's protection against cellular injury is dependent on heat shock factor-1. Am J Physiol Cell Physiol 290:C1625-32.

203. Wang J, Chen G, Pantopoulos K. 2005. Inhibition of transferrin receptor 1 transcription by a cell density response element. Biochem J 392:383-8.

204. Wang L, Adamo ML. 2000. Cell density influences insulin-like growth factor I gene expression in a cell type-specific manner. Endocrinology 141:2481-9.

205. Scalise M, Pochini L, Panni S, Pingitore P, Hedfalk K, Indiveri C. 2014. Transport mechanism and regulatory properties of the human amino acid transporter ASCT2 (SLC1A5). Amino Acids 46:2463-2475.

206. Yan Y, Vasudevan S, Nguyen H, Bork U, Sitaraman S, Merlin D. 2007. Extracellular interaction between hCD98 and the PDZ class II domain of hCASK in intestinal epithelia. J Membr Biol 215:15-26.

207. Toyoda M, Kaira K, Ohshima Y, Ishioka NS, Shino M, Sakakura K, Takayasu Y, Takahashi K, Tominaga H, Oriuchi N, Nagamori S, Kanai Y, Oyama T, Chikamatsu K. 2014. Prognostic significance of amino-acid transporter expression (LAT1, ASCT2, and xCT) in surgically resected tongue cancer. British journal of cancer 110:2506-2513.

208. Witte D, Ali N, Carlson N, Younes M. 2002. Overexpression of the neutral amino acid transporter ASCT2 in human colorectal adenocarcinoma. Anticancer Res 22:2555-7.

209. Li R, Younes M, Frolov A, Wheeler TM, Scardino P, Ohori M, Ayala G. 2003. Expression of neutral amino acid transporter ASCT2 in human prostate. Anticancer Res 23:3413-8.

210. Kaira K, Oriuchi N, Imai H, Shimizu K, Yanagitani N, Sunaga N, Hisada T, Tanaka S, Ishizuka T, Kanai Y, Endou H, Nakajima T, Mori M. 2008. Prognostic significance of L-type amino acid transporter 1 expression in resectable stage I-III nonsmall cell lung cancer. Br J Cancer 98:742-8.

211. Kaira K, Oriuchi N, Takahashi T, Nakagawa K, Ohde Y, Okumura T, Murakami H, Shukuya T, Kenmotsu H, Naito T, Kanai Y, Endo M, Kondo H, Nakajima T, Yamamoto N. 2011. LAT1 expression is closely associated with hypoxic markers and mTOR in resected non-small cell lung cancer. Am J Transl Res 3:468-78.

212. Kamphorst JJ, Nofal M, Commisso C, Hackett SR, Lu W, Grabocka E, Vander Heiden MG, Miller G, Drebin JA, Bar-Sagi D, Thompson CB, Rabinowitz JD. 2015. Human pancreatic cancer tumors are nutrient poor and tumor cells actively scavenge extracellular protein. Cancer Res 75:544-53.

213. Commisso C, Davidson SM, Soydaner-Azeloglu RG, Parker SJ, Kamphorst JJ, Hackett S, Grabocka E, Nofal M, Drebin JA, Thompson CB, Rabinowitz JD, Metallo CM, Vander Heiden MG, Bar-Sagi D. 2013. Macropinocytosis of protein is an amino acid supply route in Ras-transformed cells. Nature 497:633-7.

214. Yang L, Achreja A, Yeung TL, Mangala LS, Jiang D, Han C, Baddour J, Marini JC, Ni J, Nakahara R, Wahlig S, Chiba L, Kim SH, Morse J, Pradeep S, Nagaraja AS, Haemmerle M, Kyunghee N, Derichsweiler M, Plackemeier T, Mercado-Uribe I, Lopez-Berestein G, Moss T, Ram PT, Liu J, Lu X, Mok SC, Sood AK, Nagrath D. 2016. Targeting Stromal Glutamine Synthetase in Tumors Disrupts Tumor Microenvironment-Regulated Cancer Cell Growth. Cell Metab 24:685-700.

215. Ran T, Zhang Y, Diao N, Geng S, Chen K, Lee C, Li L. 2019. Enhanced Neutrophil Immune Homeostasis Due to Deletion of PHLPP. Frontiers in immunology 10:2127-2127.

216. Leonard D, Huang W, Izadmehr S, O'Connor CM, Wiredja DD, Wang Z, Zaware N, Chen Y, Schlatzer DM, Kiselar J, Vasireddi N, Schüchner S, Perl AL, Galsky MD, Xu W, Brautigan DL, Ogris E, Taylor DJ, Narla G. 2020. Selective PP2A Enhancement through Biased Heterotrimer Stabilization. Cell 181:688-701.e16.

217. Farrington CC, Yuan E, Mazhar S, Izadmehr S, Hurst L, Allen-Petersen BL, Janghorban M, Chung E, Wolczanski G, Galsky M, Sears R, Sangodkar J, Narla G. 2020. Protein phosphatase 2A activation as a therapeutic strategy for managing MYC-driven cancers. J Biol Chem 295:757-770.